การออกแบบเครื่องปฏิกรณ์ฟลูอิไดซ์เบดแบบหมุนเวียนสำหรับการดูดซับคาร์บอนไดออกไซด์และการทำให้คืนสภาพตัวดูดซับ

นายสุทธิชัย บุญประสพ

วิทยานิพนธ์นี้เป็นส่วนหนึ่งของการศึกษาตามหลักสูตรปริญญาวิทยาศาสตรดุษฎีบัณฑิต
สาขาวิชาเคมีเทคนิค ภาควิชาเคมีเทคนิค
คณะวิทยาศาสตร์ จุฬาลงกรณ์มหาวิทยาลัย
ปีการศึกษา 2559

DESIGN OF CIRCULATING FLUIDIZED BED REACTOR FOR CARBON DIOXIDE ADSORPTION AND SORBENT REGENERATION

Mr. Sutthichai Boonprasop

A Dissertation Submitted in Partial Fulfillment of the Requirements
for the Degree of Doctor of Philosophy Program in Chemical Technology
Department of Chemical Technology
Faculty of Science
Chulalongkorn University
Academic Year 2016

Thesis Title	DESIGN OF CIRCULATING FLUIDIZED BED REACTOR FOR CARBON DIOXIDE ADSORPTION AND SORBENT REGENERATION
By	Mr. Sutthichai Boonprasop
Field of Study	Chemical Technology
Thesis Advisor	Professor Dr. Pornpote Piumsomboon
Thesis Co-Advisor	Associate Professor Dr. Benjapon Chalermsinsuwan

Accepted by the Faculty of Science, Chulalongkorn University in Partial Fulfillment of the Requirements for the Doctoral Degree

.....Dean of the Faculty of Science
(Associate Professor Dr. Polkit Sangvanich)

THESIS COMMITTEE

.....Chairman
(Associate Professor Doctor Prasert Reubroycharoen)

.....Thesis Advisor
(Professor Dr. Pornpote Piumsomboon)

.....Thesis Co-Advisor
(Associate Professor Dr. Benjapon Chalermsinsuwan)

.....Examiner
(Associate Professor Dr. Prapan Kuchonthara)

.....Examiner
(Associate Professor Dr. Tawatchai Charinpanitkul)

.....External Examiner
(Dr. Boonrod Sajjakulnukit)

สุทธิชัย บุญประสพ : การออกแบบเครื่องปฏิกรณ์ฟลูอิไดซ์เบดแบบหมุนเวียนสำหรับการดูดซับคาร์บอนไดออกไซด์และการทำให้คืนสภาพตัวดูดซับ (DESIGN OF CIRCULATING FLUIDIZED BED REACTOR FOR CARBON DIOXIDE ADSORPTION AND SORBENT REGENERATION) อ.ที่ปรึกษาวิทยานิพนธ์หลัก: ศ. ดร. พรพจน์ เปี่ยมสมบูรณ์, อ.ที่ปรึกษาวิทยานิพนธ์ร่วม: รศ. ดร. เบญจพล เฉลิมสินสุวรรณ, 183 หน้า.

ความสูงของท่อไรเซอร์เป็นตัวแปรที่สำคัญในการออกแบบท่อไรเซอร์ที่ทำให้เกิดช่วงการไหลแบบปั่นป่วนหมุนเวียน ความสูงที่เหมาะสมจะต้องมีค่าน้อยกว่าความสูงที่มากที่สุดที่ของแข็งสามารถขยายตัวได้ในแนวดิ่ง ช่วงการไหลแบบปั่นป่วนหมุนเวียนได้รวมเอาคุณลักษณะที่ดีของช่วงการไหลแบบปั่นป่วนซึ่งมีสัดส่วนของของแข็งสูง และคงที่ตลอดแนวความสูง เข้ากับความสามารถในการหมุนเวียนของของแข็ง เช่นเดียวกับช่วงการไหลแบบความเร็วสูง อุณหภูมิที่เหมาะสมต่อการดูดซับ คือ 60 องศาเซลเซียส ปริมาณสูงสุดที่สามารถดูดซับคาร์บอนไดออกไซด์ได้คือ 295 มิลลิกรัม ต่อ กรัมของตัวดูดซับที่มีโพแทสเซียมคาร์บอเนตกระจายอยู่บนพื้นผิวคิดเป็นร้อยละ 17 โดยน้ำหนัก ตัวดูดซับที่ผ่านการใช้งานแล้วสามารถนำกลับมาใช้งานได้ใหม่ด้วยการทำให้ฟื้นฟูสภาพ (regeneration) ทั้งแบบดั้งเดิมด้วยกระบวนการทางร้อนหรือแนวคิดใหม่ด้วยการลดความดัน ดังนั้นเครื่องปฏิกรณ์ฟลูอิไดซ์เบดแบบหมุนเวียนขนาดห้องปฏิบัติการ (Lab scale) ได้ถูกสร้างขึ้นเพื่อศึกษาผลของตัวแปรดำเนินการต่อการดูดซับแบบต่อเนื่อง การเพิ่มความเร็วของแก๊สป้อนเข้าช่วยเพิ่มความสามารถในการดูดซับซึ่งถือเป็นสัญญาณที่ดีต่อการพัฒนาระบบดูดซับในระดับต้นแบบ (Pilot scale) ที่สามารถดักจับคาร์บอนไดออกไซด์ได้อย่างต่อเนื่อง การคำนวณสภาวะของการดูดซับทำได้โดยการสร้างแบบจำลองทางคณิตศาสตร์ด้วยวิธีพลศาสตร์ของไหลเชิงคำนวณ การพัฒนาหอดูดซับขนาดต้นแบบเสนอการติดตั้งท่อหล่อเย็นในท่อไรเซอร์ที่มีเส้นผ่านศูนย์กลาง 1 เมตร ความสูง 3.55 เมตร การลดอุณหภูมิภายในท่อไรเซอร์จะช่วยลดข้อจำกัดของสมดุลเคมี (chemical reaction equilibrium) ที่อุณหภูมิของท่อหล่อเย็นที่เหมาะสมสามารถดักจับคาร์บอนไดออกไซด์ได้ถึงร้อยละ 95 โดยที่ไม่ต้องใช้พลังงานในการดูดซับสูงดังเช่นในระบบดั้งเดิมที่ใช้ของเหลวเอมีนเป็นตัวดูดซับ

ภาควิชา เคมีเทคนิค ลายมือชื่อนิสิต .....

สาขาวิชา เคมีเทคนิค ลายมือชื่อ อ.ที่ปรึกษาหลัก .....

ปีการศึกษา 2559 ลายมือชื่อ อ.ที่ปรึกษาร่วม .....

5672908723 : MAJOR CHEMICAL TECHNOLOGY

KEYWORDS: CO2 CAPTURE, CIRCULATING FLUIDIZED BED , CARBONATE ADSORBENT , MULTI STAGE ADSORPTION, COMPUTATIONAL FLUID TECHNIQUE

SUTTHICHAI BOONPRASOP: DESIGN OF CIRCULATING FLUIDIZED BED REACTOR FOR CARBON DIOXIDE ADSORPTION AND SORBENT REGENERATION. ADVISOR: PROF. DR. PORNPOTE PIUMSOMBOON, CO- ADVISOR: ASSOC. PROF. DR. BENJAPON CHALERMSINSUWAN, 183 pp.

Suitable height of the riser is a crucial design parameter for operating in circulating turbulent fluidized bed regime (CTFB). It was suggested to be lower than the maximum bed expansion. The hydrodynamics of the CTFB are similar to the conventional turbulent fluidized bed which has highly uniform solid fraction while particles can circulate throughout the system as the fast fluidization. The optimum sorption temperature was found to be 60 °C where the maximum CO_2 capture capacity was 295.79 milligram of CO_2 per gram of the sorbent which loaded by 17 percentage of K_2CO_3. The used sorbent could be regenerated by either heat treatment or depressurization. Thus, the lab scale circulating fluidized bed reactor was built to study the effect of the operating parameters. The positive trend of the increasing in gas velocity showed the promise trend for the commercial use. The sorption stages of the pilot scale were determined by computational fluid technique. The alternative design suggests a riser with 1 m in diameter and 3.55 m tall with cooling tubes being set to overcome the equilibrium limitation. The optimum cooling temperatures could provide more than 95% CO_2 capture of the inlet concentration. This riser does not need a large amount of energy for regeneration as conventional amine absorber.

Department:	Chemical Technology	Student's Signature .....
Field of Study:	Chemical Technology	Advisor's Signature .....
Academic Year:	2016	Co-Advisor's Signature .....

ACKNOWLEDGEMENTS

I would like to express my deepest gratitude for my supervisor, Prof. Dr. Pornpote Piumsomboon and Assoc. Prof. Dr. Benjapon Chalermsinsuwan, offered many helpful suggestions, supervision, and encouragement throughout past three and a half years of my research. They clearly respected me more than I respected myself. They trusted in me before I will put my trust in them. Because of their love and kindness, mistaken turn to be a great lesson.

I would like to acknowledge Prof. Dr. Dimitri Gidaspow who invested his precious retirement time with me for six months in IIT, Chicago. Learning with him, a great person who modernized chemical engineering is one of the best experiences in my life. A half century of working experiences of him gave me a missing jigsaw which innovatively elevated this thesis to be a patent in future.

I wish to express my thankfulness to Sakura Project which provided a full scholarship to work at Nagoya University, Japan for three months. In this place, I had found my best friends who shared happiness and sadness together. Sincerest appreciation also extends to the 100th Anniversary Chulalongkorn University Fund for Doctoral Scholarship for full financial support of this research.

The special thanks to Mr. Chompuphol Sanyonk who help me to design and construct the first apparatus for carbon dioxide sorption.

Finally, I wish to acknowledge my beloved mother, Nittaya Boonprasop who left me temporary and waiting for me in the good place. She was born in baby blooming period. She was recognized as an illiterate single mum who sent her only son to the elite university, Chulalongkorn university. The new knowledge which had been found and was written in this thesis is due to her scarification. Hopefully, she could see the successfulness of her parenting throughout this work from the good place.

CONTENTS

Page

Page

Page

List of tables

Page

Page

List of Figures

Page

Page

Page

Page

CHAPTER I
INTRODUCTION

1.1.Background

After the industrial revolution, coal is a major source of energy which supplies to serve various purposes of humanity. Thus, the major greenhouse gas, CO_2 have increased its content from around 280 ppm since 18th century [1]. Since the Kyoto protocol was signed in 1997, the COP21 has become the most recent and important international agreement to regulate greenhouse gas emissions country by country. This agreement reflects the urgency and high priority for the reduction of CO_2 to solve global warming [2]. The result of the enforcement of CO_2 capture and storage (CCS) technology has been adopted by a number of large industrial plants in developed countries [3-5]. Although the emission rate of CO_2 in developed countries has been decreasing, the global emission rate of CO_2 has still been drastically increasing [6]. Due to the report of National Aeronautics and Space (NASA), atmospheric CO_2 concentration drastically increases since 1950 and reaches about 415 ppm in late 2017 [7, 8], thus increasing the danger to humanity as the concentration of CO_2 could soon reach a critical concentration of 580 ppm [9, 10].

In the 21st century, the large sources of CO_2 emission: fossil fuel electric generator in those heavy industries such as steel, concrete and cement are the leading sources of CO_2 mission (42%). Other large sections are transportation (23 %) and industry (20 %) [11]. The various kinds of alternative energy, which have been integrated to smart grid, play a crucial role to reduce the load of coal power plants, but

the use of non-fossil fuel has slightly increased since 1971 from 86 % of fossil fuel and 14 % of non-fossil fuel to 82 % of fossil fuel and 18 % of non-fossil fuel in 2012 [12].

Therefore, carbon capture, utilization, and storage (CCUS) technology is an alternative method to reduce CO_2 emission rate by converting CO_2 to high valuable products instead of exhaust to the atmosphere [4, 6, 13]. The large portion of investment and operating cost of CCUS are caused by CO_2 capture processes [14].

The most famous commercialized CO_2 capture unit is amine liquid stripper by using mono ethanolamine (MEA) [15]. Since this process is costly process (15-30% of the investment cost and 15 – 20% of operating cost), it does not implement in the small and middle scale factories especially those in the developing counties [14, 16]. Due to the high energy requirement and capital cost, those units only have employed in the large scale factories which have been located in the developed countries where they have been to comply with Kyoto protocol and COP 21 such as, Japan, United states and Canada [17].

Actually, carbon dioxide can be captured by various methods such as, liquid absorption, membrane separation, and dry solid adsorption [18]. Sadly, the reasonable method, that have been used in the developed countries are too expensive and require such a high standard safety utilities to prevent amine contaminating the environment. The membrane separation is difficult for scaling up. So, dry solid adsorption becomes a candidate that is inexpensive, and applicable for developing countries.

High adsorption capacity together with fast adsorption rate of potassium carbonate supported on gamma alumina ($K_2CO_3/\gamma\text{-}Al_2O_3$) is claimed to be an alternative method to improve dry adsorption process instead of stripper unit with liquid amine

which is high toxicity on the environment. Capturing of carbon dioxide by solid sorbent obeys chemical equilibrium as shown in equation (1).

$$K_2CO_{3(s)} + CO_{2(g)} + H_2O_{(g)} \leftrightarrow 2KHCO_{3(s)} + \Delta H \quad (1)$$

In the presence of one mole of water vapor, one mole of K_2CO_3 can adsorb one mole of CO_2 and can form two mol of potassium bicarbonate ($KHCO_3$). The adsorption reaction occurs under the atmospheric pressure with respect to the exothermic chemical equilibrium reaction as shown in the equation [18].

Heat regeneration (conventional method) is a primitive design for temperature swing adsorption unit. Application of energy can reverse the equilibrium as shown in equation (1). $KHCO_3$ then converts back to K_2CO_3 by releasing CO_2 which will be compressed and kept in the storage. The conventional method is classified as high energy intensity process because it requires high temperature (200 - 350 °C) and long regeneration time (30 - 90 minutes) to complete the target regeneration process. Formation of high thermal stability which occurs by the side reaction, potassium dawsonite compound ($KAl(CO_3)_2(OH)_2$), consumes more energy than $KHCO_3$ to convert back to K_2CO_3. Even, Dawsonite can be prevented by hydro treatment or multiple impregnation method, the conventional regeneration by itself, is difficult to scale up to reach the load of power plant.

Based on the chemical equilibrium in (1), the system maintains the pressure by shifting the equilibrium backward when depressurization is applied. Therefore, depressurization will be an alternative way to regenerate the sorbent. The expected advantages of this alternative method are short regeneration time and homogeneity of

sorbent after passing the regeneration without the need to use the high energy for regeneration.

Figure 1 shows the new CO_2 capture system concept. Flue gases at 55 °C are introduced into the sorber-riser at a velocity of 1 m/s. The heat of sorption is removed with water cooled tubes. The major portion of the heat of sorption can be used to regenerate the sorbent as shown in the cooling water loop which the flow rate is controlled to maintain the temperature in the range of 50 to 60 °C. The colors in Figure 1 show the temperatures inside the riser. The red color represents 60 °C, the green is 40 °C and the blue is 20 °C. Due to the equilibrium limitation, the sorbent has to be cooled to adsorb CO_2 at the low concentration. In a downer, the sorbent will be regenerated by heat from hot cooling water and heat from cooling the flue gas from 100 - 130 °C to 55 °C. Park *et al.* apparently used multiple circulating fluidized beds to accomplish the CO_2 capture [19]. Combining and optimizing these three important system components which are sorber-rier, separator-cyclone and regenerator-downer in one reactor is a major task to develop a circulating fluidized bed reactor for using in the industries.

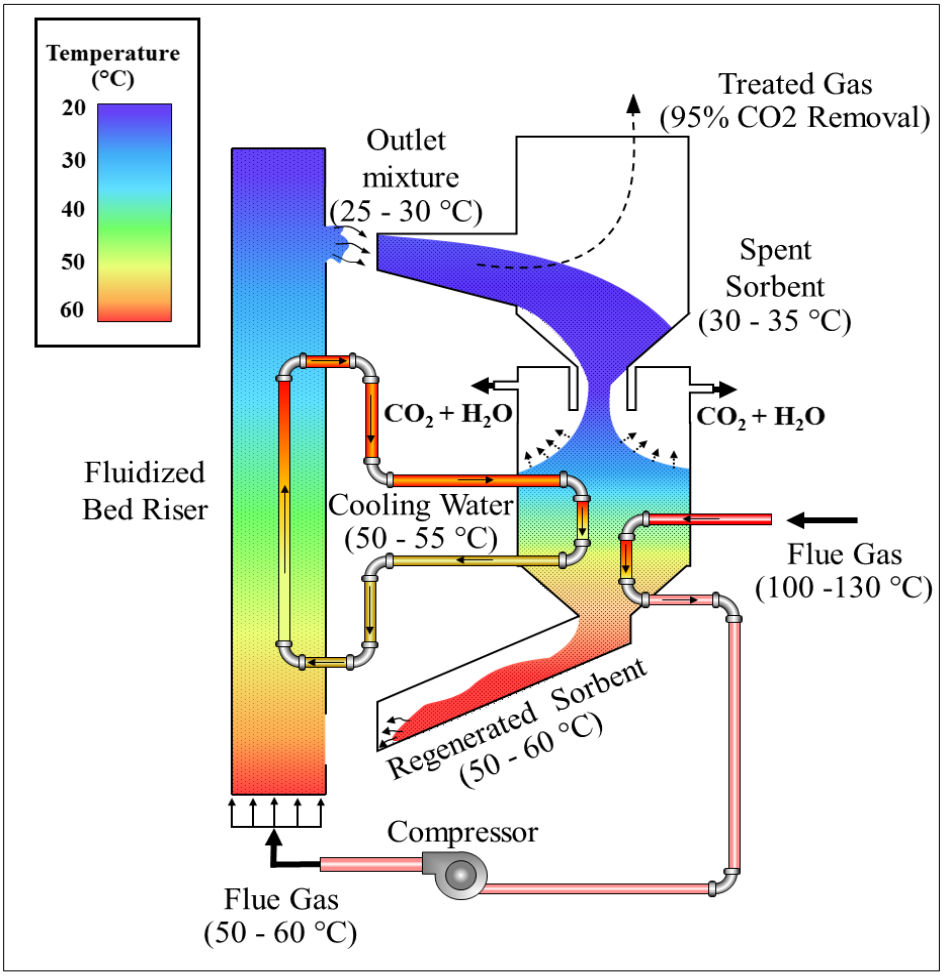

Figure 1 CO_2 capture system with heat utilization system based on CFD design

1.2. Objectives

1.2.1. To study the effect of carbon dioxide regeneration process on the performance of carbon dioxide adsorption and regeneration using solid sorbent

1.2.2. To design the circulating fluidized bed reactor for carbon dioxide adsorption and regeneration using solid sorbent

1.2.3. To optimize the operating parameters for carbon dioxide adsorption and regeneration using solid sorbent in the circulating fluidized bed reactor

1.3. Scope of dissertation

1.3.1 Determine the optimum operating condition for CO_2 sorption in turbulent fluidization regime.

1.3.2 Investigate suitable regeneration processes which has high carbon dioxide adsorption.

- Heat by heating coil/heater.
- Depressurize by diaphragm pump.

1.3.3. Design circulating fluidized bed reactor (laboratory scale).

- Investigate the circulating fluidized bed reactor design.

1.3.4. Optimize the operating parameters for carbon dioxide adsorption and regeneration using solid sorbent in the circulating fluidized bed reactor.

1.3.5. Design the circulating fluidized bed reactor (pilot scale) using computational fluid dynamics (CFD).

- CO_2 capture in multistage circulating fluidized bed reactors.
- CO_2 capture in a riser with multiple cooling section.
- Sorbent regeneration downer using waste heat from flue gas.

CHAPTER II
THEORY AND LITERATURE REVIEWS

2.1. Adsorption

Adsorption is occurred by contacting of a solid with a fluid (liquid or gas). One or more components can be attached on the adsorbent surface. The common uses of the adsorption are in purification processes. The sorbents are also known as a "filter" which employ in water or air in purifications. The adsorption is a physical phenomenon when the size of the target component is fit with the pore size of solid particle. Due to the weak attractive force, the physical sorption does not use any additional energy for removing the target component but the process takes a long time. Moreover, selectivity of physical adsorption is quite low.

Industries are more familiar with another kind of adsorption process which called "sorption". The sorption is characterized by capturing the target component via a specific chemical reaction. Therefore, the sorption can overcome the limitation of selectivity. The performance of sorption is mainly determined by the activity of the sorbent. Acidity is the most common property which can be used to screen out the potential sorbent.

In this study, the target component is CO_2 which is considered as acid. The CO_2 sorption can be easily explained as the neutralization process with the basic sorbent. Amine and carbonate of metal group I are considered as a promising basic sorbent for commercial scale. Both can capture CO_2 at the low temperature with the presence of water which is suit for post-combustion CO_2 capture.

Based on the safety, the carbonate of metal group I is more environmental friendly than the amine which is considered as a carcinogen. Due to the great availability, K_2CO_3 and Na_2CO_3 meet the criteria. Thus, understanding the mechanism of CO_2 sorption is the first and the most important step to study the new design of a circulating fluidized bed reactor for CO_2 sorption using solid sorbent.

2.1.1. Sorption models

The explanation for the work of sorbents is quite similar to the heterogeneous catalysts. The target component diffuses from the bulk gas through the gas film to react with active solid component on the sorbent surface as shown in Figure 2. The thickness of the gas film is considered as the mass transfer resistance. There are two conventional ways to reduce this resistance which are increasing in velocity of the bulk gas and decreasing the sorbent diameter.

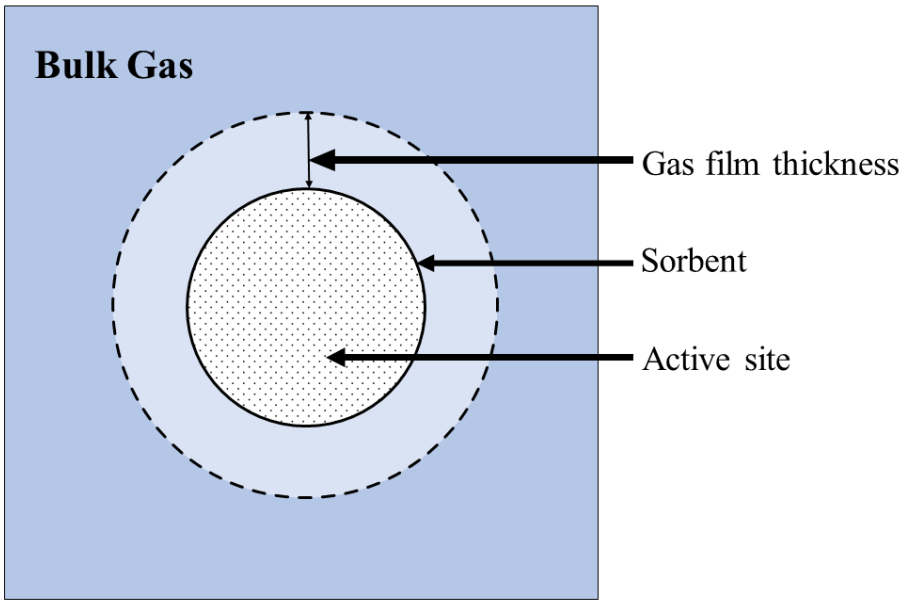

Figure 2 Gas sorption model

Another resistance of the sorption process is determined by the kinetic of the reaction between CO_2 and the active solid phase, carbonate of metal group I (M_2CO_3, M is metal group I). The sorption reaction is obeyed by the exothermic equilibrium reaction as shown in equation (2).

$$M_2CO_{3(s)} + CO_{2(g)} + H_2O_{(g)} \leftrightarrow 2MHCO_{3(s)} + \Delta H \quad (2)$$

The overall rate of reaction is presented as an effective rate constant which includes the rate of mass transfer and the rate of sorption reaction as shown in (3).

$$\frac{1}{k_{eff}} = \frac{1}{k} + \frac{1}{k_{mass}} \quad (3)$$

where; k_{eff} is the effective rate constant,

k is the rate constant of sorption reaction,

k_{mass} is the rate of mass transfer through the gas film.

Onischak *et al.* employed the CO_2 sorption in the rectangular duct which was packed with Na_2CO_3 and K_2CO_3 on the duct bottom [20]. Their kinetic study demonstrated that the k varied with sorption condition. The k of K_2CO_3 was higher than Na_2CO_3. However, the rate constants were in the same order of magnitude. The concentration profile of CO_2 could be used to determine k_{eff}. Figure 3 shows an example of the breakthrough curve for CO_2 concentration profile with the length of the duct sorption reactor. The concentration of CO_2 was dropped along the length and then

became constant due to the equilibrium as shown in Figure 3. k_{eff} is approximated by the equation (4) [21].

$$k_{eff} = \frac{\Delta C}{C} \cdot \frac{v}{L} \tag{4}$$

Where; L is the shortest length that CO_2 is constant,

v is gas velocity,

ΔC is the difference between the inlet and outlet CO_2 concentrations,

C is the average concentration between inlet and outlet of each stage.

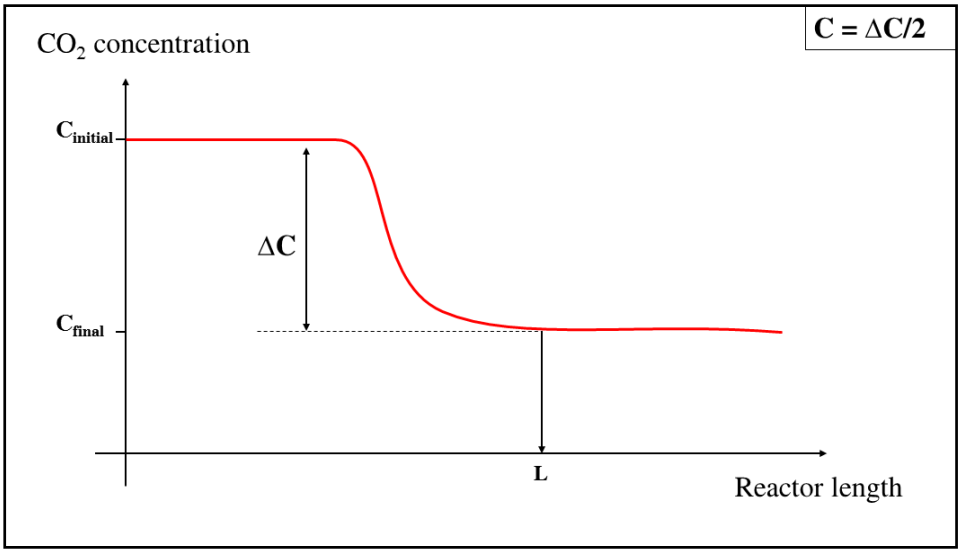

Figure 3 Breakthrough curve for CO_2 sorption

After obtained k from the experiment and k_{eff} from the approximation, solving equation (3) will give k_{mass}. The calculation shows that k is greater than k_{eff} for two

order of magnitude. Therefore, the rate limiting step of CO_2 sorption using carbonate of metal group I is mass transfer limitation.

2.1.2. Regeneration

Figure 4 shows the well-known sorption process which composes of two adsorption vessels. The sorption will be performed in only one vessel (vessel number 1) for a certain period of time. Then, the sorption will be switched to another vessel while the temperature in vessel number 1 is increased for regeneration. The alternate sorption and regeneration between the 2 vessels is the conventionally continuous process. It is called the temperature swing sorption for the CO_2 capture using solid sorbent.

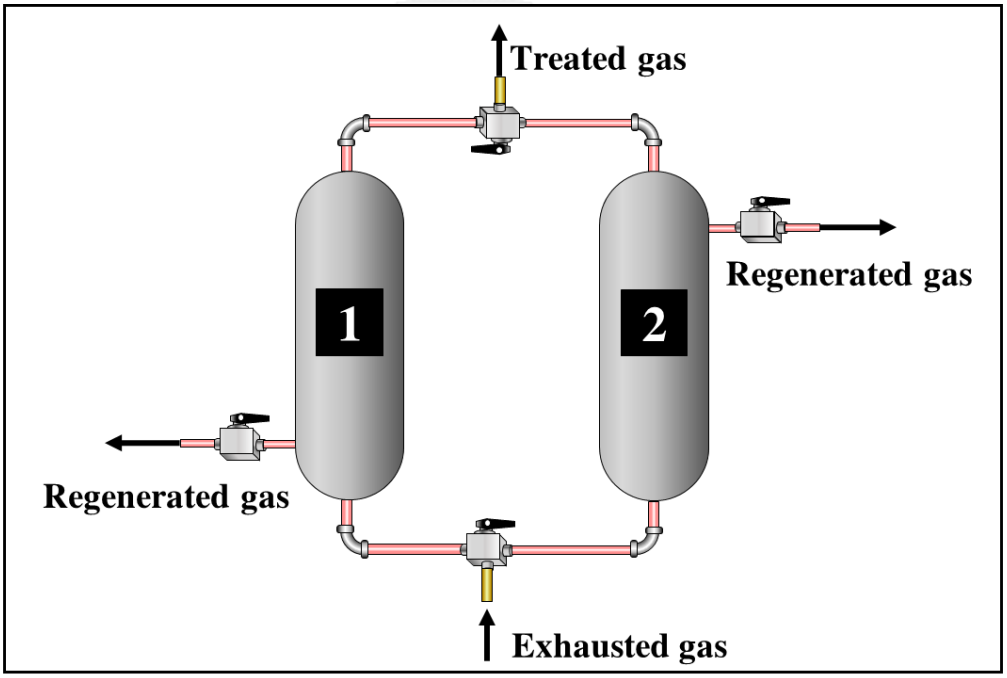

Figure 4 Temperature swing sorption unit [14]

2.1.2.1. Temperature swing

The application of heat into the spent sorbent is the conventional regeneration process. Due to the physical phenomenon, the raise in temperature will increase the kinetic energy of the gas molecule. The high kinetic energy molecules can easily escape from the pore of the sorbent, then the spent sorbent become active again.

The heat regeneration can consider as the chemical process especially for the spent at sorbent from CO_2 sorption. Equations (1) and (2) show that the heat will release after the sorption due to exothermic equilibrium. This heat which obtained from the sorption is about one third of the heat from the coal combustion [14]. Due to the exothermic equilibrium, the application of heat can increase the backward rate of reaction. Therefore, potassium bicarbonate can convert back to potassium carbonate.

The range of regenerating temperature of K_2CO_3 is an issue which is waiting for the discussions. Some of the researcher showed that the regeneration temperature should be higher than 200 °C but some results showed that the regeneration should be as low temperature as 60 °C due to the equilibrium. Focusing on the sorbent preparation, the higher regeneration temperature was found in the sorbents which was prepared by the impregnation on the support gamma alumina. Another group of sorbent which was employed at the low regeneration temperature, was the use of pure carbonate sorbent or mixing carbonate with alumina at a certain ratio. Due to the fast rate of reaction, the clear mechanism for the CO_2 sorption using carbonate sorbent still unclear.

2.1.2.2. Pressure swing

Depressurization is an alternative method for regeneration. The short regenerating time and high homogeneity to the regenerated sorbent are the benefits of using depressurized regeneration. However, this entire regeneration energy is depend on electricity while the heat regeneration, some of regeneration energy can be utilized from the waste heat which was obtained from the exhausted gas. Therefore, the comparison between the conventional and the alternative regeneration is required.

Equation (2) shows that a mole of carbonate compound, a mole of CO_2 and a mole of water is reduced after the sorption process to form two moles of solid potassium bicarbonate. The equilibrium will shift backward to increase the pressure in the system when the pressure is reduced by the vacuum pump. Therefore, the bicarbonate is also converted to be the carbonate as mentioned in the pressure swing regeneration.

2.1.3. CO_2 Capture concepts

State of the art of CO_2 capture technologies for existing fossil energy power plants are limited to amine absorbers [22]. They have been used for removal of CO_2 from natural gas for decades. The continuous CO_2 removal up to 90 % could not be achieved due to reaction equilibrium [23]. The regeneration of these solvents consumes 15 to 30 percent of the energy of the power plant due to the use of produced steam. Furthermore, for a conventional coal fired 329 MW plant [24], it requires 4 absorber columns, 8.8 m diameter and 24.0 m height. The stripper will have a diameter of 4.9 m and a height of 22.9 m. The heights are large due to low rates and low diffusion coefficients in liquids.

The solid potassium carbonate and sodium carbonate sorbents developed at IIT by Onischak and Gidaspow [25, 26] and at RTI by Nelson *et al.* [23, 27] both showed

the high sorption rates of using solid sorbent. The effective rate constant for CO_2 sorption was as high as 10 reciprocal seconds. Such high rates lead to much shorter columns. The sorbent carbonate of alkali metal group I which is prepared by the impregnation method is one of the promise sorbent due to suitable textural properties, good physical properties and high thermal stability [28]. Moreover, the sorbent preparation can be modified by calcination to improve both sorption and regeneration properties [29]. Normally, CO_2 adsorption exhibits two routes, the first forming $MHCO_3$ and latter, a few amount $MAl(CO_3)_2(OH)_2$ compound which M is group I alkali metal [28]. Excellent regeneration properties can be obtained when $KHCO_3$ is the only component formed [29]. Zhou *et al.* suggested that $MAl(CO_3)_2(OH)_2$ compound formation could be eliminated by hydrotreatment to obtain $K_2CO_3.1.5\ H_2O$ phase before entering the sorption [18, 30]. The regeneration properties of K_2CO_3 sorbent, such as adsorption capacity after multi-cycles adsorption, less regenerative energy and short time regeneration, have been shown to be improving continuously by many researchers [3, 31-34].

There are several kinds of reactor to remove CO_2 from flue gases using alkali metal group I carbonate sorbents such as bubbling fluidized beds used at RTI [35], batch turbulent fluidized beds used in Thailand [36, 37], circulating fluidized beds used in Korea [19, 38] and moving beds [39]. There are also a couple ways to regenerate the sorbents which are the application of heat and depressurization treatments [14]. However, reducing the pressure requires additional electrical energy for a vacuum compressor besides the energy needed for a compressor to circulate the sorbent. An alternative method is to utilize heat recovered from sorption reaction which was considered to be one third of the heat of combustion together with the waste heat from

the power plant. Kongkitisupchai and Gidaspow have also shown that one sorption stage is insufficient to remove 90 % of CO_2 in flue gas due to equilibrium limitations [14]. Park *et al.* have patented the idea of using multi-stage CFBs for CO_2 capture process [19].

2.2 Fluidization

Fluidization is the phenomenon that the solid (particle) behave like fluid for example it can flow from high pressure to the low pressure and the segregation of solid bed from high density to low density is observed. The fluidization have been employed in the miner industrial to separate the high value metal from the rocks.

Fluidization had been modernized in the world war II era. United States technologist tried to increase the fraction of gasoline in the refinery process which mainly depended on domestic petroleum crude oil. Fluid catalytic cracking (FCC) used the heterogenous catalyst to cut the chain of hydrocarbon molecules to a shorter molecules. Moreover, FCC which had been employed in a batch process could not improve availability of gasoline. Therefore, the development of a circulating fluidization system had been used for the continuous FCC unit.

The experiment data in fluidization study introduced the branch of pure science which was the multiphase flow operation. The complexity of the new subject is due to the combination of the classical mechanic of Newton with the partial differential equations. Thus, most of the equations which had been used to explain the particle behavior was obtained from the experiment. The different behaviors of the multi-phase flow was called regimes which dominated the design of the heterogenous reactor for several decades.

Due to some pro and cons in each fluidization regime, the fluidization regime study is the next important step for the new design of CO_2 sorption. Selection of the appropriate fluidization regime leads to the high performance compact unit.

2.2.1 Fluidization CFD History

The computational fluid dynamics (CFD) fluidization design of this study, sorber-regenerator for the capture of carbon dioxide (CO_2), is historically based on the early research of Roy Jackson [40, 41] and papers with Anderson and Jackson [42], Sinclair and Jackson [43], Hrenya and Sinclair [44] and others as reviewed in Roy Jackson's book [45]. Based on the paper published by Sinclair and Jackson [43], the designers of oil refineries (Reza Mostofi [46], Gidaspow [47]), developed the new technique to measure catalytic cracking (FCC) particle concentration distributions in a circulating fluidization using gamma ray densitometers. They found that the FCC particle concentrations in their risers were dilute in the center and dense at the walls. Such a flow regime was called the core-annular flow regime in multiphase flow [48]. Until the publication of Sinclair and Jackson's paper [43], the oil industry believed that the core-annular flow occurred only in small diameter risers found in universities. In 1988, the explanation of the velocity distribution in a large riser diameter used in EXXON Company and the small riser used in the IIT laboratory was an initial step to modernize the method for multiphase computational fluid dynamics codes to design fluidized bed reactors with reasonable confidence to flow regimes. For fluidized bed reactor design, Breault [49, 50], Chalermsinsuwan *et al.* [51], Kashyap and Gidaspow [52, 53] and others explained the fifty year old puzzle of the low Sherwood and Nusselt numbers in fluidized beds. They are below the theoretical limit of two due to the

formation of particle clusters in risers. The chapters in the recent book edited by Pannala *et al.* [54] showed the change in paradigm that had taken place in this field when compared to those papers in "Fluidization", edited by Davidson and Harrison [55].

2.2.2. Fluidization Phenomenon

Figure 5 exhibits the free body diagram of a particle in a space where occupies by the upward gas flow. The downward force weight of the particle is due to the gravity. The up thrust is the summation between force which are drag and buoyancy. The upward forces are shown by the steamlines as shown in Figure 5. At a certain velocity, the up trust is greater than the weight, the particle then can move against the gravity as fluid which their motion is dominated by the pressure gradient. The fluid behavior of solid particle is called fluidization which is the concept that used in various kind of industries.

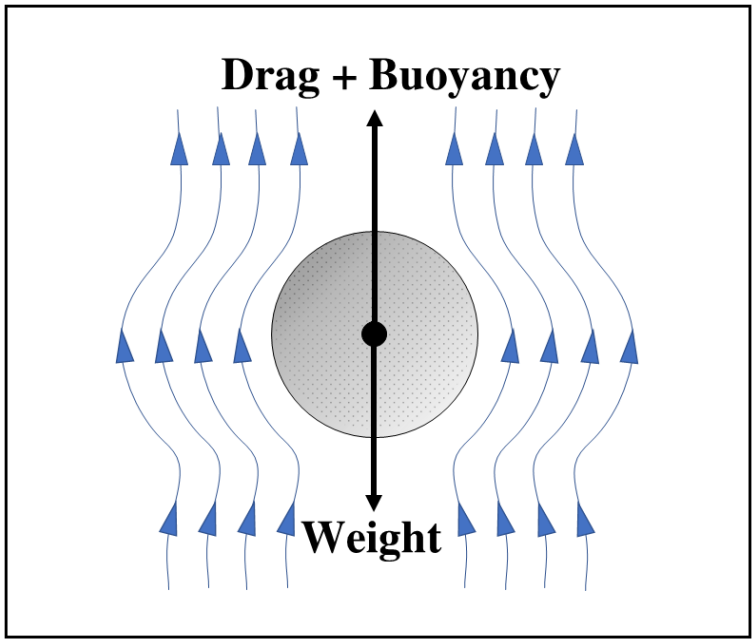

Figure 5 Free body diagram of particle

The types of gas and particle have highly affected to the shape of the steamlines which resulted on the up thrust. Roughly, classification is due to the densities of gas and solid particle and the particle diameter. In 1973, Geldart proposed the scientific concept for the particle classification as shown in Figure 6 [56].

Group C is the group of extremely fine particles which has high cohesive force. The size of the particle is ranging from 20 to 30 μm. Due to the strong cohesive force, the particles are hardly to fluidize. Group A is a particle in the range between 20 and 100 μm, and the density is typically less than 1.4 g/cm^3. Most catalyst powder is classified in this group. These bed particles can expand by the increasing in gas velocity. Group B is the particle size between 40 and 500 μm and the particle density between 1.4-4 g/cm^3. The carbonate sorbent is located in this group. This group typically forms the gas bubble immediately at incipient fluidization. Group D is the group of the large particles with the diameter greater than 600 μm and typically have high density. Fluidization of this group requires such a high gas velocity to overcome the weight of of the partcles.

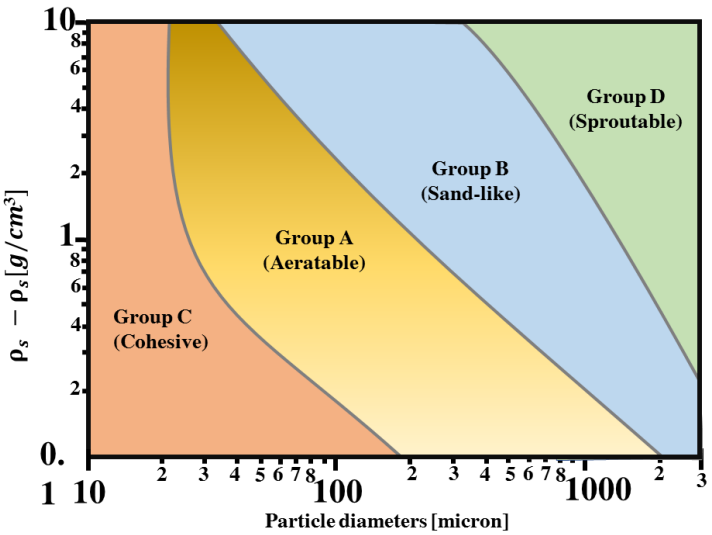

Figure 6 Geldart classification [56]

2.2.3. Conventional fluidization regime

Due to the good mixing property between gas and solid phase, fluidization is a concept which have been widely used in many applications such as combustion, heterogenous reactor (FCC), drying, gasification and fast pyrolysis [57-60]. The interaction between gas and solid phase or the transient flow behavior called regimes determine the advantage of high heat and mass transfers. The fluidization regime can be changed by adjusting the superficial gas velocity (U_g) [61].

The regime development is shown in Figure 7. At the low U_g, the system cannot develop the up thrust greater than the weight of the individual particle. Therefore, the solid bed is still stand with the maximum packing capacity which is determined by ratio of the solid volume in the system to the total volume of the system. Generally, the maximum packing capacity of solid particles is about 0.63 [51, 62-65]. Consequently, the gaseous phase is flown through the void between the particles. The fixed bed is terminated when U_g is equal to the minimum fluidization velocity (U_{mf}) which the up thrust is greater than weight of the particle.

Bubbling fluidized bed regime is performed when the U_g is increased to minimum bubbling fluidized bed (U_{mb}). For the Geldart group B particles, U_{mb} can consider to be the same as U_{mf} but in The Geldart group A, U_{mb} is about 1 to 2 times greater than U_{mf}. In this regime, the accumulation of gas is formed above the gas distributor and then the flow in the vertical direction as shown in Figure 7. The application of this regime is in the mine industries which use to separate the high value metal from the rocks. The number of the bubble depends on the type of the distributor and the magnitude of U_g.

Increasing the U_g, the bubble are disappeared and the solid particles move randomly in every direction as shown in Figure 7. This velocity is defined as the critical velocity (U_c) which considered as the final stage of bubbling fluidization and the beginning of turbulent fluidized bed. This is characterized by the great mixing property but it can apply in the batch processes [66]. The development of U_g causes the bed expansion into the vertical direction. The expansion can easily explain by the increase of the distance between the particles. Therefore, the solid volume fraction decreases when the bed is expanded.

The continuous process is employed by performing fast fluidized bed regime (circulating fluidized bed) [67-70]. This application begins when the U_g is set higher than the transport velocity (U_{tr}) which is considered as the final stage of the turbulent bed. The fast bed regime is characterized by S-shape on both the pressure and solid volume fraction profile along the vertical direction [71, 72]. The concern of using this regime is core annulus formation which can be monitored by low solid fraction (< 5% of the riser volume) at the middle of the riser as compared to the high solid volume fraction at the wall regions (estimated to be about 20% or higher as compared to the riser volume) as shown in Figure 7. The unique characteristics of fast fluidized bed leads to poor mixing property in the riser. Therefore, the riser which is used in the industries are designed with such the high height to compensate its poor mixing properties.

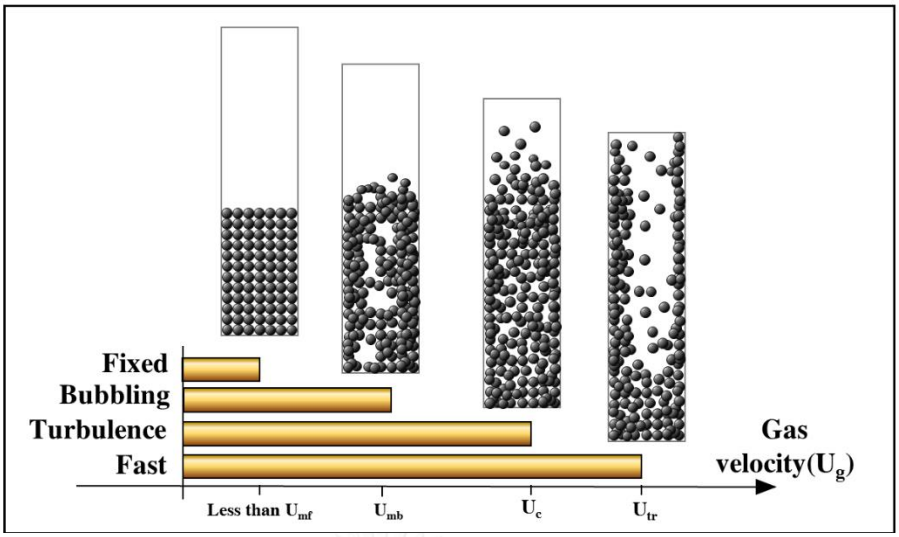

Figure 7 Conventional fluidization regimes [68]

2.3 The numerical method

Due the competition in space program between the Soviet Union and the United States to send the first human into the space, the numerical method had been developed for solving the partial differential equation in the multi-phase flow equations during the turbulent flow at the escape velocity. The precision of the numerical method revealed the safety returning flight of the Friendship 7 spacecraft at the exactly predicted location in the southeast of KSC in the vicinity of Grand Turk Island.

At the beginning of NASA, the iterative calculations had been considered as a kind of the labor job which were handled by colored mathematician department. The first generation mainframe computer invented by IBM that could calculate 240,000 iteration per second almost lid the job of the colored mathematicians. Dorothy Vaughan transformed her position from mathematicians to be the first programmer who was expert in Fortran card code which improved the accuracy of the numerical method to the next level. Since the successful mission of the Apollo 13, the numerical method

using Fortran code shifted the paradigm of applied science. The new numerical schemes had been proposed to solve governing equations and constitutive equations. Therefore, numerical methods have become one of the most important subject in engineering world.

The improvement of the personal computer, modernized the complex Fortran code into the more user friendly program. Simulation program becomes such a common engineering tool. Understanding the numerical method tailors the simulation program to construct the alternative design for CO_2 sorption in a circulating fluidized bed reactor. The validated model computed by the simulator can reveal the real performance and the costs of the new design which provide the fair comparison with the conventional liquid absorber.

2.3.1. The finite volume method

The finite volume method (FVM) is a discretization technique which transformed partial differential equations which derived by Physics laws, especially conservation of mass, energy, and momentum to the sets of algebra equations. FVM defines the volume of the interested space and then solve the problem with a partitioned volume. FVM is commonly used with the computational fluid dynamics (CFD).

Figure 8 is a diagram which explains the concept of FVM in the CFD. The calculation domain can be the volume in case of 3-dimensional model or the area in case of 2-dimensional model which are the space where is occupied by the multiphase flow. Area is divided into a small cell with triangle shape at the first step. The boundary conditions send the input to the adjacent calculation. The equations will be solved simultaneously in each cell. The results in the cell will be used as the boundary

condition to the next contacting cells. The calculations then march out through n cell of the calculation number until the last cell of the calculation domains.

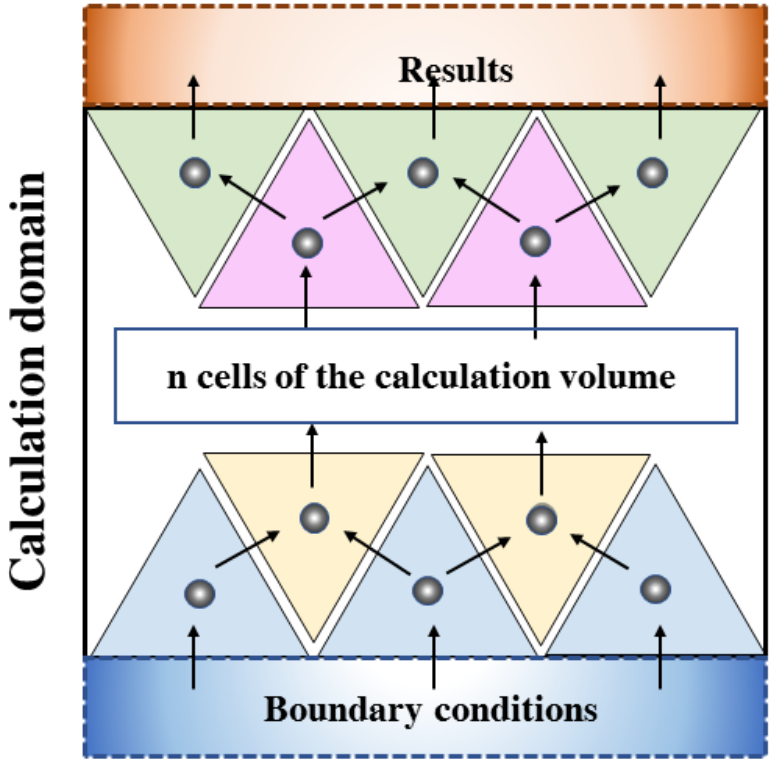

Figure 8 Compuational fluid dynamics concept

The obtained results are the important parameters which always measure in actual unit such as solid volume fraction, velocity, temperature and concentration of the substance in the mixture. Solid volume fraction is one of the most important parameters in the multiphase flow study. The actual solid volume fraction requires such an expensive and dangerous measurement technique similar to the x-ray which uses in the hospital. In contrast of FVM, only conservation of momentum is required to determine the fraction of the solid that occupied the space in each cell. The integration of the results of the cells within the calculation domain can be presented as the solid volume

fraction contour as can be seen in Figure 9. The output solid volume fractions are used as the initial condition of each cell for next time step. Compiling the results of each time step, the dynamics behavior of solid volume fraction is revealed the cluster formation as shown in the enlarge section of the riser top of Figure 9.

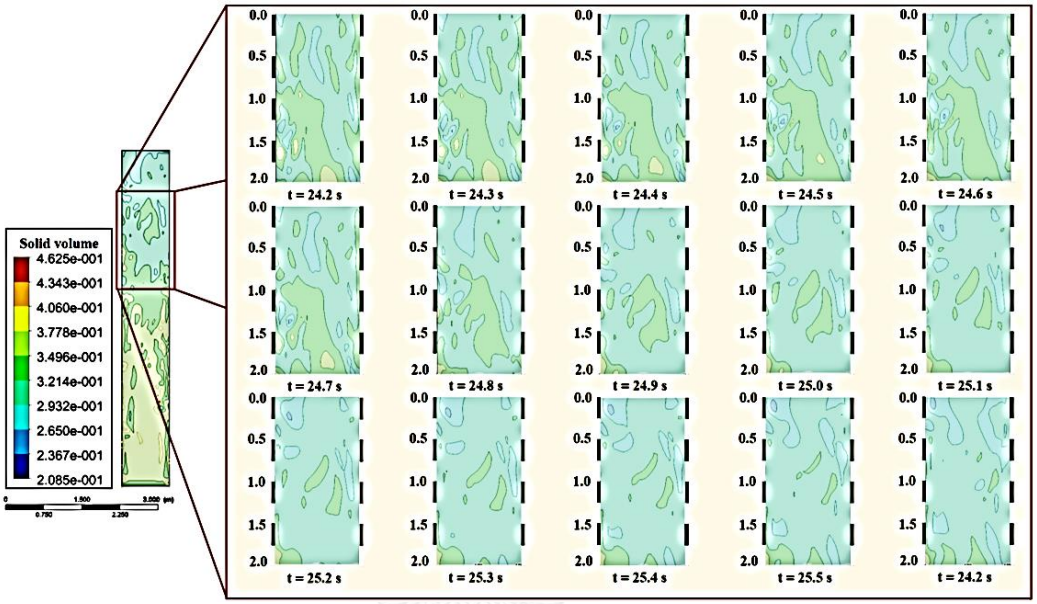

Figure 9 Cluster development

2.3.2. Grid refinement study

The size of calculation cell has highly affected on the output results. The smaller size of the cell provides the higher resolution. Therefore, grid refinement study is the first and the important step for FVM. The calculation domain is divided into the various sizes of cells (mesh) as shown in Figure 10. Normally, the mesh number can start from the certain specific number and can double it for the next trails of the simulation. The objective of the grid refinement study is to determine the minimum mesh number that the output will be the same as the results obtained from the higher mesh.

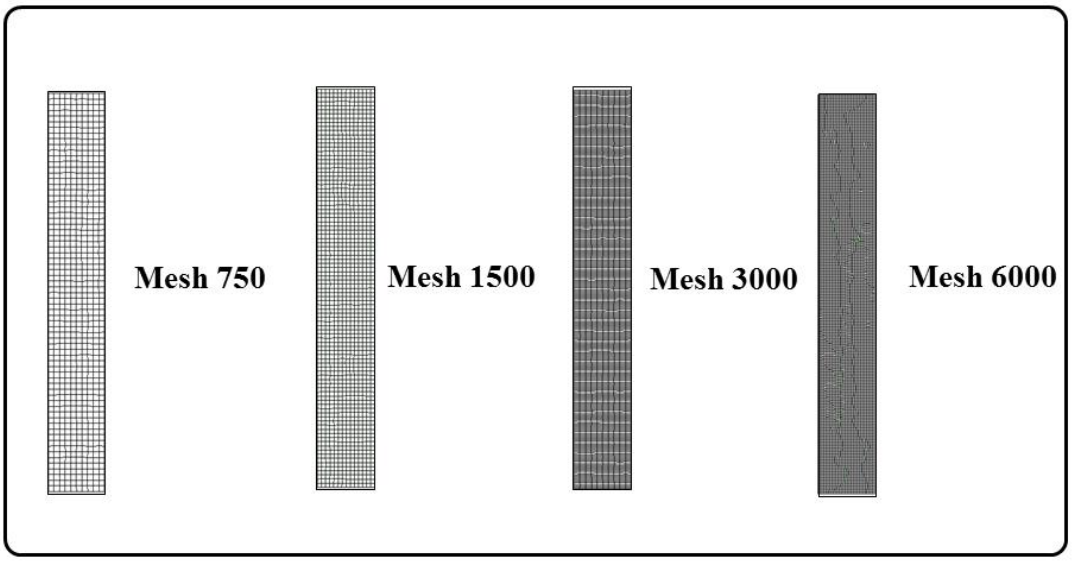

Figure 10 Grid refinement study

2.3.3. **Discretization**

Discretization is the method that was developed by mathematicians to convert the set of partial differential equation to be algebraric equations. The most well known method is Euler and Newtons-Ralphson method. Then, the algebra equations are solved numerically by the integrative calculation. Numerical scheme is the tools that is used to deal with the millions of the iterative calculation. There are the common set of the numerical scheme used in such as first or second order upwinds and QUICK. FLUENT version 17.0 is the computational program that employs discretization with the selected numerical scheme. The mathematical codes are covered by the user-friendly interface. The residual from each iteration is presented during the simulation as shown in Figure 11. If the residual is not in the acceptable reason, the grid refinement, discretization and numerical scheme will be revised by the user.

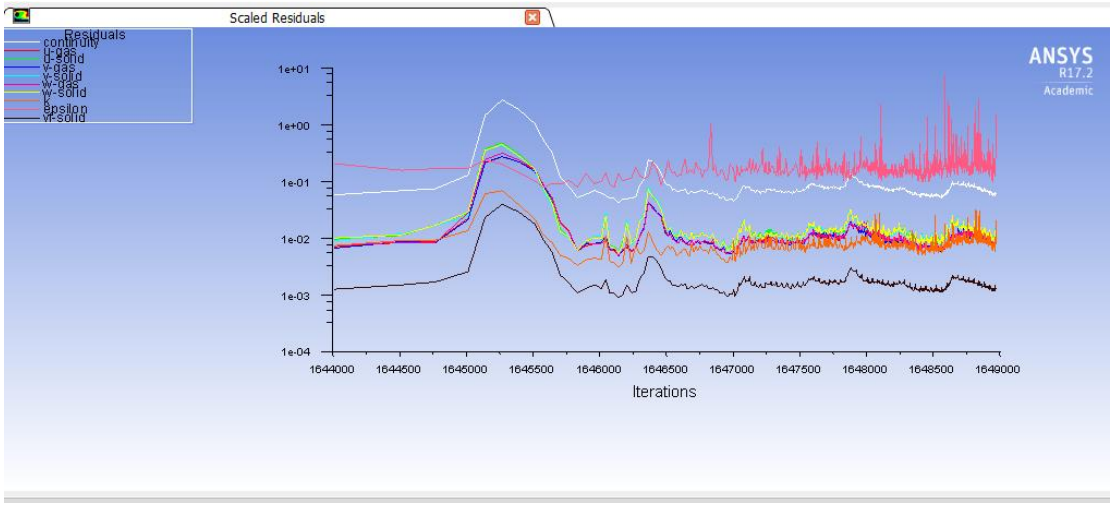

Figure 11 Residual of the iterative calculation

2.4 Literature reviews

Potassium carbonate is an inexpensive reagent to impregnate on the support [18] Based on the availability, pricing and physical properties, alpha (α-) and gamma (γ-) alumina (Al_2O_3) were widely used as supporting materials. Potassium carbonate supported on gamma alumina (K_2CO_3/γ-Al_2O_3) performed with higher capture capacity than potassium carbonate supported on alpha alumina ($K_2CO_3/\ \alpha$-Al_2O_3) [29]. In addition, K_2CO_3/γ-Al_2O_3 that had higher surface area than was more practical than $K_2CO_3/\ \alpha$-Al_2O_3 that had low surface area. A number of literature studies presented the modification method to further improve the regeneration property of K_2CO_3/γ-Al_2O_3.

Calcination temperature affected an inactive metal ($KAl(CO_3)(OH)_2$) that formed during carbonation. Increasing calcination temperature made K_2CO_3/γ-Al_2O_3 more homogenous crystallinity which could prevent the occurrence of inactive metal [73]. High basicity of solution in impregnation procedure was importance to the homogeneity of K_2CO_3/γ-Al_2O_3. Therefore, adding NaOH in the solution provided the

solid sorbent that could be used in many continuous cycles similar to increasing calcination temperature [37]. From the characterization, it showed that $KAl(CO_3)(OH)_2$ was occurred at the edge of deflected crystalline structure. Bubbling carbon dioxide gas into K_2CO_3 solution during the impregnation procedure converted K_2CO_3 locating at deflect structures to $KHCO_3$. Thus, the possibility of producing $KAl(CO_3)(OH)_2$ (Dasownite) during the adsorption was reduced [74]. Impregnating polyethyleneimine ($H(CH_2CH_2NH_2)nNH_2$) and K_2CO_3 on γ-Al_2O_3 performed an outstanding sorbent that had high capture capacity as the conventional impregnation preparation and had high regeneration property as the sorbent from the modification methods [75].

Understanding the effect of operating parameters on both adsorption and regeneration was important to develop continuous reacting system which can be used instead of amine stripper [76]. From the literature, the suitable adsorption temperature was found in the range of 60 to 70 °C [18]. The excess water in mixed gas caused the side reaction which gave $K_2CO_3 1.5H_2O$ as the intermediate. This intermediate lead the adsorption reaction to occur faster than the one in equation (1) and (2) [77]. Also the literature revealed the possibility that depressurization by vacuum fan could regenerate the used sorbent [14]. The high homogeneity of regenerated sorbent was an outstanding advantage of depressurization process than the thermal process. Although there were a lot of studies on adsorption and regeneration processes, dry sorbent still have not applied in the industry. Therefore, the study of continuous circulation fluidization was prioritized in order to use this processes in the real industry.

Due to the good mixing property, gas-solid particle fluidized beds have been widely used in the industries, such as coal combustion, fluid catalytic cracking, drying

and gasification [57, 58]. Inside the system, the advantage of high heat and mass transfers depends on transient flow behavior called regimes [78, 79] which can be changed by adjusting superficial gas velocity [61] and solid particle circulation rate. Bubbling and turbulent fluidized beds are the conventional fluidized bed regime which is always applied in batch processes at low U_g [80, 81]. Application of fluidization in continuous processes begins when U_g is higher than the highest velocity which solid particles can remain inside the reactor called transport velocity (U_{tr}) [67, 82]. The system performing with fast fluidized bed regime (in circulating fluidized bed) shows solid particle recirculation between riser and downer sections with the "S-shape" solid volume fraction profile in vertical direction and the core annulus solid volume fraction profile in radial direction [69, 83]. Limitation of those reactors is affiliated by the unique characteristics of hydrodynamics in each fluidization regime.

As a result, a large number of literature studies tried to explore the new fluidization flow patterns inside the system [70]. High-density fluidized bed [84-86] dense suspension up flow [87], and circulating turbulent fluidized bed (CTFB) [88, 89], were investigated as new fluidization regimes in the last decade. Focusing on CTFB, the uniform and high solid concentration along the riser height as turbulent fluidized bed with solid circulation from riser to downer sections as fast fluidized bed and no core annular were observed [90]. In the literatures experimental study, the circulating turbulent fluidized bed was composed of bubbling fluidized bed at dense phase region at low riser height and fast fluidized bed at high riser height above secondary feed gas injection [91]. Then, the gas-solid particle behavior in dense phase and dilute phases were extensively studied. Particle-particle interaction dominated dense phase region but dilute phase region was dominated by interaction between gas

and solid particle [92]. Contact efficiency in CTFB was higher than high density fluidized bed which means that the CTFB reactor had better performance under the same conditions. This provided an alternative to operate fluidized bed reactor with higher performance [93, 94]. Secondary feed gas injection provided the good advantage in circulating fluidized bed boiler in order to operate the system for completely combustion [95]. Selectivity of oxidative hydrogenation of ethane to ethylene was increased by adding secondary feed gas injection [96]. The circulating fluidized bed incinerators with secondary feed gas injection could operate at low temperature which lead to less emission of heavy metal [97].

On the other hand, secondary feed gas injection might affect reactant concentration, kinetic of the reaction and temperature distribution which is leading to poor conversion in some chemical reactions. Therefore, a circulating fluidized flow pattern with high solid concentration in single gas feed injection should be studied. Besides, the computational fluid dynamics result of Chalermsinsuwan *et al.* examined transient flow behavior of gas-solid particles in 2-dimensional fluidized bed reactor with single feed gas. Their results showed that solid particles could circulate between riser and downer with high solid concentration at U_g lower than transport velocity (U_{tr}) [31, 98]. The transition flow between turbulent and fast fluidized bed in single gas feed system will provide a suitably interesting flow pattern to chemical processes [99].

Applying fluidized bed system to adsorb carbon dioxide by K2CO3/γ-Al2O3 could be the way to made dry adsorption practical for commercial scale. At 12 wt.% of carbon dioxide, the adsorption capacity depended on U_g. The highest capture capacity was in turbulent fluidized bed [99]. The appropriated design of circulating fluidized

bed system together with U_g could perform CTFB that would be the first prototype of continuous dry solid adsorption unit [100].

CHAPTER III
EXPERIMENTAL APPARATUS AND METHOD

3.1. The new flow regime study in a two-dimensional circulating fluidized bed (CFB) reactor with single feed stage

A full understanding of the transient flow behavior in the CFB reactor with single feed gas injection is needed to validate the computational fluid dynamics (CFD) results which is one of the most important tools to design an alternative CO_2 sorption unit. The new sorption design is expected to be less complex and more efficient. The effect of U_g between conventional turbulent and fast fluidized beds is determined by the bed expansion. The intersection of linear solid volume fraction trend on the y-axis represents the bed front. The bed height is the length from the riser bottom to the bed front, which becomes a new spectacle parameter to monitor the new flow regime, circulating turbulent fluidized bed reactor (CTFB), which contains the good mixing property as conventional turbulent fluidized bed regime and the possibility to operate continuously as operated under fast fluidized bed regime. The results in this part demonstrate the possibility to perform CTFB using a single feed system.

3.1.1. Fluidization particles

Sand particles were sieved by standard 60- and 80-mesh sieves. The two sizes of sand particles and commercial grade PVC particles (Thai Plastic and Chemicals Public Company Limited) were measured to determine the particle size distributions as seen in Figure 12 by using a laser particle size analyzer (Malvern, model mastersizer 2000) and then determine the mean particle diameters by the weight average method.

The interpretation of the particle size distribution showed that the mean diameter of sand particles were 260 and 126 micron and the mean diameter of PVC was 161 micron.

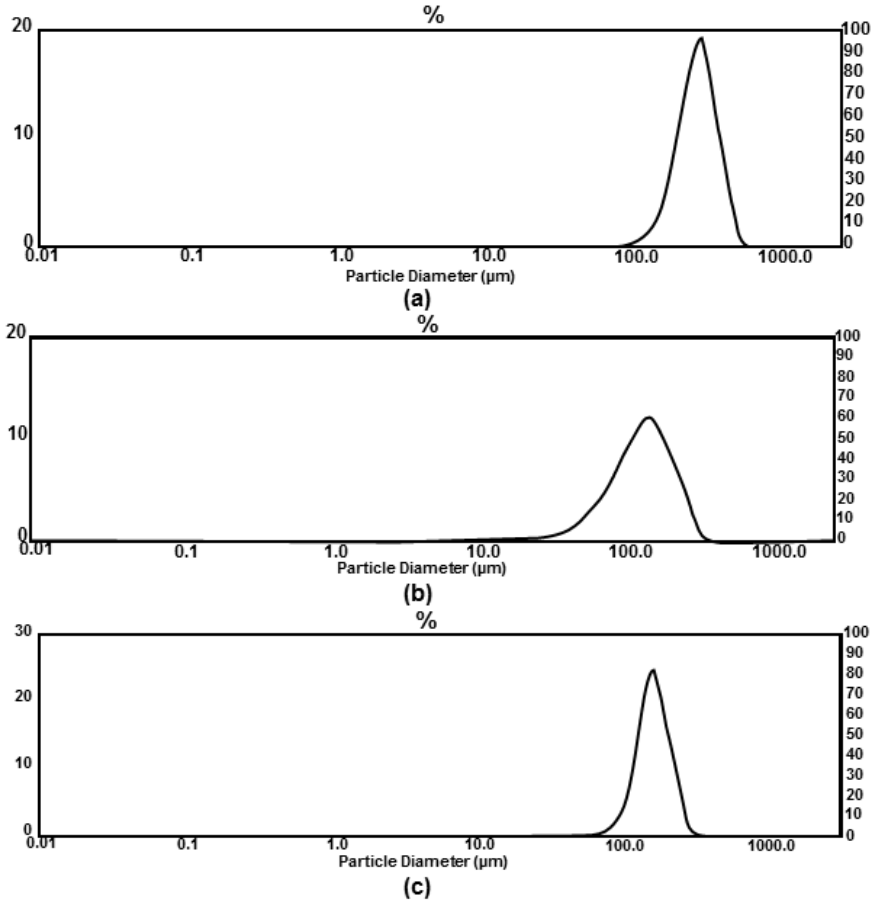

Figure 12 Particle size distribution

(a) Sand with mean diameter of 260 micron

(b) Sand with mean diameter of 126 micron

(c) PVC with mean diameter of 161 micron

The true density of the particles was measured using the pycnometer method. The density of solid particles was the ratio of the mass and volume of particles which

was substituted by the displaced volume of water after put the particles into the cylinder. The densities of sand particles and PVC were 2,650 and 1,400 $kg.m^{-3}$, respectively.

3.1.2. Two - dimensional circulating fluidized bed reactor

Figure 13 shows an acrylic circulating fluidized riser with dimension of 0.15 m width, 0.05 m depth and 2.00 m height. At the initial step, the solid particle was load into the downer (d) and then air was introduced to the reactor through the air box (a) at the riser bottom. The gas encountered with the solid particles above a screen which was installed as the wind box distributor. Gas-solid mixture flowed to the riser (b) and moved to the cyclone (c) where gas and solid particles were then separated. Gas was vented out at the cyclone top, and solid particles fell to the downcomer (d) which had the dimension of 0.30 m width, 0.05 m depth and 0.9 m height. The overall G_s were controlled by the percent opening of a ball valve (e) which located between the downcomer and riser bottom together with an auxiliary air (f) which fed at the lower downcomer to assist the solid flow to the riser. The employed G_s was ranging from 2 to 911 $kg/s.m^2$. Air was compressed by a compressor (Fu Sheng) at room temperature and passed through a dehumidifier air regulator (g) (CHFC model AW 5000-06) at constant pressure of 2 bar. The U_g was controlled by a rotameter (h) at the bottom of the circulating fluidized bed riser.

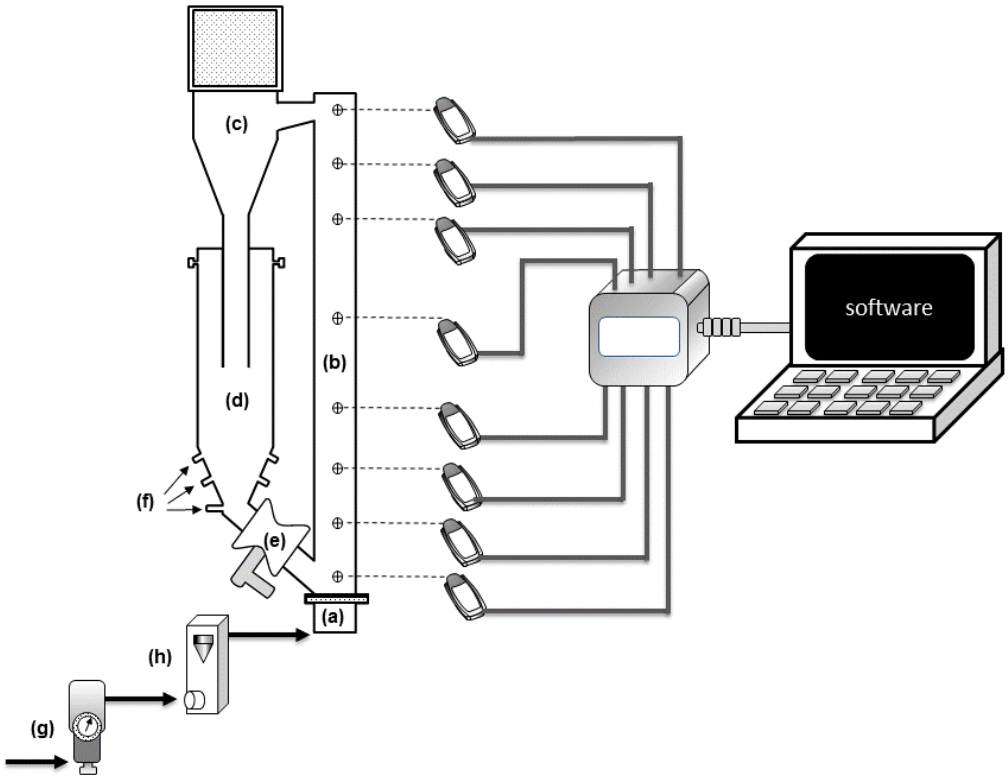

Figure 13 Two-dimensional fluidized bed reactor

(a) Wind box (b) Riser (c) Cyclone (d) Downcomer

(e) Ball valve (f) Auxiliary air (g) Regulator (h) Rotameter

3.1.3. Measuring system

The pressures along the riser were measured by digital pressure sensors (Fourier DT 150-1150 mbar, accuracy ± 1%, resolution 0.25 mbar). The measurement was employed with sampling rate of 500 times per second. The outputs were received and then send to a computer by a Fourier data logger. The difference among each averaged absolute pressure along the riser height was a pressure drop, which used to calculate the

ε_s by using equation (5). The plot of solid volume fraction versus the dimensionless riser height (*h/H*) was used to investigate the hydrodynamics of conventional fluidized bed regimes.

$$\varepsilon_s = \frac{\Delta P}{\rho_p g \Delta h} \tag{5}$$

Where:

ε_s = the solid volume fraction [-],

h = the instantaneous riser height where the pressure is being measured [m],

Δh = the height difference between two measured positions (h) [m],

ΔP = the pressure drop between two measured positions [Pa]

H = the total riser height [m], ρ_p = the particle density [kg/m^3],

g = the gravity [m/s^2].

The design and operating parameters were combined in terms of *Ar*, *Re* and *V**. *Ar* is a dimensionless number that is used to demonstrate the relationship of gas and solid particle properties as calculated by equation (6). Gas and solid particle properties are the most important design parameters to predict the fluidization regimes. The effects of other operating parameters, especially U_g, were included in Re as shown in equation (7). U_g was the important factor to characterize the fluidized bed regimes. *V** was another important parameter that merged batch and continuous processes together by the G_s in the second term as shown in the equation (8). In the batch processes, there

was no solid recirculation which led G_s to zero, while it had a positive value in the continuous processes.

$$Ar = \frac{\rho_g(\rho_p - \rho_g)g{d_p}^3}{\mu^2} \tag{6}$$

$$Re = \frac{\rho_g d_p U_g}{\mu} \tag{7}$$

$$V^* = \left[\frac{{\rho_g}^2}{g\mu_g(\rho_p - \rho_g)}\right]^{\frac{1}{3}}\left[U_g - \frac{G_s\varepsilon_s}{\rho_p(1-\varepsilon_s)}\right] \tag{8}$$

Where:

ρ_g = the air density [kg/m^3], ρ_p = the particles density [kg/m^3],

d_p = the mean particle diameter [m], μ = the dynamic viscosity of the gas [Pa.s],

U_g = the superficial gas velocity [m/s], G_s = the solid recirculating rate [kg/m^2.s],

ε_s = the average solid volume fraction along the riser height [-].

3.2. The optimum condition for CO_2 sorption under turbulent fluidized bed regime in a riser-sorber

Turbulent fluidized bed regime is an attractive operating regime to improve the performance of CO_2 adsorption with a solid sorbent because of its excellent mixing property of gas phase and solid phase. The promising solid sorbent, potassium carbonate (K_2CO_3), supported on gamma alumina (γ-Al_2O_3) was prepared through impregnation and inserted into the adsorption column to determine the optimum

operating parameters. 2^3 factorial design plus center points were carried out and the results were analyzed to identify the main effect and interaction between the operating parameters.

3.2.1. Sorbent

High adsorption capacity together with fast adsorption rate of potassium carbonate supported on gamma alumina ($K_2CO_3/\gamma\text{-}Al_2O_3$) was claimed to be an alternative method to improve dry sorption process instead of stripper unit with liquid amine which was highly toxicity to the environment.

3.2.1.1 Sorbent preparation

5 g of K_2CO_3 (QReC, AR grade) and 5 g γ-Al_2O_3 (Merck, activity stage I) were measured and mixed with 25 mL of distilled water in flasks. The flasks were then placed in a shaker (WiseShake, model SHO-2D) with rotational speed of 230 rpm for 24 hours. The precursor, comprising of the remaining particles on filtration paper, was dehydrated in an oven (Binder, model ED 115) at 105 °C for 24 hrs. In the last step, the dry precursor was pulverized and calcined in a furnace (Carbolite, CWF 13) with a heating rate of 3 °C per minute from room temperature to 600 °C and held for up to 3 hours.

3.2.1.2 Textural properties of the sorbent

Figure 14 shows textural properties of support $\gamma\text{-}Al_2O_3$ before and after impregnation. The support had a smooth surface with sharp edges as shown in Figure 14 (a) while the sorbent which is prepared by the impregnation method as mention in section 3.2.1.1 would be identified as a round particle with rough surface as andFigure 14 (b). The round shape of the sorbent was attributed to a grinding process when the

support was incorporated into a K_2CO_3 solution for a duration of 24 hours. The collision among particles cracked the extended edges and resulted in rounder particles, which enchanced the sorption because it helped to minimize erosion on the reactor walls. At low calcination temperature (less than 600 °c), the energy was not high enough to reduce K_2CO_3 to obtain C=O group nor K atom [101]. Thus, the purpose of calcination in this study was to increase the stability of active-site K_2CO_3 on the support.

The EDX result of support γ-Al_2O_3 and sorbent is shown in Figure 14 (c) and Figure 14 (d). On the support alumina, only oxygen and alumina peaks were found. The appearance of potassium peaks (K) in Figure 14 (d) confirmed the completion of impregnation. Thus, it can be concluded that agglomeration of active-site K_2CO_3 might be the cause of the rough surfaces as shown in Figure 14 (b). The loading percent of the active site was confirmed by XRF technique. The percent by weight of K_2CO_3 loading on γ-Al_2O_3 was around 18%.

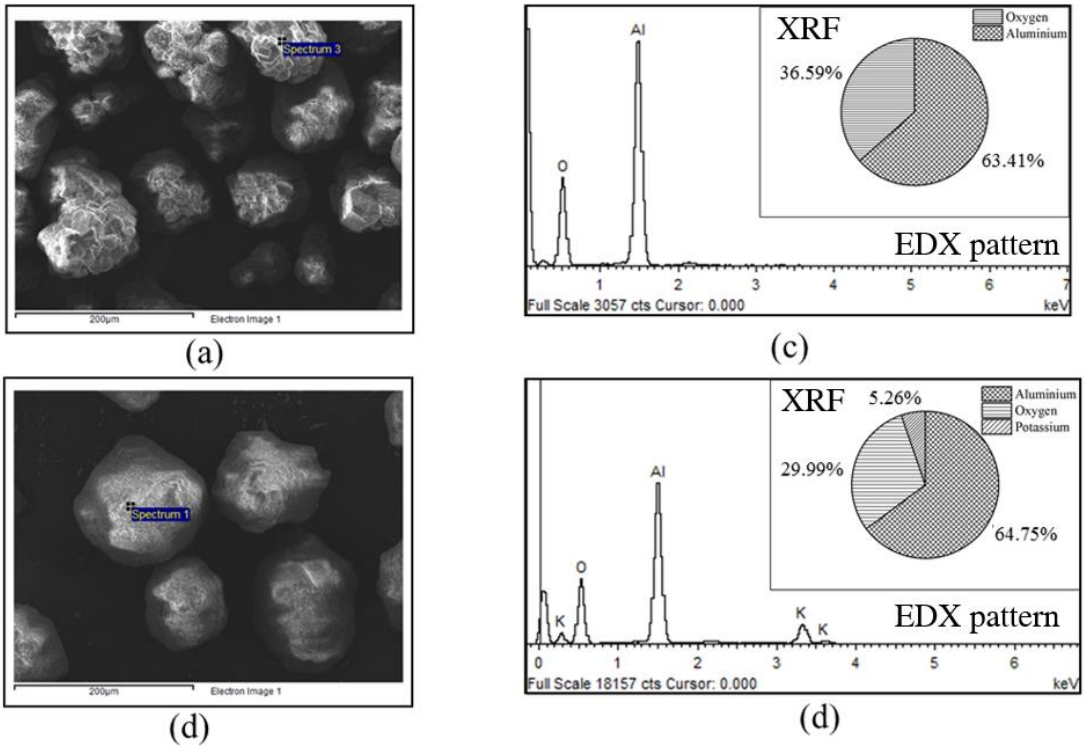

Figure 14 Textural properties of support γ-Al2O3 before and after impregnation

(a) SEM image of γ-Al_2O_3

(b) SEM image of sorbent

(c) EDX pattern of γ-Al_2O_3

(d) EDX pattern of sorbent

The loading percent in this study was a crucial variable that could be used to determine the capture capacity, as seen in equation (9). Based on the results of SEM-EDX in Figure 14, the sorbent was strictly prepared by the same procedures and loaded into the turbulent fluidized bed reactor at the different trials with changing conditions, ultimately to determine the optimum operating parameters for capturing CO_2.

$$q = \frac{1}{m}\int_{o}^{t} Q(C_{in} - C_{out})dt \qquad (9)$$

Where:

q = the capture capacity [mg of CO_2/g of sorbent [mg of CO_2/g of sorbent],

m = the mass of active site on sorbent [g],

C_{in} = the inlet concentration of CO_2 (% mass) [-],

C_{out} =the outlet concentration of CO_2 (% mass) [-].

Q = the gas flow rate [g/s],

t = the sorption time [s].

3.2.2. Sorption apparatus

Figure 15 demonstrates a fluidized bed reactor for CO_2 adsorption study. A cylinder (A) of the mixed gas with 11 ± 1 % volume of CO_2 balanced by nitrogen (Thai-Japanese Gas) was controlled by a rotameter (B) (Nitto, model K-2014 (Air)). The gas first entered the steam generator (C), maintained at a temperature of 60 °C. Water was added water and the mixture was passed through an sorbent bed in the fluidization riser (D) (outer diameter of 0.025 m). In the riser, the gas-solid flow was characterized in the turbulent flow regime. CO_2 was removed according to the following exothermic equilibrium equation:

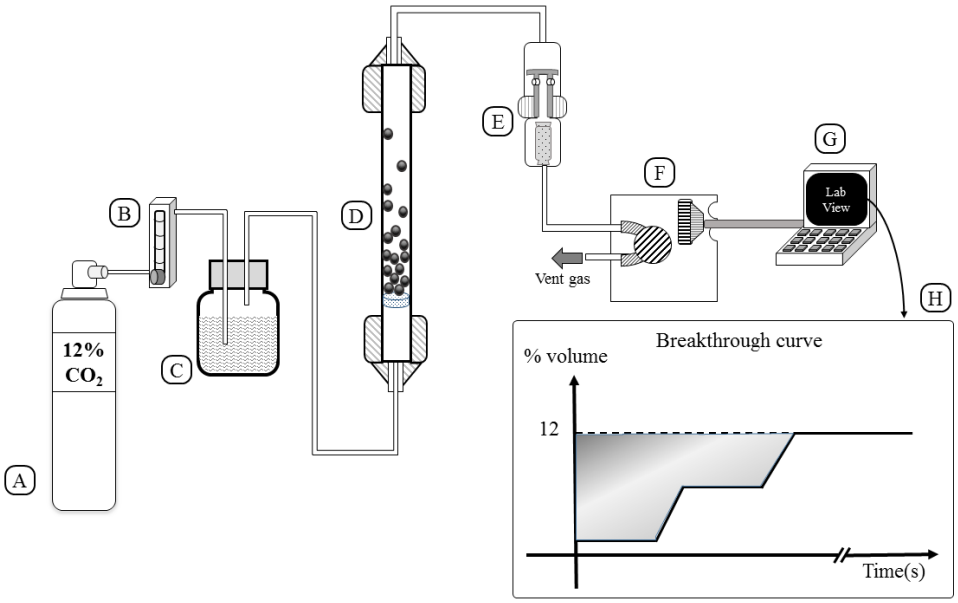

Figure 15 Fluidization adsorption system

The freeboard sorbent particles and excess moisture were removed by a filter (E). The amount of CO_2 in the treated gas, which was released from the riser, was detected by the sensor ((F), CO_2 METER, K-33 BLG CO_2) with a sampling rate of 1 sample per second. The real-time outputs from the sensor were %RH, gas temperature and percent by volume of CO_2. These values were sent to be analyzed and stored by a code developed under the LabVIEW System Design Software ((G), National Instruments). The adsorption profiles were obtained as an output from the program. The plot of break-through curves (H) was done when the concentration of measured gas was equal to its initial concentration. The shaded area between the initial concentration line and the break-through curve were integrated to determine the capture capacity in unit of milligram of CO_2 per gram of sorbent (mg-CO_2/ g-sorbent) by the following equation (9).

3.2.3. Experimental design for the optimum sorption condition

The three operating parameters in this experiment consisted of the following properties: the amount of sorbent loaded, ranging from 5 - 15 grams; the adsorption temperature, ranging from 50 - 70 °C; and lastly, the gas flow rate, ranging from 5-7 liters/minute.

The results from 2^k factorial design plus center points as shown in Figure 16 were ultimately used to determine the optimum operating parameters. A constant k was an integer number equating to the number of interesting operating parameters, which were adsorption temperature (A), gas flow rate (B) and sorbent loading (C). Thus, the k value in this study was 3, and the 2^3 factorial conditions are shown in Figure 16 (a). The center point condition occurred when two of the operating parameters were fixed at the medium values, while another parameter was varied either to maximum or minimum value as shown in Figure 16 (b).

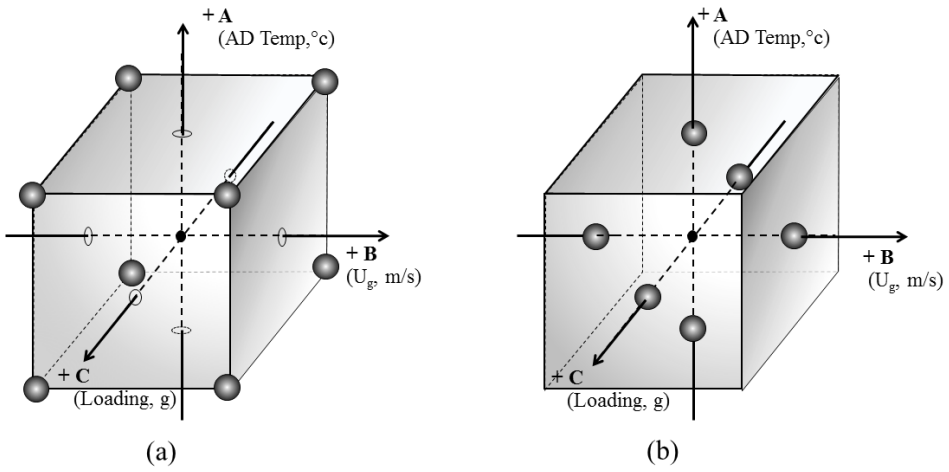

Figure 16 2^3 factorial design plus center points

3.3. Sorbent regeneration study

Due to an excellence in both thermal and physical properties, K_2CO_3/γ-Al_2O_3 was selected to be the sorbent in this study. The support γ-Al_2O_3 had such a strong interaction with water. This helped to improve the diffusivity through the gas film resistance. However, the study of porous supported material of alkali metal sorbent showed that gamma alumina (γ-Al_2O_3) enhanced the adsorption of CO_2 [102]. Due to the cost efficiency, potassium carbonate was an outstanding metal compared to those carbonate compounds of the metal alkali earth [103]. The adsorption of CO_2 by using potassium carbonate supported on gamma alumina (K_2CO_3/γ-Al_2O_3) reached the criteria to be used in the pilot scale. The regeneration properties of the sorbent, which was prepared by the conventional method and captured CO_2 in the optimum operating condition, had not been studied yet. Therefore, the next step was the regeneration study which meant to determine re-usability of the sorbent.

3.3.1. Conventional heat regeneration

The necessity to further extend the scope of this study was addressed to determine the optimum conditions of the conventional heat regeneration method. The parameters to be investigated consists of regeneration temperature, regeneration time, and regeneration cycle. The data obtained from each trial of the experiment will be plotted the concentration of CO_2 versus time to show breakthrough curves and CO_2 capture capacity (mg-CO_2/g-sorbent) determined by integrating the area of adsorption rate with respect to time. The results would further be analyzed by 2^k Factorial Design to indicate the optimum condition of the operating parameters as well as to fit regression models of adsorption capacity. Moreover, the suitable heat regeneration will provide

the crucial both design and parameters for an alternative design of a continuous CO_2 sorption unit in a circulating fluidized bed reactor using K_2CO_3 sorbent. These results are expected to be a bridge which connects the results from a number of the experiments in the laboratory scale apparatus to the design of the pilot scale study.

3.3.1.1. Conventional heat regeneration procedure

Figure 17 demonstrates a fluidized bed reactor for CO_2 adsorption study. A cylinder of nitrogen (a) (99.99%, Thai-Japanese Gas) was controlled by a rotameter (b) (Nitto, model K-2014 (Air)) at the rate of 2 liters per minute. The gas first entered the steam generator (c), maintained the temperature at 60 °C, for adding water and passed through sorbent bed in the fluidization riser (d) (outer diameter of 0.025 m) to initiate the hydro treatment process for 20 minutes [18, 30].

The adsorption performed after hydro treatment process. Three ways valve (e) twisted to the opposite position to let mixed gas with 11 ± 1 % volume of CO_2 balanced by nitrogen (f) (Thai-Japanese Gas) flew to a rotameter. The gas flow rate was regulated at 5 liters per minute, which was sufficient to maintain TFB flow regime in the riser. Once again, the moisture was added to the mixed gas by the steam generator and the mixed gas was introduced to the active sorbent bed loaded above the porous glass filter. The freeboard particles and unreacted water were separated out of the treated gas in the filter (g). The amount of CO_2 in the treated gas, which exhausted out of the adsorption riser, would be detected by the sensor ((h), CO_2 METER, K-33 BLG CO_2) with a sampling rate of 1 sample per second. These values were sent to be analyzed and stored by the computer code developed under the LabVIEW System Design Software ((i), National Instruments).

The adsorption profiles would be obtained as an output from the developed computer code. The plot of break-through curves (j) was done when the concentration of measured gas was equal to its initial concentration and the shaded area between the initial concentration line and the break-through curve would be integrated to determine the CO_2 capture capacity in the unit of milligram of CO_2 per gram of sorbent (mg-CO_2/g-sorbent) by following equation (9). To investigate the regeneration capacity of the sorbent, spent sorbent was put in a crucible and placed in a furnace (k, Carbolite CWF 13/13, power max 3,100 watt, holding power 1,800 watt).

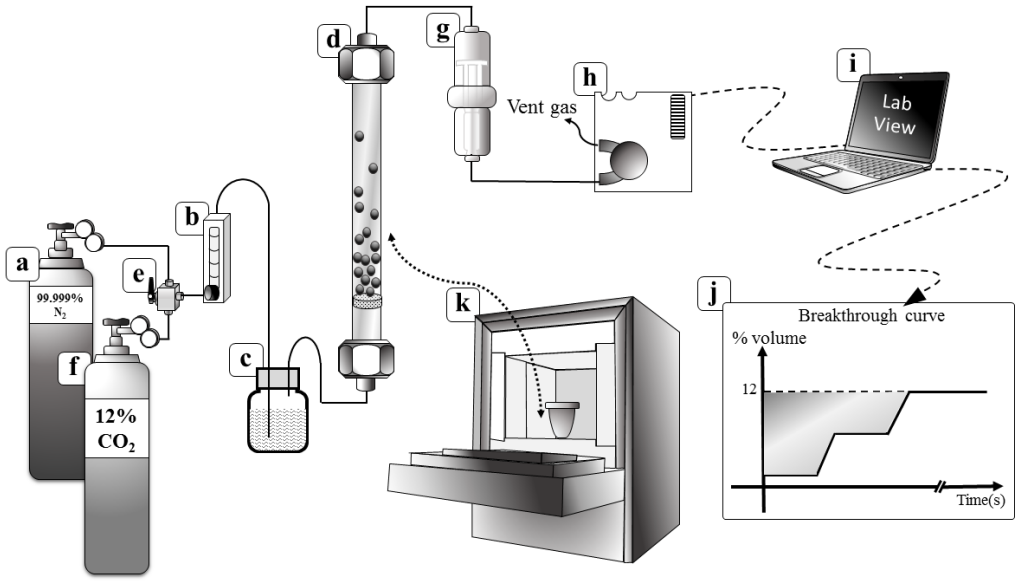

Figure 17 Schematic diagram of CO_2 fluidization adsorption system and conventional heat regeneration system

3.3.1.2. Experimental design for the optimum condition of conventional heat regeneration

There were three operating parameters to be investigated in this experiment, consisting of the following properties: the regeneration temperature, ranging from 200 - 300 °C; the regeneration time, ranging from 2 – 20 minutes; and lastly, the regeneration cycle, ranging from 1-3 cycles.

The results would ultimately be used to determine the optimum operating parameters by 2^k factorial design. A constant k was an integer number equating to the number of the interested operating parameters; regeneration temperature (A), the regeneration time (B) and regeneration cycle (C). Thus, the k value in the study was 3 and the 2^3 factorial conditions were shown in Table 1.

Table 1 Experiment ranges and level of the regeneration operating parameters

Operating Parameter	Symbol	Unit	Code of Level		
			-1	0	1
Regeneration Temperature	*A*	°C	200	-	300
Regeneration Time	*B*	minute	2	-	20
Regeneration Cycle	*C*	round	1	2	3

3.3.2. Depressurization regeneration

Heat regeneration (conventional method) is a primitive design for temperature swing adsorption unit. Application of energy can reverse the equilibrium as shown in equation (1). $KHCO_3$ converts to be K_2CO_3 by releasing CO_2 which will be compressed and keeps in the storage. The conventional method is classified as high energy intensity process because it requires high temperature (200 - 350 °C) and long regeneration time (30 - 90 minute) to complete the regeneration process. Formation of high thermal stability compound, potassium dawsonite compound ($KAl(CO_3)_2(OH)_2$) which

occurred by the side reaction, consumes more energy than $KHCO_3$ to convert to K_2CO_3. However, dawsonite can be prevented by hydro-treatment or multiple impregnation method. The conventional regeneration by itself is difficult to scale up to match with the load of power plants.

Based on the chemical equilibrium in equation (1), the system maintains the pressure by shifting the equilibrium backward when depressurization is applied. Therefore, depressurization it will be an alternative way to regenerate the sorbent. The expected advantages of this alternative method are short regeneration time and homogeneity of sorbent after passing the regeneration without the need to use the thermal regeneration. The regeneration of the sorbent via depressurization, where the sorbent is prepared by the impregnation method and captured CO_2 under turbulent fluidized bed regime, has not yet been studied. The scope of this study is to determine the optimum conditions of this alternative method. The parameters to be investigated consist of regeneration pressure, regeneration time, and regeneration cycle. The data of CO_2 concentration versus time obtained from each trial of experiment will be plotted to show a breakthrough curve and CO_2 capture capacity (mg-CO_2/g-sorbent) which will be determined by integrating the area of adsorption rate with respect to time. The results will further be analyzed by 2^k factorial design to indicate the optimum condition of operating parameters as well as to fit the regression models of adsorption capacity.

3.3.2.1. Depressurization regeneration procedure

Figure 18 demonstrates a fluidized bed reactor for CO_2 adsorption study. A cylinder of nitrogen (A) (99.99 %, Thai-Japanese Gas) was controlled by a rotameter (B) (Nitto, model K-2014 (Air)) at the rate of 2 liters per minute. The gas first entered

the steam generator (C), maintained the temperature at 60 °C, for adding water and passed through sorbent bed in the fluidization riser (D) with outer diameter of 0.025 m to initiate the hydro treatment process for 20 minutes [18, 30].

The adsorption was performed after hydro treatment process. Three ways valve (E) was twisted to the opposite position to let mixed gas with 12 ± 1 % volume of CO_2 balanced by nitrogen (F) (Thai-Japanese Gas) to flow to a rotameter. The gas flow rate was regulated at 5 liters per minute, which was sufficient to maintain turbulent flow regime in the riser. Once again, the moisture was added to the mixed gas in the steam generator and the mixed gas was introduced to the active sorbent bed loaded above the porous glass filter. The free board particles and unreacted water were separated out of the treated gas in the filter (G). The amount of CO_2 in the treated gas, which was released from the adsorption riser, would be detected by a sensor (H) (CO_2 METER, K-33 BLG CO_2) with a sampling rate of 1 sample per second. These values were sent to be analyzed and stored by the computer code developed under the LabVIEW System Design Software (I) (National Instruments).

The adsorption profiles would be obtained as an output from the developed computer code. The plot of break-through curves (J) was done when the concentration of measured gas was equal to its initial concentration and the shaded area between the initial concentration line and the break-through curve would be integrated to determine the CO_2 capture capacity in the unit of milligram of CO_2 per gram of sorbent (mg-CO_2/g-sorbent) by following equation (9).

To investigate the regeneration capacity of the sorbent, the rotameter was closed and three valve (K) was twisted to a vacuum pump (L). The pressure of the riser-sorber, which was loaded by the spent sorbent, was reduced by the action of the vacuum pump.

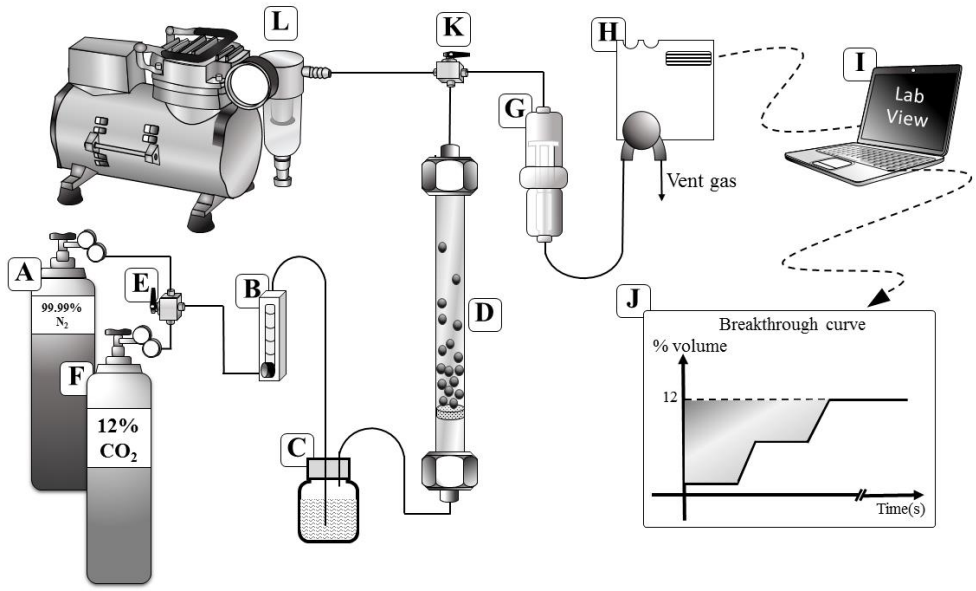

Figure 18 Schematic diagram of CO_2 fluidization sorption system and depressurized regeneration system

3.3.1.2. Experimental design for the optimum condition of depressurization regeneration

There were three operating parameters to be investigated in this experiment, consisting of the following properties: the regeneration pressure, ranging from 0.8 - 0.2 atm; the regeneration time, ranging from 2 – 20 minutes; and lastly, the regeneration cycle, ranging from 1-3 cycles. The regeneration temperature was kept at the same as sorption temperature of 60 °C. The results would ultimately be used to determine the optimum operating parameters by 2^k factorial design plus 4 runs at second regeneration cycle. A constant k was an integer number equating to the number of the interested

operating parameters; regeneration temperature (A), the regeneration time (B) and regeneration cycle (C). Thus, the k value in the study was 3 and the 2^3 factorial conditions were shown in Table 2 .

Table 2 Experiment ranges and level of operating parameters of the depressurized regeneration

Operating Parameter	Symbol	Unit	Code of Level		
			-1	0	1
Regeneration Pressure	A	atm	0.8	-	0.2
Regeneration Time	B	minute	2	-	20
Regeneration Cycle	C	-	1	2	3

3. 4. CO_2 sorption in a circulating fluidized bed under circulating turbulent fluidized bed regime

The limitation of solid sorbent adsorption was the type of the sorption vessel which was classified as a batch process. Therefore, the used of solid sorbent was limited the laboratory scale or the small production rate plant only. After the optimum conditions for CO_2 sorption and regeneration were revealed, the next step was attempting the sorption in a circulating fluidized bed reactor which consisted of three important parts: sorber-riser, gas-solid separator cyclone and regeneration-downer as seen in Figure 1 of the chapter I.

3.4.1. Circulating fluidized bed apparatus

Figure 19 shows the complete system of the CFB reactor which was designed to perform the continuously CO_2 sorption. The fresh sorbent was loaded in the downer (A) (crossectional area of 30*10 cm^2 and height of 35 cm). An one inch butterfly valve (B_1) was installed beneath the bottom downer to control solid recirculating rate of the sorbent to the riser (C) bottom at the sorption temperature of 60 °C. The valve was modified with a pneumatic system which alternately injected air to open and close (I). The longer the close valve, the less solid recirculating flow would be. The simulated wet flue gas, 12 % CO_2 balance by N_2 were introduced to the bottom of the riser (diameter of 2.5 cm and height of 100 cm). The inlet gas velocity were varied in the range which could maintain the circulating turbulent fluidization regime. The sorption in the sorber riser is obeyed an exothermal equilibrium reaction as shown in equation (1).

After the sorption process, the mixture flew out of the riser top to separate gas and solid. The cyclone inlet tube was 2.5 cm in diameter and the rest dimension are followed Lapple design. The used sorbent fell down to another butterfly valve (B_2) and then entered the downer. The close and open position were controlled by the pneumatic mechanisim. The opening of this valve was adjusted to accumulate the sorbent about 4 cm above the bottom of the cyclone.

The treated gas which had low CO_2 content vented out of the cyclone top. A few amount of the outlet gas was sampled every one second to mesure the concentration of CO_2 by the infrared CO_2 sensor (F) (CO_2 METER, K-33 BLG CO_2). These values were sent to be analyzed and stored by the computer code developed under the

LabVIEW System Design Software (G) (National Instruments). The sorption profiles would be obtained as an output from the developed computer code. The plot of break-through curves (H) was done when the concentration of measured gas was equal to its initial concentration and the shaded area between the initial concentration line and the break-through curve would be integrated to determine the CO_2 capture capacity in the unit of milligram of CO_2 per gram of sorbent (mg-CO_2/g-sorbent) by following equation (9).

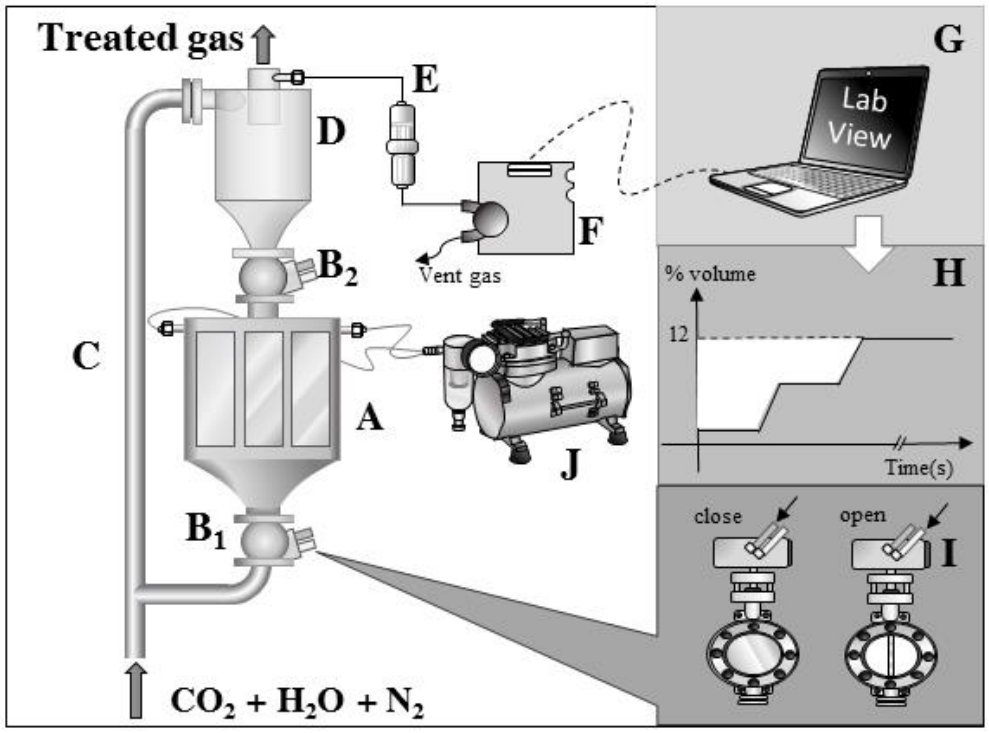

Figure 19 Schematic diagram of circulating fluidized bed for CO_2 sorption

3.4.2. Experimental design for the optimum operating condition for CO_2 sorption using circulating fluidized bed reactor

After the reaching breakthrough concentration (12 percent CO_2 by volume) valve B_1 was closed while the valve B_2 was open for several minutes to circulate the sorbent back to downer for depressurized regeneration. Then, the valve B_2 was closed

and the pressure was reduced on the downer to 0.2 atm by using diaphragm pump (J) to initiate the sorbent regeneration.

The results would ultimately be used to determine the optimum operating parameters by 2^k factorial design. A constant k was an integer number equating to the number of the interested operating parameters, Superficial gas velocity (A), Solid circulation rate (B), initial sorbent loading (C) and regeneration time (D). Thus, the k value in the study was 4 and the 2^4 factorial conditions were shown in Table 3.

Table 3 Experiment ranges and level in the circulating fluidized bed reactor

Operating Parameter	Symbol	unit	Level	
			Low (-1)	High (+1)
Superficial gas velocity	A	m/s	1	1.5
Solid circulation rate	B	kg/m^2.s	50	100
Initial sorbent loading	C	g	300	600
Regeneration time (Depressurized)	D	minute	1	12

3.5. An alternative design of the pilot scale CO_2 sorption unit using computational fluid dynamic

The most common technology for post-combustion of the CO_2 capture is the amine solvent scrubber. The energy consumption for capturing CO_2 from flue gases using amine solvent technology is 15 to 30% of the power plant electricity production [14]. Hence, there is a need to develop more efficient methods of removing CO_2. A circulating fluidized bed using sodium or potassium carbonates is potentially such a process, since their high decomposition pressures allow regeneration at low temperatures using waste heat rather than steam from the power plant. But equilibrium data for the sorbents require the use of several cooled stages to achieve high CO_2

conversions. Here a method of computing such a number of stages for a given CO_2 conversion was developed using multiphase computational fluid dynamics.

3.5.1. CFD equations in FLUENT version 17

In this study, a set of governing equations for conservation of mass, momentum, energy and species and the constitutive equations were solved numerically, very similar to the circulating fluidized bed study of Chalermsinsuwan *et al.* [38]. The constitutive equations were based on the kinetic theory of granular flow, as reviewed by Gidaspow [47]. This theory has been used by many researchers. The commercial CFD program FLUENT 17.0 was chosen for modeling and simulating the system. A summary of the governing equations and constitutive equations is given in Table 4.

Table 4 A summary of the governing equations and constitution equations

A. Governing Equations

(a) Conservation of mass;

- Solid phase;

$$\frac{\partial}{\partial t}\left(\varepsilon_s \rho_s\right)+\nabla.\left(\varepsilon_s \rho_s v_s\right)=0 \quad (10)$$

- Gas phase;

$$\frac{\partial}{\partial t}\left(\varepsilon_g \rho_g\right)+\nabla.\left(\varepsilon_g \rho_g v_g\right)=0 \quad (11)$$

(b) Conservation of momentum;

- Solid phase;

$$\frac{\partial}{\partial t}\left(\varepsilon_s \rho_s v_s\right)+\nabla.\left(\varepsilon_s \rho_s v_s v_s\right)=-\varepsilon_s \nabla P+\nabla.\tau_s-\nabla P_s+\varepsilon_s \rho_s g-\beta_{gs}\left(v_g+v_s\right) \quad (12)$$

- Gas phase

$$\frac{\partial}{\partial t}\left(\varepsilon_g \rho_g v_g\right)+\nabla.\left(\varepsilon_g \rho_g v_g v_g\right)=-\varepsilon_g \nabla P+\nabla.\tau_g+\varepsilon_g \rho_g g-\beta_{gs}\left(v_g-v_s\right) \quad (13)$$

(c) Conservation of energy;

- Solid phase;

$$\frac{\partial}{\partial t}\left(\varepsilon_s \rho_s H_s\right)+\nabla.\left(\varepsilon_s \rho_s v_s H_s\right)=-\varepsilon_s \frac{\partial p_s}{\partial t}+\tau_s:\nabla.v_s+S_s+Q_{gs} \quad (14)$$

with $H_s = \int c_{ps} dT_s$

- Gas phase;

$$\frac{\partial}{\partial t}\left(\varepsilon_g \rho_g H_g\right) + \nabla.\left(\varepsilon_g \rho_g v_g H_g\right) = -\varepsilon_g \frac{\partial p_g}{\partial t} + \tau_g : \nabla.v_g + S_g + Q_{sg} \quad (15)$$

with $H_s = \int c_{pg} dT_g$

(d) Conservation of species;

- Solid phase;

$$\frac{\partial}{\partial t}\left(\varepsilon_s \rho_s y_i\right) + \nabla.\left(\varepsilon_s \rho_s v_s y_i\right) = R_j \quad (16)$$

- Gas phase;

$$\frac{\partial}{\partial t}\left(\varepsilon_g \rho_g y_i\right) + \nabla.\left(\varepsilon_g \rho_g v_g y_i\right) = R_j \quad (17)$$

(e) Conservation of solid phase fluctuation energy;

$$\frac{3}{2}\left[\frac{\partial}{\partial t}\left(\varepsilon_s \rho_s \theta\right) + \nabla.\left(\varepsilon_s \rho_s \theta\right) v_s\right] = \left(-\nabla p_s I + \tau_s\right) : \nabla v_s + \nabla.\left(k_s \nabla \theta\right) - \gamma_s \quad (18)$$

B. Constitutive Equations;

(a) Solid phase stress;

$$\tau_s = \varepsilon_s \mu_s \left[\nabla v_s + \left(\nabla v_s\right)^T\right] - \varepsilon_s \left(\xi_s - \frac{2}{3}\mu_s\right) \nabla.v_s I \quad (19)$$

(b) Gas phase stress;

$$\tau_g = \varepsilon_g \mu_g \left[\nabla v_g + \left(\nabla v_g\right)^T\right] - \frac{2}{3}\varepsilon_g \mu_g \left(\nabla.v_g\right) I \quad (20)$$

(c) Collisional dissipation of solid fluctuating energy;

$$\gamma_s = 3(1-e^2)\varepsilon_s^{\,2} \rho_s g_0 \theta \left(\frac{4}{d_p}\sqrt{\frac{\theta}{\pi}}\right) \quad (21)$$

(d) Radial distribution function;

$$g_0 = \left[1 - \left(\frac{\varepsilon_s}{\varepsilon_{s,\max}}\right)^{1/3}\right]^{-1} \quad (22)$$

(e) Solid phase pressure;

$$p_s = \varepsilon_s \rho_s \theta \left[1 + 2 g_0 \varepsilon_s (1-e)\right] \quad (23)$$

(f) Solid phase shear viscosity;

$$\mu_s = \frac{4}{5}\varepsilon_s \rho_s d_p g_0 (1-e)\sqrt{\frac{\theta}{\pi}} + \frac{10 \rho_s d_p \sqrt{\pi\theta}}{96(1-e)\varepsilon_s g_0}\left[1 + \frac{4}{5}\varepsilon_s g_0 (1-e)\right]^2 \quad (24)$$

(g) Solid phase bulk viscosity;

$$\xi_s = \frac{4}{3}\varepsilon_s \rho_s d_p g_0 (1-e)\sqrt{\frac{\theta}{\pi}} \quad (25)$$

(h) Conductivity of fluctuating energy;

$$k_s = \frac{150\rho_s d_p \sqrt{\pi\theta}}{380(1-e)g_0}\left[1+\frac{6}{5}\varepsilon_s g_0(1-e)\right]^2 + 2\varepsilon_s{}^2\rho_s d_p g_0(1-e)\sqrt{\frac{\theta}{\pi}} \quad (26)$$

(i) Gas-solid phase interphase exchange coefficient;

When $\varepsilon_s \le 0.80$;

$$\beta_s = 150\frac{(1-\varepsilon_g)^2\mu_g}{\varepsilon_g d_p{}^2} + 1.75\frac{(1-\varepsilon_g)^2\rho_g|v_g - v_s|}{d_p} \quad (27)$$

When $\varepsilon_s > 0.80$;

$$\beta_s = \frac{3}{4}\frac{(1-\varepsilon_g)\varepsilon_g}{d_p}\rho_g|v_g - v_s|C_{D0}\varepsilon_g{}^{-2.65} \quad (28)$$

With

$$\mathrm{Re}_k < 1000\ ; C_{D0} = \frac{24}{\mathrm{Re}_k}(1+0.15\mathrm{Re}_k{}^{0.687})\ ;\ \mathrm{Re}_k = \frac{\rho_g\varepsilon_g|v_g - v_s|d_p}{\mu_g}$$

$$\mathrm{Re}_k \ge 1000\ ;\ C_{D0} = 0.44$$

3.5.2. Kinetic equations with the equilibrium limitation

Capturing of CO_2 using sodium carbonate sorbents is restricted by the equilibrium for the reaction shown below.

$$CO_{2(g)} + H_2O_{(g)} + Na_2CO_{3(s)} \leftrightarrow 2NaHCO_{3(s)} + 129kJ \quad (29)$$

When the bicarbonate reaches its decomposition pressure, the capture of CO_2 will stop [14]. Hence, to adsorb the lower concentrations of CO_2, the temperature of the sorbent must be lower. Normally, the rate of CO_2 sorption using solid sorbent is assumed by the first order reaction but, in this study, the forward and backward reactions were employed as shown below as a function of concentrations of CO_2 and water vapor and the reaction temperature.

$$-r_{fw} = k_{fw}[CO_2]^{n'}[H_2O]^{n'} \quad (30)$$

$$k_{fw} = k_0'[e^{(E_a'/RT)}] \quad (31)$$

$$+r_{bw} = k_{bw}(1/[CO_2]^{n''})(1/[H_2O]^{n''}) \quad (32)$$

$$k_{bw} = k_0^{''}[e^{(E_a^{''}/RT)}] \quad (33)$$

The variables shown in equations (30) – (33) were determined via a logical loop, as shown in Figure 20. $[CO_2]_{eq}$ represents molar CO_2 which obtained from the equilibrium study as shown in equation (34) [29].

$$[CO_2]_{eq} = (1\times10^{-9})T^4 - (2\times10^{-7})T^3 + (2\times10^{-5})T^2 - (5\times10^{-4})T + 0.0045 \quad (34)$$

r_{eff} is the effective rate of reaction which is determined by the difference between the forward and backward reaction rates as shown in equation (35). If the molar concentration of CO_2 is larger than $[CO_2]_{eq}$ then it will occur a sorption reaction which represents by negative sign. The system will reduce CO_2 by a formation of $NaHCO_3$ which the rate determined by the forward reaction as expressed in equation (30) and (31). The system will reach equilibrium when r_{eff} becomes zero. On the other hand, if $[CO_2]$ is lower than $[CO_2]_{eq}$, for the regeneration process, r_{eff} becomes positive. The $NaHCO_3$ will decompose and form CO_2 which is explained by the backward reaction as expressed in equation (32) and (33).

$$r_{eff} = r_{bw} - r_{fw} \quad (35)$$

To determine the reaction parameters, the logical loop started by calculating $[CO_2]_{eq}$ using equation (34) at the temperature of 45 °C. Then, the obtained equilibrium carbon dioxide concentration was substituted into equations (30) – (33). Use the iterative calculations to determine those kinetic constants that make the r_{eff} become zero

with $[CO_2]_{eq}$ at sorption temperature of 45 °C. After that for selected temperatures between 20 to 70 °C, use those kinetic constants to calculate the carbon dioxide concentration using equation (30) – (33) and compare the result with those obtained from the prediction of empirical equation (34) at each specific temperature. If the $[CO_2]_{eq}$ deviation between those obtained from equation (34) and from kinetic equations is greater than 5 percent, the new iteration will start to obtain a new set of kinetic parameters. However, the above described procedure will stop when the set of kinetic parameters can predict the carbon dioxide concentration via the kinetic equations within 5 percent deviation compared to those obtained from empirical equation, was found for all selected temperature. After finding the proper set of kinetic parameters, these parameters and equations were coded in the user defined function of the FLUENT 17.0 program as shown in equations (36) – (39).

$$r_{fw} = k_{fw}[CO_2]^{0.4}[H_2O]^{0.4} \quad (36)$$

$$k_{fw} = 1*10^{-10}[e^{(70/RT)}] \quad (37)$$

$$r_{bw} = k_{bw}(1/[CO_2])^{0.15}(1/[H_2O])^{0.15} \quad (38)$$

$$k_{bw} = 7.83*10^{-3}[e^{(-0.000502/RT)}] \quad (39)$$

Conventionally, the kinetic models for CO_2 sorption were fit as first order reaction which were presented by the multiplication between the rate constant and molar concentration of CO_2. This model is just the rough approximation by considering CO_2 sorption as only forward exothermic reaction. Thus, that model cannot completely described the sorption system which the reactions were limited by the equilibrium of the reactions. In this study, both forward and backward kinetic models, as mentioned in equation (36) to (39), were used to represent the sorption reaction in the riser and

their model parameters were determined. Figure 21 shows the equilibrium curve (Line AB) obtained from the experiment [14]. This curve was used for determining the kinetic parameters of the equilibrium sorption reaction. The computed equilibrium CO_2 concentration from kinetic models at varying temperature shows a very good agreement the equilibrium curve. Thus, this obtained kinetic models are the good representative reaction rate for studying CO_2 sorption in a circulating fluidized bed reactor.

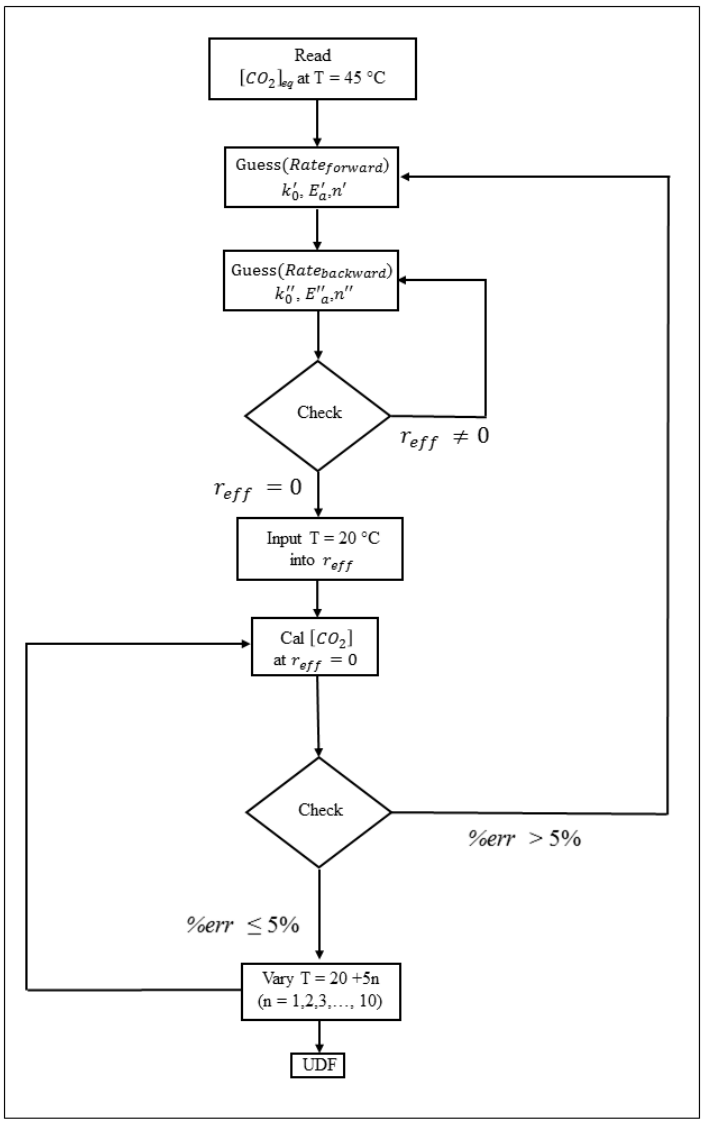

Figure 20 Logical loop of thermal equilibrium for CO_2 sorption using Na_2CO_3 sorbent

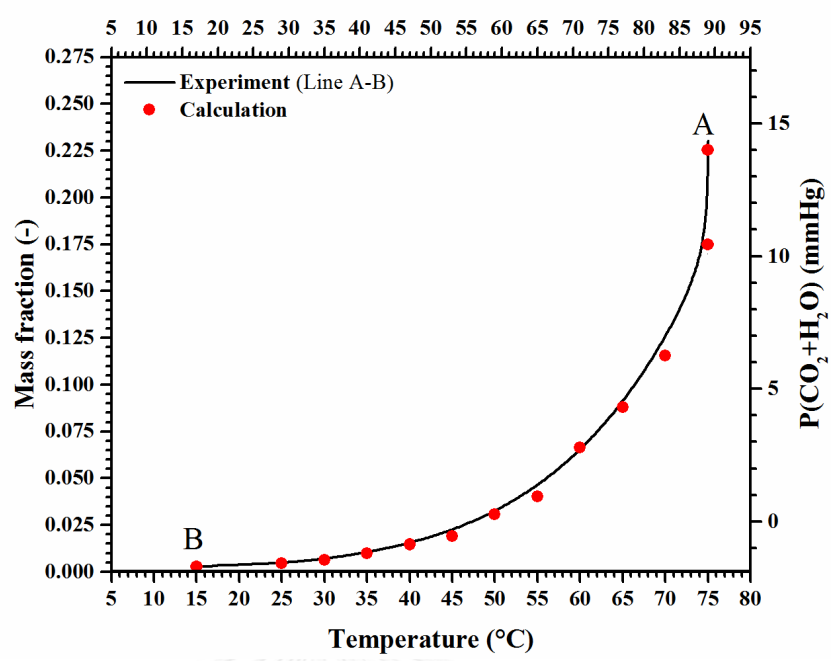

Figure 21 Kinetic model validation [14]

3.5.3. Multi single-stage sorber-risers

In of this CFD study meant to show the possibility to capture CO_2 with 95 percentage removal which is the milestone for the sorption process. The conventional liquid amine absorber could not capture CO_2 higher than 90 percent due to the equilibrium limitation. Multiple risers similar to that in the Park et. al. patent is used. The design was obtained using multiphase CFD following the equilibrium curve of sodium carbonate and sodium bicarbonate.

The sorption temperature is a crucial variable in this study. The inlet gas and solid temperatures in the first stage were kept at 50 and 55 °C, respectively. CO_2 and H_2O were set as an input into the sorber-riser as shown in Figure 22, with an equi-molar fraction of 0.15. The concentration of CO_2 obtained from the outlet becomes the inlet for the next stage as shown Table 5. The inlet temperature gas and solid phase was

reduced by 5 °C in the next stage, while the other properties were kept at constant, as shown in Table 6.

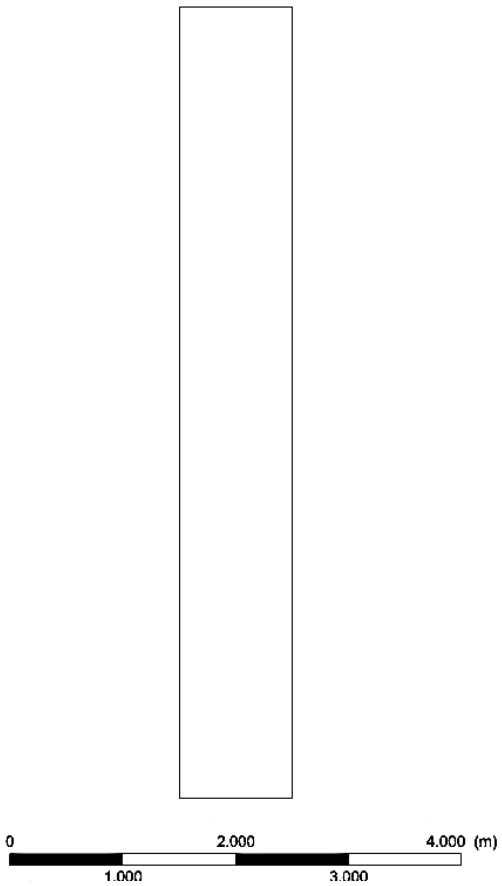

Figure 22 2-dimensional sorber-riser

Table 5 Operating parameters of each single stage sorption-riser

Sorber-riser	Inlet Temperature		Input CO_2 Mass fraction
	Gas Phase [°C]	Solid Phase [°C]	
Stage 1	50	55	0.227
Stage 2	45	50	outlet of Stage 1
Stage 3	40	45	outlet of Stage 2
Stage 4	35	40	outlet of Stage 3
Stage 5	30	35	outlet of Stage 4
Stage 6	25	30	outlet of Stage 5

Table 6 Properties and inlet conditions of the single stage sorber-riser

Symbol	Description	Value	Unit
ρ_g	Gas density	1.04	kg/m^3
μ_g	Gas viscosity	2×10^{-5}	kg/m s
ρ_S	Solid density	500	kg/m^3
d_p	Solid sorbent diameter	500	micron
Gs	Solid sorbent circulation rate	48	kg/s
e	Restitution coefficient between particles	0.9	-
e_w	Restitution coefficient between particles and wall	0.9	-
ϕ	Specularity coefficient	0.1	-
v_g	Inlet gas velocity	1.0	m/s
v_s	Inlet solid velocity	0.27	m/s
$\varepsilon_{s(in)}$	Solid volume fraction of inlet solid phase	0.4	-
$\varepsilon_{s(\max)}$	Maximum packing capacity	0.63	-

3.5.4. Multi-stage sorber-riser

The next part of the CFD study in this disstertation, new design was proposed of a compact sorption riser which has the multi-stage sorption inside a single riser. The riser is also equiped with cooling water tubes to cool down the sorbent for the next stage sorption. This design makes it possible to capture CO_2 up to 95 percent. The energy balances showed that sorbent regeneration could utilize the heat from the sorption reaction and from flue gas without the need of additiontal heat from external sources, except small amount of electricity for supporting fluidization in the riser.

Figure 23 shows a schematic diagram of the multi-stage riser with cooling tube sections and its dimension. The flue gas having equimolar of 0.15 CO_2 and H_2O balanced by N_2 was input at velocity of 1 m/s into the multi-stage riser. The CO_2

sorption started at section A above the riser entrance. The solid-gas mixture entered section B where the cooling tubes were set up and then the cooled mixture entered the sorption sections (section C and E) and followed by the cooling sections (section D and F), respectively. The outlet mixture was measured at the top of the section G which was considered as the results of this alternative design.

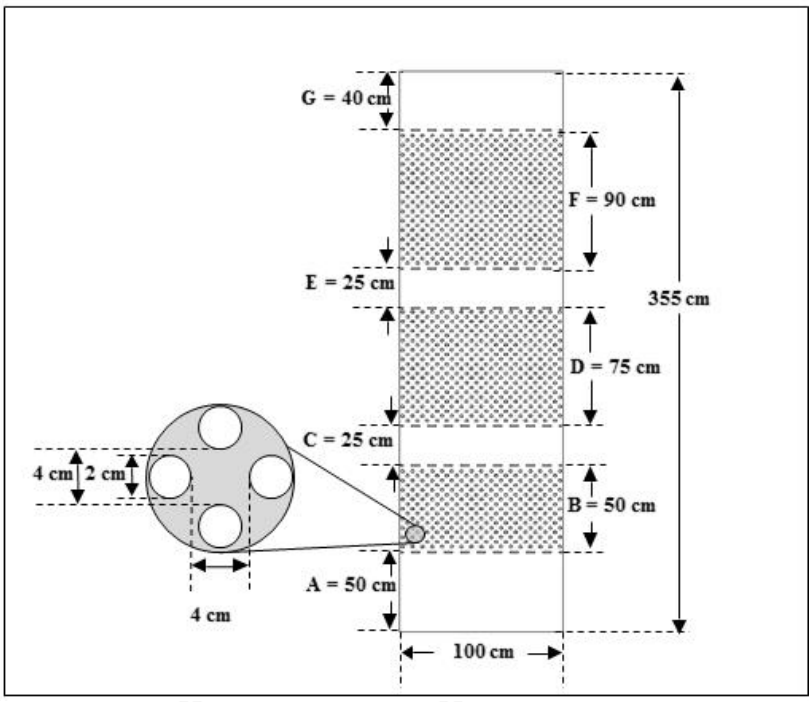

Figure 23 Schematic diagram of riser with cooling tubes

Table 7 shows the details in each riser-sorber section. There are different number of the cooling tubes in each section and three different sets of surface temperatures of the cooling tubes as shown in Table 7. The surface temperature of the cooling tubes in section B was fixed at 50 °C. The temperature in the next section was reduced by 10 °C in operation I and 5 °C in operation II, but it was kept unchange (at 50 °C) in operation III.

Table 7 Variation of cooling tubes temperatures

Section Name	Symbol	Exchanger Tube			
			Temperature [°C]		
		Number [-]	Operation I	Operation II	Operation III
Stage 1	A	none	none	None	none
Cooling 1	B	281	50	50	50
Stage 2	C	none	none	none	none
Cooling 2	D	413	40	45	50
Stage 3	E	none	none	none	none
Cooling 3	F	479	30	40	50
Stage 4	G	none	none	none	none

Table 8 shows the physical properties and inlet conditions which are the same as Kongkitisupchai et al [14]. The sorbent particle was classified in Geldart group B [56]. The multiphase flow regime in the multi-stage riser was characterized by a CTFB regime [63, 104]

Table 8 Properties and inlet conditions for mutistage sorber-riser

Symbol	Description	Value	Unit
ρ_g	Gas density	1.04	kg/m^3
μ_g	Gas viscosity	2×10^{-5}	kg/m.s
ρ_g	Gas density	1.04	kg/m^3
ρ_S	Solid density	500	kg/m^3
d_p	Solid sorbent diameter	500	micron
G_s	Solid sorbent circulation rate	48	kg/s
e	Restitution coefficient between particles	0.9	-
e_w	Restitution coefficient between particles and wall	0.9	-
ϕ	Specularity coefficient	0.1	-
v_g	Inlet gas velocity	1.0	m/s
v_s	Inlet solid velocity	0.27	m/s
$\varepsilon_{s(in)}$	Solid volume fraction of inlet solid phase	0.4	-
$\varepsilon_{s(\max)}$	Maximum packing capacity	0.63	-

3.5.5. Downer regenerator

Figure 24 shows the dimensions of the cyclone and regeneration-downer. The inlet boundary condition is the output of the multi stage sorber-riser tube in the previously section. The mixture was introduced horizontally and perdendicular to the inlet of the tube which connected to the riser exit. The tube was expanded from 10 to 15 cm. The total height of the cyclone is 45 cm and 35 cm in diameter. The bottom of the cyclone is reduced to 20 cm with the inclination length of 15 cm. The treated gas will be vented out at the exit of the cyclone. Spent sorbent is separated downward by the gravity and collided with baffles.

Those buffles help distributing sorbent before entering to the downer. The small tubes diamter of 2 cm beneath the baffles were set as the outlet which meant to deliver CO_2 and H_2O which obtained from the reverse reaction during the regeneration out of the downer when the heat was applied via the tubes in the downer. The first half of the tubes which located at the upper downer were set as wall which their temperature were set as a constant value of 60 °C which equate the outlet temperature of the mixture in the exchanger represented by section B of Figure 24 in the previous section. The temperatures of the rest of the tube were set at 130 °C which is equaled to stack gas from the power plant.

The condition for the sorbent regeneration was mainly determined by the solid temperature and mass fraction of $NaHCO_3$. The temperature of solid should be equal to the inlet temperature of inlet solid temperature of riser (55 °C). In addition, all of $NaHCO_3$ must be changed to Na_2CO_3. The complete regenerated sorbent was fed back through an inclined tube which designed to conncect downer bottom to the riser bottom.

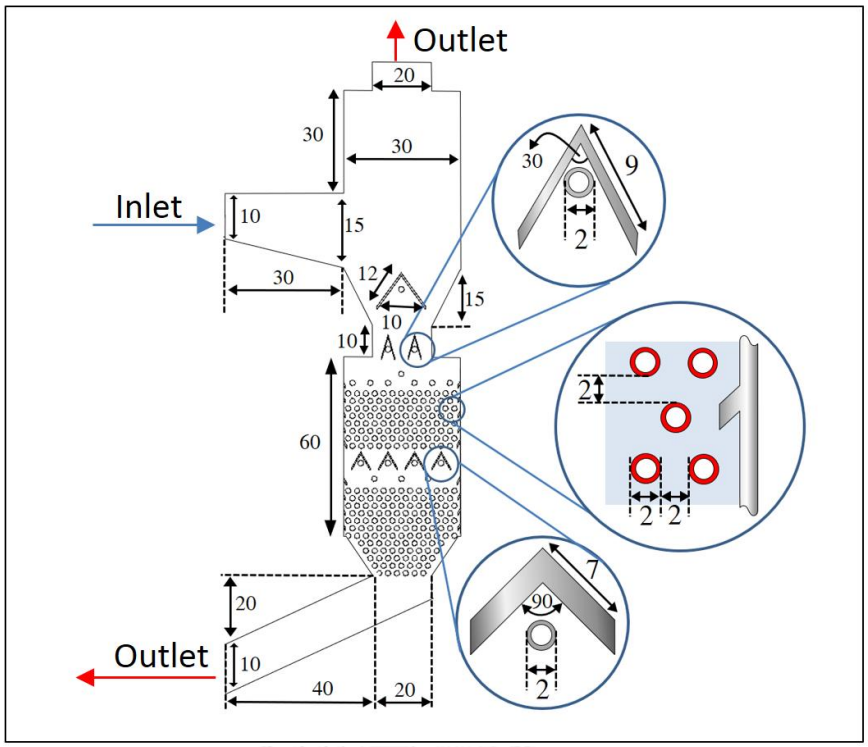

Figure 24 Schematic diagram of regenerator-downer with heat tubes

(the number are in the unit of cm)

CHAPTER IV
RESULTS AND DISCUSSION

4.1. Design parameters for performing circulating turbulent fluidization with single feed stage fluidized bed reactor

The possibility for performing CTFB using only single feed gas injection is studied in a circulating fluidization reactor. Geldart classification and Archimedes number (*Ar*) are included in design parameters. Two sizes of sand (126 and 260 micron) represented the Geldart group B, while a PVC (161 micron) represented the Geldart group A. The superficial gas velocity (U_g) ranged from 0.2 to 1.4 m/s with various solid recirculation rates adjust in order to study the effect of the operating parameters. Solid volume fraction profile along riser height is used to determine the bed front. The appearance of CTFB in the system was indicated by the disappearance of the bed front along the riser height. The suitable height of the riser was the crucial design to perform CTFB. The height suggests to be lower than the maximum solid bed expansion of each particles.

4.1.1 Effect of particle properties to the transient flow behaviors

4.1.1.1. Geldart group B particles

Figure 25 shows ε_s profiles of sand (260 micron) at varying regulating G_s. The (conventional) turbulent fluidized bed (TFB) started when the U_g was equal to 0.7 m/s which is considered as the critical velocity as shown in Figure 7. High ε_s region was observed at the bottom of the riser as shown in the region I of Figure 25 (a) – (d). This region can be divided into two parts which are the accelerating region and the dense

phase region. In the fluidized bed reactors, particles are fed to the riser from the downer. This always shows an entrance effect that causes extremely high ε_s close to the maximum packing capacity ($\varepsilon_{s\ (max)}$ = 0.6 - 0.63). The acceleration zone is the region II at the middle riser part. This region is characterized by the second gradient (h/H = 0.2 - 0.8) on the profile. Due to the fluctuation of ε_s , TFB is known as the high mixing property regime which is an outstanding advantage for the CO_2 sorption. The trend of ε_s profile of region II in Figure 25 (a) – (d) showed linear trend and y-interceptions (bed front) obtained from the extrapolation of the linear fitting curve were defined as the terminal position of acceleration region. The turbulent bed or bed height was defined the height of region I and II. The recirculation of particles in the bed was the reason for high □$_s$ in the bed. Above the bed to the riser exit (h/H = 0.9), the ε_s was extremely low. Region III was called the freeboard zone which occurred because high kinetic energy (K.E.) particles escape from the bed.

Figure 25 (a) revealed effect of U_g at constant G_s of 120 ± 10 kg/s.m^2. Increasing Ug causes the dilution of ε_s in region I. In the higher U_g system K.E. is higher than the slow U_g system which resulted in more solid moving upward. The higher value of U_g also dramatically increased the gradients of ε_s in region II. Focusing on y-interceptions obtained by the extrapolation in region II, bed fronts moved to the higher position. Thus, U_g directly affected on bed height but not ε_s in region III.

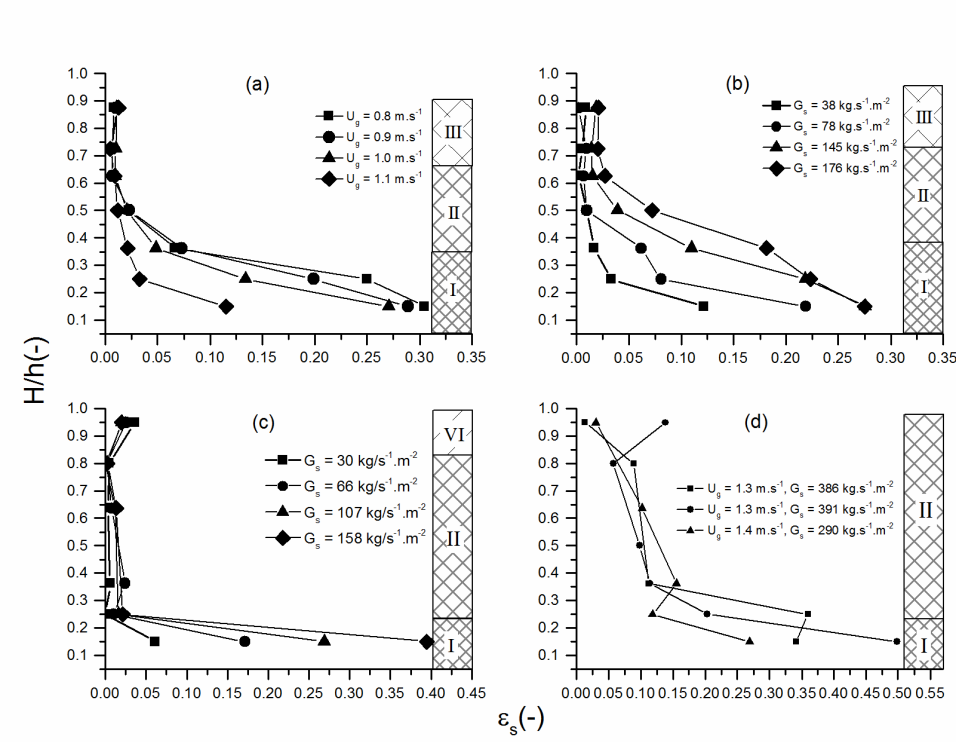

Figure 25 Solid volume fraction profile of 260 micron sand

(a) G_s was constant in the range 120 to 130 kg/s.m^2

(b) Constant U_g of 1.0 m/s

(c) Constant U_g of 1.1 m/s

(d) Circulating turbulent fluidized bed (CTFB) profiles

On the other hand, G_s has such a large effect on the ε_s in the bed. As shown in Figure 25 (b), the bed is denser due to increasing of G_s. U_g of the fluid affected the magnitude of both drag force and buoyancy force which are the upthrust on particles. The summation of them against the weight of that particle, which became the principle of fluidized beds. The magnitudes of the upthrust which distributed on each particle decreased when G_s increased. Therefore, the average K.E of particles decreased, which reduced amount of free board particles and probability of the exit effect at low U_g. So, the ε_s in the bed increased. The bed height was independent from G_s due to the same

position of y- interception when G_s had varied. Theoretically, particle velocity is determined by the rate of impulse from air in front of the air distributor which is installed on the riser bottom. Then, the K. E. of the particles turns to be gravitational potential energy represented by the bed expansion. The transformation between K. E. and gravitational potential energy of each particle is independent of the mass of the particles in the system. Consequently, the bed expansion depended on U_g, due to the conservation of energy in the fluidized bed system.

Figure 25 (c) shows the result of the ε_s profile when increasing G_s while U_g was maintained constant at 1.1 m/s. The more G_s value caused the denser solid ε_s in region I but not in the region II and III as mention in Figure 25 (b). The more G_s did not affect ε_s in the region II. Moreover, ε_s increased again at the high riser part because the accumulation in the top of the riser, instead of region II. Fluid could provide enough energy to generated high speed particles that could escape out of the region II, then their K. E. reduced after collision with the riser top before entering the cyclone. The accumulation of particles at the riser exit became the cause of the exit effect which represented in region VI. Therefore, at low U_g, a few amount of particles could escape from the region II. So, the exit effect was not observed.

In Figure 25 (d), at U_g of 1.3 m/s and high flux G_s in system (G_s = 386 to 391 kg/s.m^2) presented an interesting characteristic on their profiles. No bed front appeared in the middle part of the riser (h/H = 0.2-0.8) because the bed expanded all over the riser and seemed to have a uniform ε_s at high concentration along the riser height and high G_s caused by the exit effect. Particles circulated from the top of the riser to the cyclone in a similar characteristic of CTFB, which was also noted by Qi et al [90-94].

Furthermore, this special characteristic also showed at the higher U_g of 1.4 m/s and G_s of 290 $kg/s.m^2$. This could be concluded that CTFB could occur in single feed gas fluidization. The difference between CTFB with single feed and that with a secondary gas feed injection system was the particle velocity profile. CTFB with single feed injection was similar to a conventional TFB with might has the back mixing near the riser wall, but the CTFB with secondary gas feed injection had a more uniform particle velocity profile with positive value in the radial direction [90-94].

Figure 26 shows the ε_s of sand particles with an average diameter of 126 micron. It noticed that no bed fronts appeared in the riser as the interception in the range of the riser height (h/H = 0.0 – 1.0) when the extrapolation. CTFB could be found at the lower U_g with the different conditions as shown in Figure 26 (a) and (b). CTFB was denser when G_s was increased as shown in the region I II and VI.

Furthermore, when comparing the sand bed particles of 126 micron (Figure 26) and 260 micron (Figure 25), it was also found that the less average particle diameters, CTFB could operate at the lower U_g. Therefore, the bed of finer particles had higher potential to expand.

The result of the CTFB at U_g equal to 1.1 m/s is shown in Figure 25 (c) (it shows a different characteristic from other CTFBs that occurred at lower gas velocity). The trend on solid fraction profile is seen to be highly linear with the bed height when compared to others.

Figure 25 (d) shows the S-shape profile on its ε_s profile. At U_g equal to 1.2 m/s, the result revealed the occurrence of a fast fluidized bed. The bed of CTFB was collapsed due to the velocity gradient between gas and particles in the bed. The greater gradient caused the short contact time between particles and gas. Only the particles in

the center of the riser could move with such a high velocity and then escape from the bed. The dilute region, core annular was presented by a low ε_s value at the middle height of the riser. High ε_s at the riser top and bottom were influenced by the exit and entrance effects, respectively.

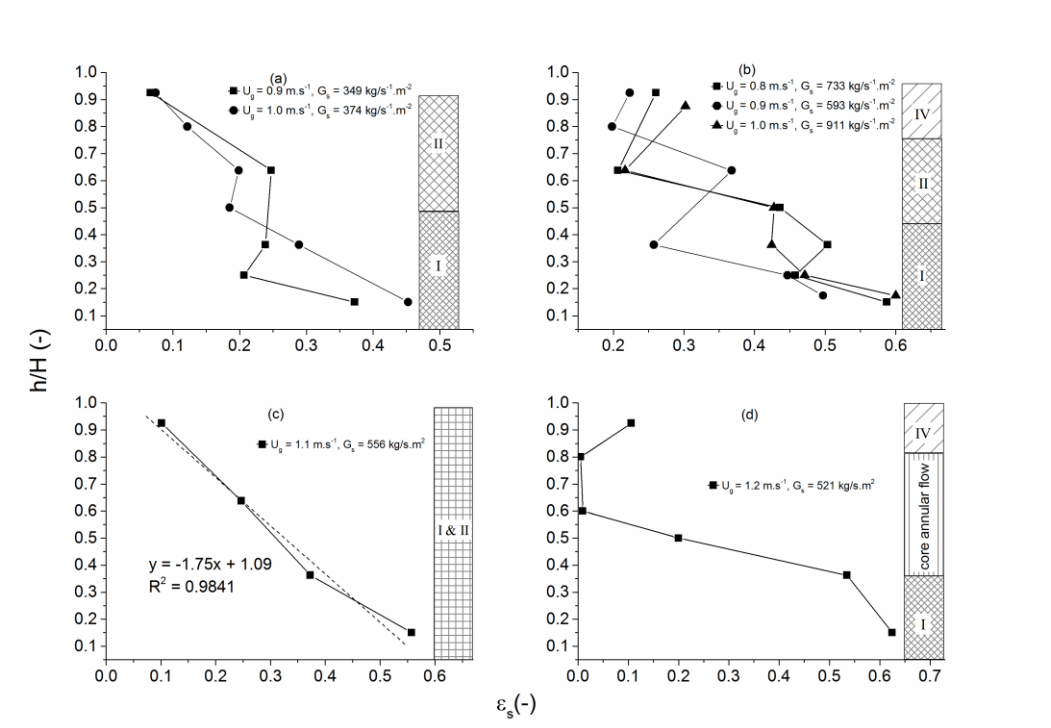

Figure 26 Solid volume fraction profile of 126 micron sand

(a) CTFB profile of sand 126 micron with no exit effect

(b) CTFB profile of sand 126 micron with exit effect

(c) Transition profile between CTFB and fast fluidized bed

(d) Fast fluidized bed

Figure 26 shows the time taken to remove sand with the average diameter of 126 micron out of the riser. There were two negative gradients. The intersection position could be projected on the superficial gas velocity axis to determine U_{tr}, which was used to terminate the turbulent fluidized bed or the beginning of fast fluidized bed

[69]. U_{tr} of sand with average diameter of 126 micron is about 1.16 m/s. This is consistent as shown in Figure 26 (c) and (d), which show the transition CTFB and fast fluidized bed at U_g = 1.1 m/s and then fully developed fast fluidized bed at U_g = 1.2 m/s. This implies that the CTFB took place in the same range as TFB before fast fluidized bed.

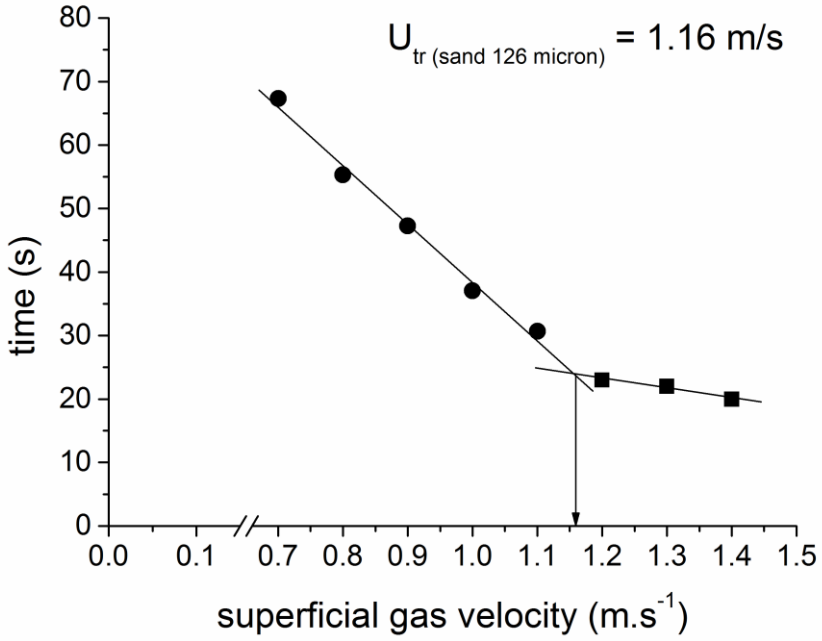

Figure 27 Transport velocity of 126 micron sand particle

4.1.1.2. Geldart Group A particle

Figure 28 shows the ε_s of PVC particles with average diameter of 164 micron. The movement of the bed noticed at lower U_g than either of size of sand. Because the PVC particles are smaller and lighter, the freeboard were observed at U_g of 0.2 m/s as shown in Figure 28 (a). The initial bed height was the same as sand particles but the bed of PVC slightly expanded with the increasing of U_g ranging: 0.2 to 1.0 m/s. The exit effect were found at the high value of U_g even in such a small condition of G_s (29

kg/s.m^2). This is due to the electrostatic charge taking place among PVC particles. Figure 28 (b) shows the effect of G_s at high U_g system of 1.1 m/s. ε_s in region I II and VI were dominated by G_s. In the region I, the ε_s dramatically increased together with the change in Gs but ε_s slightly increased in region II and VI.

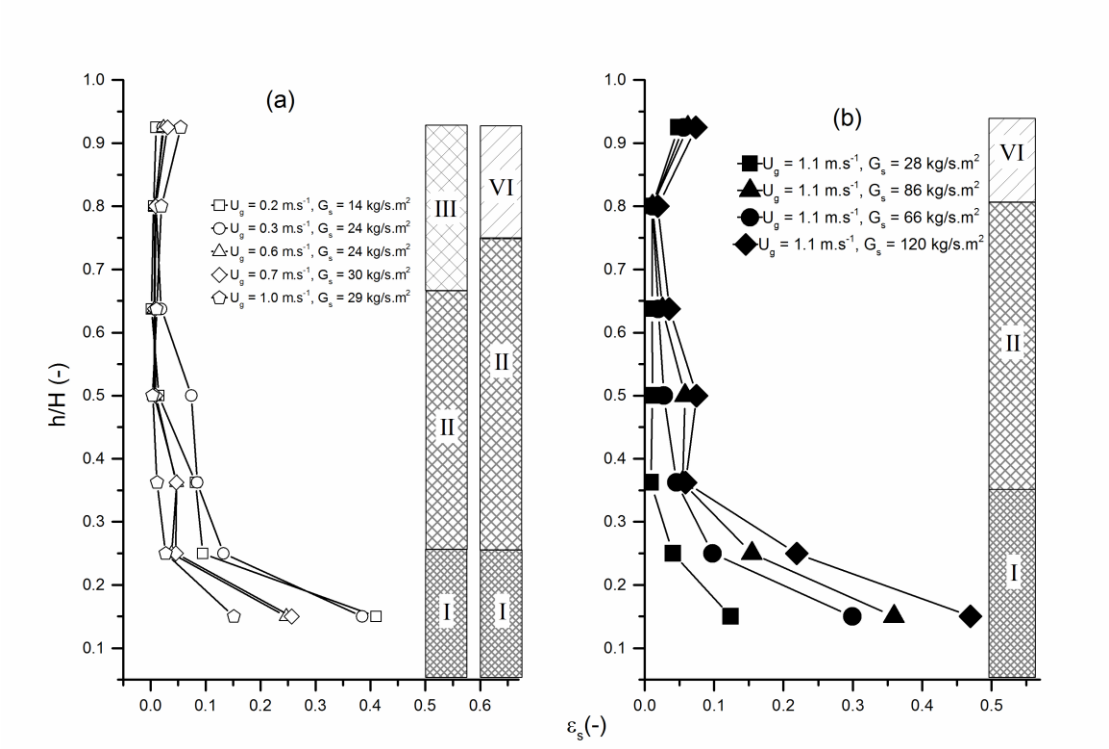

Figure 28 Solid volume fraction profile of 161 micron PVC

(a) Bed expansion at varying U_g and G_s

(b) Fast fluidized bed profile

When the PVC particles were operated under in TFB, particles collided with the riser walls. Friction and air resistance causes unbalanced on PVC particles. Electrostatic attractive force was generated by unlike charges, which then formed a particle cluster near to the walls region especially the riser top where PVC hit the wall harder. When

the clusters of PVC were formed, the particles had a large inter-particle force and agglomerated together, which reduced the particles ability to expand into the vertical direction as sand particles. Thus, the bed expansion was so small at low U_g and seemed to be unchanged at high U_g.

The intersection between the two different gradients in Figure 29 shows that the U_{tr} of the PVC particles is approximately 0.69 m/s. For U_g beyond U_{tr}, the fast fluidized regime took place at as shown in Figure 28 (b). The y-interception of region II was constant at 65 percent of riser height (h/H = 0.65) as shown in Figure 28 (a). Therefore, the bed expansion could be an alternative method to determine the transition between the TFB and fast fluidized bed as presented in sand particles. This could be concluded that the bed expansion was affected by U_g only in TFB, but not in the fast fluidized bed.

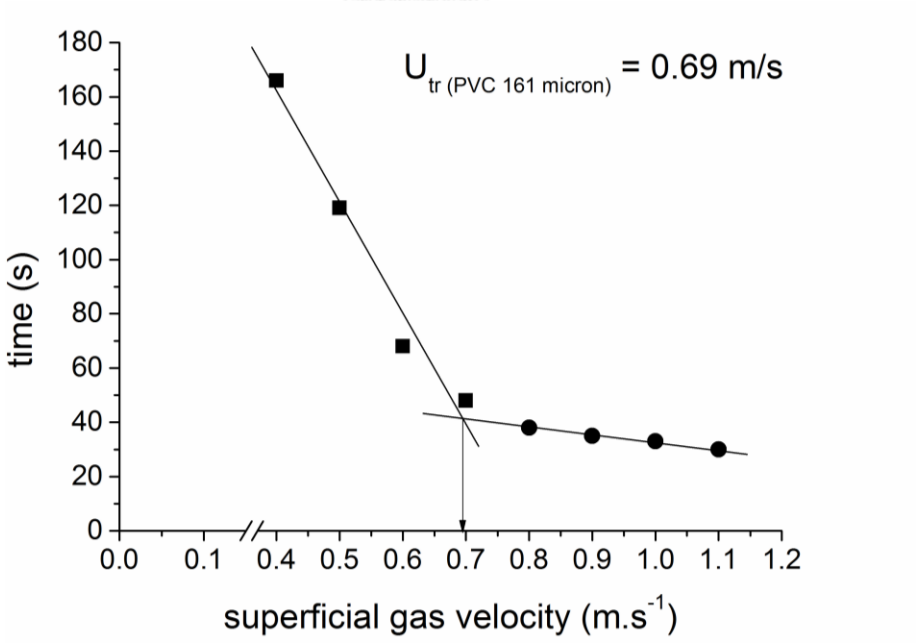

Figure 29 Transport velocity of 126 micron PVC particles

An appropriate height of the riser was an important factor to perform the CTFB in the single gas feed stage system. The bed could be developed until it was higher than the riser exit at the top of the riser. CTFB had been addressed with a high ε_s profile as a conventional turbulent fluidized bed together with the circulation of the particle to the cyclone. Performing the CTFB, the riser height must be lower than the maximum bed expansion height, which occurred when U_g was equal to U_{tr} which the highest U_g to maintain turbulent bed of TFB. If the designed riser height was higher than that the maximum bed expansion height, the fluidized bed would transform from a conventional turbulent fluidized bed regime to a fast fluidized bed regime without the existence of CTFB.

4.1.2 Identification of CTFB using flow regimes diagram

Figure 30 shows the position of CTFB on the parameter V^* versus the dimensionless $Ar^{1/3}$ on the conventional fluidization flow regime diagram. The Ar for 126 micron sand was 146 and that for 260 micron sand was 1352. Equation (8) was used to determine V^*. The position of V^* in the conventional turbulent fluidized bed region and uniform high solid fraction along the riser height without bed front confirmed the appearance of CTFB in a single feed state fluidized bed system. Therefore, the hydrodynamics is identical as the conventional turbulent fluidized bed. Furthermore, the system had very mixing property as TFB, but also circulated out of the riser to the cyclone like fast fluidized bed.

The results from this study also showed that a riser height lower than the maximum bed expansion is a crucial design parameter for performing CTFB in the circulating fluidized bed reactor with single feed state system. The maximum bed

expansion is approximated to be at the position of the front bed at U_{tr}. *Ar* and Geldart classification were expected to be the important factors that affected the maximum bed expansion of different solid particles [56].

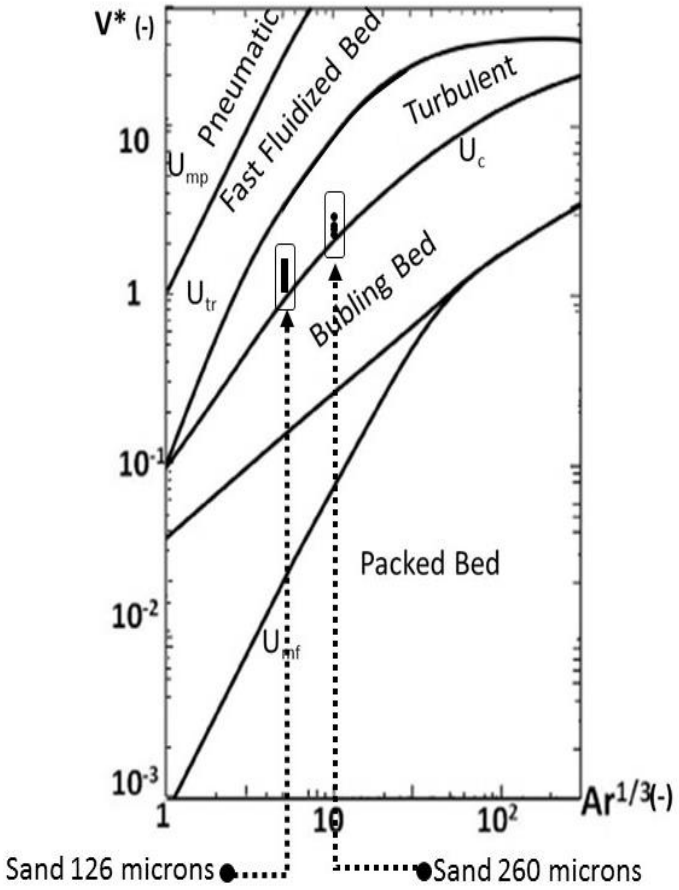

Figure 30 Position of CTFB on the flow regime diagram *[61]*

4.2. Optimum operating parameters of CO_2 adsorption in turbulent fluidized bed regime using potassium carbonate supported on gamma alumina solid sorbent

Turbulent fluidized bed regime is an attractive alternative to improve the performance of CO_2 adsorption using a solid sorbent because of its excellent mixing property of a gas phase and solid phase. The promising solid sorbent, potassium

carbonate (K_2CO_3), supported on gamma alumina (γ-Al_2O_3) was prepared through impregnation by insertion into the adsorption column to determine the optimum operating parameters. An adsorption temperature of 60 °C, superficial gas velocity of 0.22 m/s and initial sorbent loading of 5 g provided the highest CO_2 adsorption capacity of 295.79 mg of CO_2/ g of sorbent. 2^3 factorial design plus center points were used to analyze the result of the main effect and interaction between the operating parameters. From the obtained interpretation, interaction of sorption temperature with superficial gas velocity and adsorption temperature with initial sorbent loading had a statistically significant effect on CO_2 capture capacity. CO_2 adsorption profile was characterized by the similarity of breakthrough CO_2 adsorption capacity and total CO_2 capture capacity. The calculations showed that 87.8 percent of the active K_2CO_3 reacted with CO_2, and the content of CO_2 in the treated gas was reduced at a constant 18.8 percent of the initial concentration. This distinguishing breakthrough behavior provided a step forward to design a continuous reactor to capture CO_2 using a solid sorbent. However, a major obstacle for this design is the formation of Hydrated potassium dawsonite ($KAl(CO_3)(OH)_2H_2O$)), which always occurs in a fluidization reactor.

4.2.1. Statistical study to determine the optimum condition for CO_2 sorption

Table 9 shows the capture capacity of various sets of operating parameters. From the data, the range of capture capacity varied from 44 to 280 mg-CO_2/g-adsorbent. The 3 selected operating parameters had a strong effect on the CO_2 capture capacity of adsorbent. Focusing on the column titled "Loading" in Table 9, the low sorption capacity (less than 100 mg-CO_2/g-sorbent) resulted from sorbent loading larger than 5 g. The effect of sorption temperature was further investigated using the comparison of

2 pairs of the experiments; the first pair was Run 3 and Run 7, and the second pair was Run 1 together with Run 5. For the first pair, gas flow rate and sorbent load were kept at the same conditions at maximum value. The higher the temperature, the higher was the adsorption capacity. In comparison, the second pair was also subject to the same manner as the first; however, different results were obtained. The capture capacity of the first pair increased as the adsorption temperature increased, while the second pair showed the opposite result. Thus, it can be inferred that this contradiction is due to the interaction between parameters.

Table 9 Effect of operating parameters on sorption capacity

Run	AD. Temp [°c]	U_g [m/s]	Loading [g]	Capacity [mg-CO_2/g-sorbent]
1	50	0.31	5	249.21
2	50	0.31	15	97.79
3	50	0.13	5	100.66
4	50	0.13	15	44.07
5	70	0.31	5	131.84
6	70	0.31	15	103.73
7	70	0.13	5	149.07
8	70	0.13	15	77.17
9	60	0.22	10	104.99
10	60	0.22	5	279.95
11	60	0.22	15	75.02
12	60	0.13	10	90.78
13	60	0.31	10	96.85
14	70	0.22	10	125.7
15	50	0.22	10	91.12

Table 9 also shows that the maximum capture capacity was obtained by Run 10, which was operated on medium values of adsorption temperature and a gas flow rate of 60 °C and 0.22 m/s respectively with a minimum adsorbent loading of 5 g. The result

in Table 9 reveals some details about the effect of the operating parameters, but this is insufficent to determine the optimum operating parameters. Thus, statistical analysis of 2^3 factorial design plus center points was required to accomplish the research objective.

Table 10 Analysis of variance (ANOVA) of the capture capacity

Sources	Sum of squares	Degree of freedom	Mean Square	F-Value	P-Value
Model	2.7E-04	6	4.47E-05	16.86	0.0008
Ad. Temperature (A)	2.3E-05	1	2.34E-05	8.83	0.0208
Ug (B)	3.7E-05	1	3.69E-05	13.92	0.0074
Loading (C)	1.6E-04	1	1.55E-04	58.37	0.001
(A) + (B)	2.3E-05	1	2.33E-05	8.77	0.0211
(A) + (C)	2.1E-05	1	2.10E-05	7.93	0.0259
(B) + (C)	8.9E-06	1	8.89E-06	3.35	0.1089
Curvature	1.3E-05	1	1.27E-05	0.18	0.6875
Residual	2.7E-05	7	2.65E-06		
Total	5.8E-04	14			

The parameters that were relevant to the CO_2 sorption capacity were analyzed using the analysis of variance (ANOVA). Table 9 also shows that the maximum capture capacity was obtained by Run 10, which was operated on medium values of adsorption temperature and a gas flow rate of 60 °C and 0.22 m/s respectively with a minimum adsorbent loading of 5 g. The result in Table 9 reveals some details about the effect of the operating parameters, but this is insufficent to determine the optimum operating parameters. Thus, statistical analysis of 23 factorial design plus center points was required to accomplish the research objective. displays a summary of 2^3 factorial design analysis from the screened parameters obtained from the normal probability plot. The column titled “p-value”, with values less than 0.05, statistically demonstrates that those factors significantly affected CO_2 adsorption capacity. Table 10 also shows these factors are adsorption temperature (A), superficial gas velocity (B) and adsorbent

loading (C). The interaction between adsorption temperature and superficial gas velocity (AB) also played more important role than that between the adsorption temperature and superficial gas velocity (AC). Because there are no modifications on curvature, the regression model of capture capacity is represented in the first degree as shown in the following section.

The assessment of the adequacy of the model was supported by the analysis of normal probability and residual plot as shown in Figure 31. The optimum points, observed in Figure 32 (a) and (b), are influenced by adsorption temperature and superficial gas velocity respectively. Sorbent loading shows a trend that differs from those of the first two operating parameters, with increasing sorbent loading having a negative effect on the capture capacity.. In the normal plot shown in Figure 31 (a), all plots are laid on an imaginary straight line, which implies that predicted values were close to the experimental results. Moreover, the acceptance of the model was confirmed by the residual plot in Figure 31 (b), which showed no obvious pattern in the data distribution.

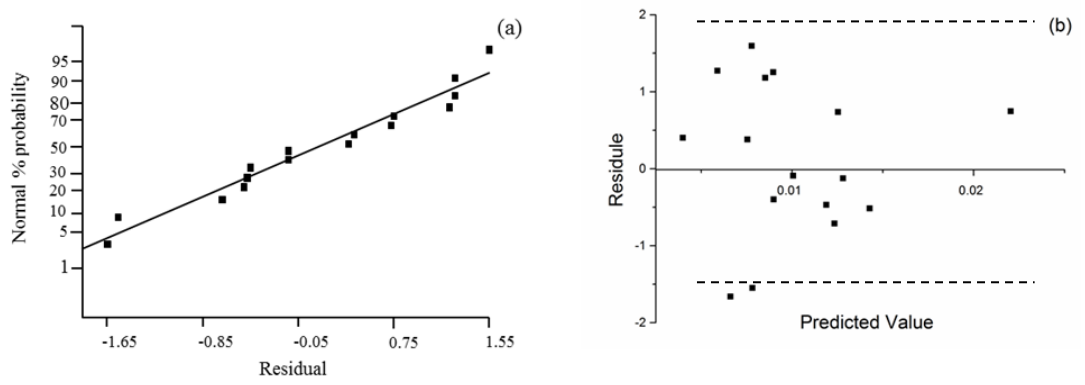

Figure 31 Assessment of the adequacy of regression model

(a) Normal probability vs. residual

(b) Residual vs. predicted value

The main effect graphs were the plots between the inverse of CO_2 capture capacity and each of the individual operating parameters while keeping other untested parameters at median value, as shown in Figure 32. The optimum points, observed in Figure 32 (a) and (b), are influenced by adsorption temperature and superficial gas velocity respectively. Sorbent loading shows a trend that differs from those of the first two operating parameters, with increasing sorbent loading having a negative effect on the capture capacity.

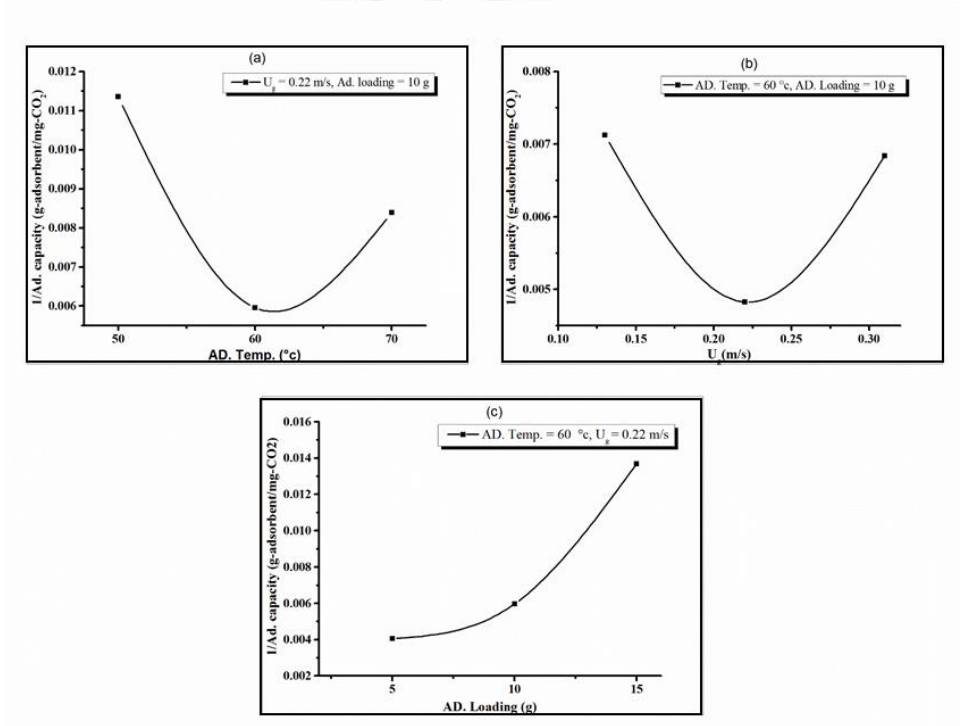

Figure 32 Main effect of operating parameters

(a) Effect of adsorption temperature

(b) Effect of superficial gas velocity

(c) Sorbent loading

Focusing on Figure 32 (a), increasing adsorption temperature from 50 °C to 60 °C encourages CO_2 adsorption capacity, but once the temperature passes 60 °C to 70 °C, the trend changes in the opposite direction. Chemical kinetics of adsorption and thermodynamics are the concepts which account for this phenomenon. At the first period of increasing temperature, heat added provides sufficient energy to the system. The increase in kinetic energy allows gaseous molecules to diffuse through the gas film that covers sorbent particle. In addition, a portion of the energy was used to overcome the activation energy of adsorption. However, thermodynamics dominated the system when the adsorption temperature was higher than 60 °C [9]. Due to the exothermic chemical equilibrium of adsorption, increase in adsorption temperature caused the equilibrium to shift backward. Thus, the CO_2 adsorption capacity was reduced after the optimum temperature at 60 °C.

The transport phenomena could be used to explain the optimum superficial gas velocity in Figure 32 (b). Here, the thickness of gas film resistance is seen to decrease when velocity of gas increases in the first period. The gas molecule took a shorter time to reach the active site on the support. Thus, the increasing gas velocity from 0.11 m/s to 0. 22 improves the mixing properties between gas and solid phase which demonstrated by higher the capture capacity. On the contrary, in the turbulent fluidization regime, when gas velocity is introduced faster than this optimum value, it creates a more expanded turbulent bed. The expansion of the bed at a constant initial sorbent loading is caused by the void between particles and low residence time. This ultimately results in low mixing properties, which lead to low CO_2 capture capacity in the second period of increasing gas velocity (0.22 to 0.33 m/s). Thus, the result shows

the optimal value for superficial gas velocity at 0.22 m/s for the maximum CO_2 capture capacity.

As seen in Figure 32 (c), higher sorbent loading is characterized by poor mixing properties. Fluidized bed occurs when the summation of upward force (drag force) and buoyancy force are larger than particle weight (downward force). Increasing the amount of sorbent at constant superficial gas velocity reduces the magnitude of upward force that distributes on the sorbent particles. As a result, particles had less mobility. Thus, only a few regions in the higher loading system could enhance adsorption, with some of the regions in the higher loading system performing adsorption very well. Meanwhile, the rest of the regions performed poorly.

The merit of the ANOVA table is that it identifies the interaction between operating parameters that are statistically significant. The interaction between adsorption temperature and superficial gas velocity is shown in Figure 33 (a) – (c) are plots between pairs of operating parameters at their maximum and minimum values versus the inverse value of capture capacity, while the other parameters are plotted according to their average values.

The interaction between adsorption temperature and superficial gas velocity is shown in Figure 33 (a). At minimum gas velocity, increase in temperature promotes adsorption reaction. Once again, mass transport can be appropriately explained by the graphs in Figure 33 (a). Because of the occurrence of a thick film gas layer at lower superficial gas velocity, gas molecules require higher temperature for kinetic energy to diffuse through the resistance film and react with the active site on the sorbent surface. Under excess energy at higher temperature, the chemical equilibrium shifts backward.

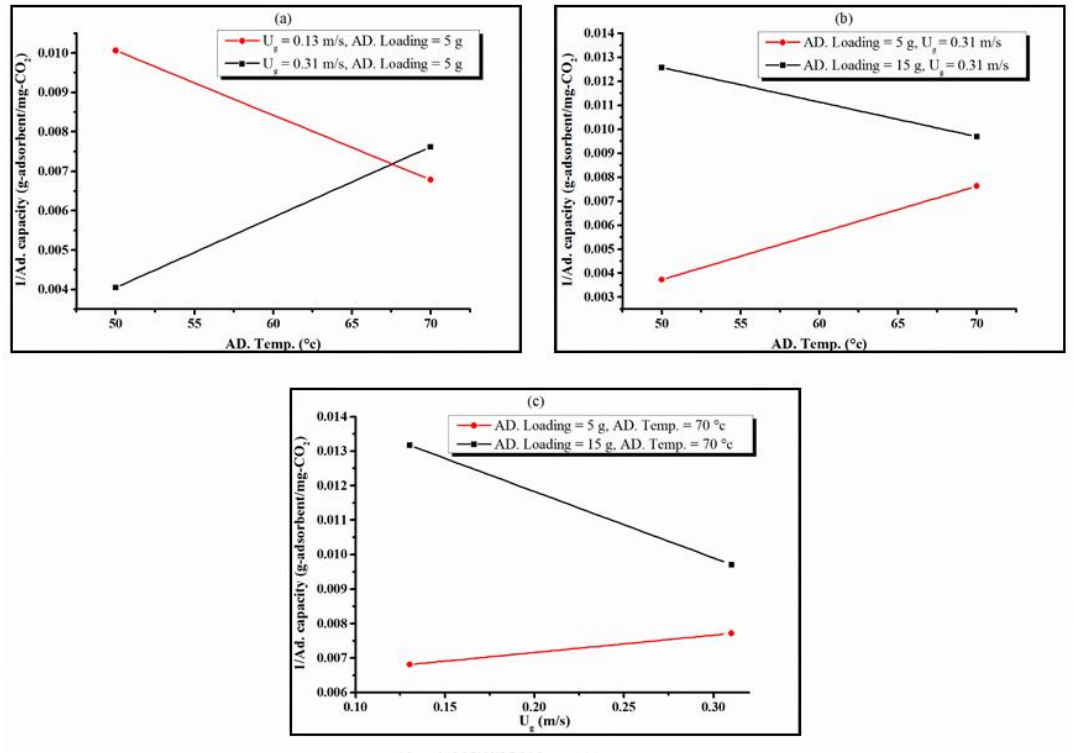

Figure 33 Interaction effect between operating parameters

(a) Interaction of adsorption temperature and superficial gas velocity

(b) Interaction of adsorption temperature and sorbent loading

(c) Interaction of superficial gas velocity and sorbent loading

Figure 33 (b) shows the interaction between sorbent loading and adsorption temperature. Higher loading at the constant of gas velocity led to poorer mixing properties. Increasing adsorption temperature, though, could compensate for the negative impact of the high sorbent loading system. Due to the additional heat in the system, gas molecules gained more kinetic energy and moved faster at higher temperature. This ultimately increased the probability for CO_2 to be captured by K_2CO_3 on γ-Al_2O_3.

The results of the interaction between sorbent loading and gas velocity are presented in Figure 33 (c). At sorbent loading of 15 g, increasing gas velocity provides a higher sorption capacity. This implies that gas velocity provides more opportunity for CO_2 to be adsorbed due to the reduction of the film layer as well as better mixing in the turbulent bed. Thus, the enhanced capture capacity was affected by the superficial gas velocity. The major concern is that the negative effect of gas velocity which is occurred at lower sorbent loading of 5 g. Increasing gas velocity causes the dilute turbulent bed which leads to the less mixing property between gas and solid phase.

The obtained results then provided fundamental groundwork for the design of a fluidized bed reactor for heterogeneous reactions. The operating temperature played a significant role in the perspectives of transport phenomena, kinetics and thermodynamics. Moreover, it could be used to optimize the system when the system was subject to increase in superficial gas velocity and sorbent loading. The highest adsorption capacity was 295.79 mg of CO_2/g of sorbent which was obtained by Run 10.

Figure 34 shows the concentration profile of CO_2 with respect to time in the adsorption column. Within the first 19 seconds, 81.2 percent of CO_2 was captured by the sorbent. The concentration of treated gas is then equivalent to its initial concentration (12 % volume). Calculating the amount of the initial loading of 18 percent active species on the support revealed that the CO_2 capacity obtained from Run 10 was about 87.8 percent of maximum CO_2 captured capacity. Thus, this validated that turbulent fluidized bed regime could overcome the limitation of mass transport in a heterogeneous reaction.

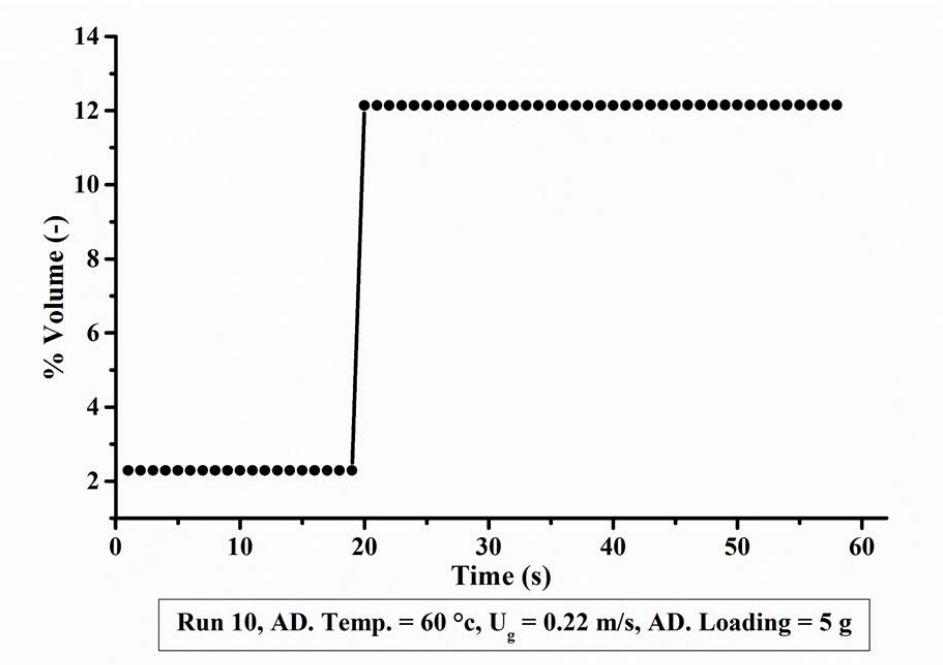

Figure 34 Breakthrough curve of the optimum operating condition

Focusing on the 19th and 20th seconds of the adsorption time, the concentration of CO_2 abruptly shifted back to its initial feed concentration. Thus, the adsorption profile of CO_2 in the turbulent fluidized bed regime was characterized by the equivalent of breakthrough CO_2 capture capacity and total CO_2 capture capacity. This outstanding adsorption profile is a promising characteristic for designing a continuous process to capture CO_2 using solid sorbent. The adsorption risers could be placed in series while sharing only a single unit of the regenerator. The results obtained from this work validate the possibility of further study on designing a circulating fluidized bed adsorption reactor using solid sorbent.

4.2.2. Characterization study of the sorbent

Figure 35 shows XRD patterns of the sorbent both before and after the adsorption in Run 10. The pattern of fresh sorbent demonstrates the peaks of K_2CO_3

and γ- Al_2O_3. After adsorption, species of $KHCO_3$ and potassium dawsonite ($KAl(CO_3)(OH)_2$) were found [36]. The appearance of $KHCO_3$ confirmed the completion of the reaction as shown in equation (1), but the appearance of dawsonite did not. Dawsonite is a byproduct of the adsorption taking place in both the fixed bed and fluidized bed systems.

The mechanism of dawsonite formation in the adsorption process is still not fully understood. Due to its high thermal stability, dawsonite is a major obstacle to sorbent regeneration. There have been several researchers who have successfully improved impregnation to avoid dawsonite[18, 36, 103]. Using the sorbent obtained from those modified impregnation methods in the optimum operating parameters obtained from this work will be a step forward closer in the study of CO_2 capture storage technology.

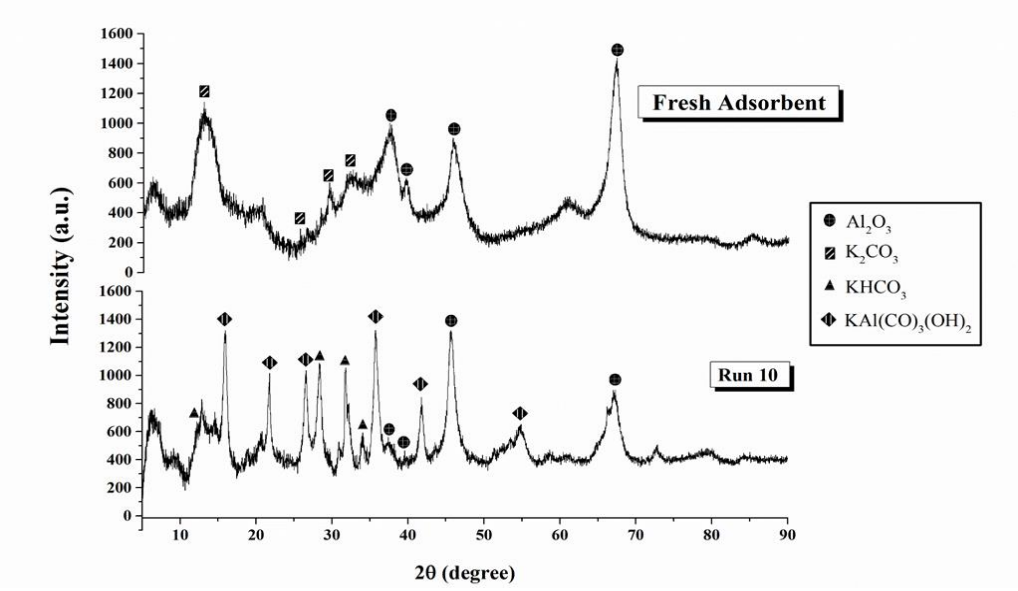

Figure 35 XRD pattern of sorbent before and after CO_2 adsorption

4.3. Effect of operating parameters of sorbent potassium carbonate supported on gamma alumina (K_2CO_3/γ-Al_2O_3) on CO_2 capture capacity using conventional heat regeneration

4.3.1. Statistical analysis (2^3 factorial design) of the heat regeneration operating parameter

The effect of regeneration operating parameters and their interactions on CO_2 fluidization adsorption system was mainly evaluated by capture capacity which directly displays the amount of CO_2 in unit of milligram per gram of active site (or sorbent). The results from the varying parameters in the certain range using 2^3 factorial design analyses are shown in

Table 11. The maximum CO_2 adsorption capacity of 355.62 mg-CO_2/g-sorbent obtained from Run 8 which all operating parameters were kept at the maximum values. The lowest range of CO_2 adsorption capacity (less than 100 mg-CO_2/g-sorbent) were tendency to be provided by the low value of regeneration temperature, together with long duration of regeneration (Run 3, Run 4 and Run 9). Other combinations of regeneration temperature and time caused the medium values of CO_2 adsorption capacity (100-300 mg-CO_2/g-sorbent).

The normal probability plot in Figure 36 was used to screen out the effected operating parameters and interactions that had statistical meaning to the change of CO_2 adsorption capacity. Due to the deviation from the normal line, regeneration temperature and regeneration time and their interaction were considered as the effected parameters.

The result from Figure 36 shows that the main effect of regeneration cycle and its interaction are located in the linear trend of the normal line. Regeneration cycle has no effect to the CO_2 adsorption capacity. Thus, the sorbent which has been prepared and passed the adsorption process following the explanations in the Methodology is re-useable by the application of heat regeneration processes.

Table 12 shows that all of effected parameters and interaction analyzed by normal probability plot had P- value less than 0. 05. Thus, the results of normal probability plot were verified. Focusing on the P-value, the value that is much less than 0. 05, the more influence it has on an output. This could be concluded that interaction between regeneration temperature and regeneration time and the main effect of regeneration temperature have the same degree on the change of the adsorption capacity which is much higher than the main effect of the regeneration time.

Table 11 Effect of operating regeneration parameters to CO_2 capture capacity

Run	*A*	*B*	*C*	Capture capacity (mg-CO_2/g-sorbent)
1	-1	-1	-1	194.65
2	-1	-1	1	186.03
3	-1	1	-1	84.30
4	-1	1	1	97.84
5	1	-1	-1	133.99
6	1	-1	1	142.01
7	1	1	-1	331.02
8	1	1	1	355.62
9	-1	1	0	84.56
10	1	-1	0	132.74
11	1	1	0	313.67
12	-1	-1	0	250.38

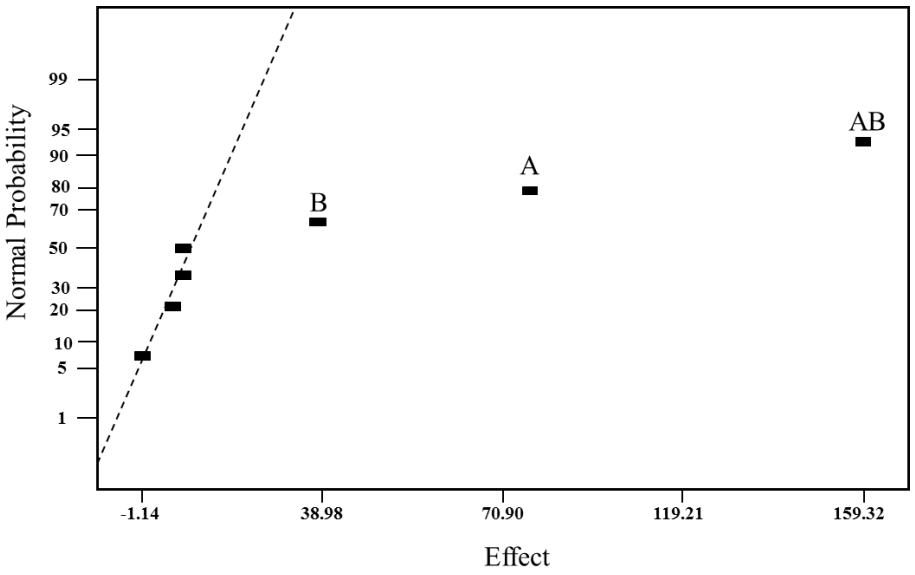

Figure 36 Normal probability plot of effected parameters

Table 12 The analysis of variance (ANOVA) of the heat regeneration operating parameters

Sources	Sum of squares	Degree of freedom	Mean Square	F-Value	P-Value
Model	1.02E+05	3	34079.21	77.91	0.0001
A	2.18E+04	1	21784.93	49.81	0.0001
B	4.30E+03	1	4302.51	9.84	0.0139
AB	7.62E+04	1	76150.18	174.10	0.0001
Residual	3.50E+03	8	437.40		
Total	1.06E+05	11			

Figure 37 shows an influence of main effect parameters and their interaction on CO_2 adsorption capacity. Main effect graphs were the plots between the CO_2 capture capacity and each of the individual operating parameters while keeping other untested parameters at their average values. Increasing in regeneration temperature and

regeneration time exhibit the positive trend to the magnitude of CO_2 adsorption capacity as shown in Figure 37 (a) and (b). The intersection as shown in Figure 37 (a) clearly displays the interaction of regeneration temperature and regeneration time. The regeneration temperature has a positive effect on CO2 adsorption capacity when increasing regeneration temperature, while keeping the regeneration time at high value. On the other hand, while keeping the regeneration time at low value increasing regeneration temperature shows negative effect on CO2 adsorption capacity respectively. Focusing on their gradients, the effect of regeneration temperature has steeper slope than the effect of regeneration time.

The intersection as shown in Figure 37 clearly displays the interaction of regeneration temperature and regeneration time. The regeneration temperature has a positive effect on CO_2 adsorption capacity when increasing regeneration temperature, while keeping the regeneration time at high value. On the other hand, while keeping the regeneration time at low value increasing regeneration temperature shows negative effect on CO_2 adsorption capacity.

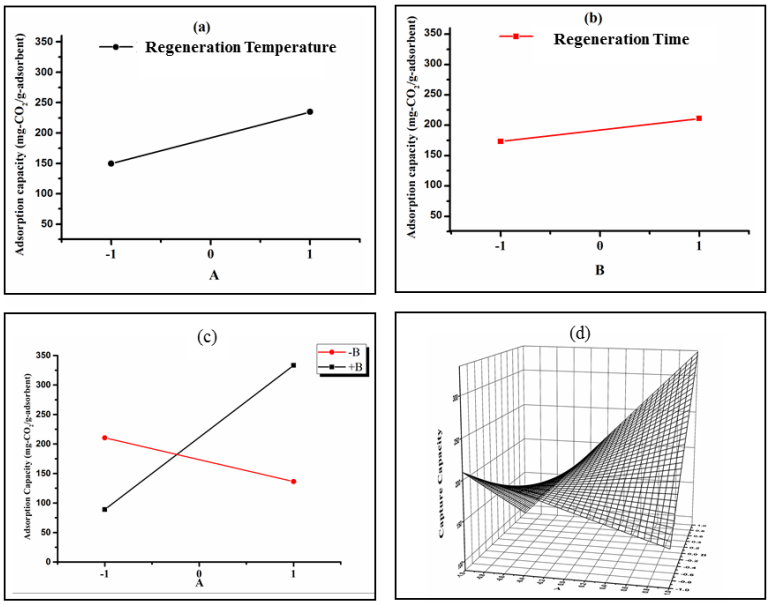

Figure 37 Effect of operating heat regeneration parameters and interaction

(a) Effect of regeneration temperature

(b) Effect of regeneration time

(c) Interaction effect between operating parameters

(d) Response surface

The response surface shown in Figure 37 (d) constructed by a regression models in equation (41) represents the CO_2 capture capacity (Y) as the function of the regeneration operating parameters in coded form.

$$Y(A,B) = 192.23 + 42.61A + 18.94B + 79.66AB \qquad (41)$$

The model above was tested for accuracy by evaluating the residual and revealed no severe indication of non- normality, nor any possible of an outlier or inequalities of variance in addition to a clear agreement with the predicted values. The

maximum CO_2 capture capacity was found at the operating parameters of high regeneration temperature and regeneration time.

Due to the curvature of the response surface, the capture capacity was increased when both regeneration temperature and regeneration time were decreased. The regeneration process at low regeneration temperature and regeneration time might be an alternative method to design a continuous adsorption unit using a solid sorbent. Since the sorbent in the continuous unit does not fully utilize its CO_2 capture capacity, as it does in case of the batch processes such as fixed bed, bubbling bed and turbulent bed, thus the energy and time requirements for the sorbent regeneration will be less than those required in the batch processes.

4.3.2. Adsorption characterization of the sorbent regenerated with heat

Figure 38 shows concentration profiles of CO_2 with respect to time of simulated gas which passed the sorption process. CO_2 capture capacity of the sorbent which passed various heat regeneration conditions were labelled on each concentration profile. Figure 38 (a) displays concentration profile of the treated gas leaving the column that was loaded by fresh sorbent. Within the first 23 seconds, 89.42 percent of CO_2 was captured by the sorbent. The concentration of treated gas was then equivalent to its initial concentration (12 % ± 1 % volume). Then, the concentration of CO_2 abruptly shifted back to its initial feed concentration. The capture capacity of the fresh sorbent was used as the reference value to compare the effectiveness of those operating regeneration conditions.

Thermal mass decomposition of the fresh sorbent by the STA was chosen to explain the interaction between regeneration temperature and regeneration time. In (b)

– (d) exhibit the concentration profiles of varying regeneration conditions of the first, the second and the third regenerations, respectively. The CO_2 capture capacity of the sorbent after passing heat regeneration was briefly estimated from the size of the space between y-axis and the filled area. In each regeneration cycle, the CO_2 capture capacity was ranked from excellent, good, fair and poor by the condition of both high regeneration temperature and regeneration time (+A,+B), the condition of both low regeneration temperature and regeneration time (-A,-B), the condition of high regeneration temperature together with low regeneration time (+A-B) and the condition of low regeneration temperature but high regeneration time (-A,+B). Focusing on CO_2 capture capacity of each heat regeneration condition, the magnitudes are independence from the number of the regeneration cycles as mentioned in the statistical analysis.

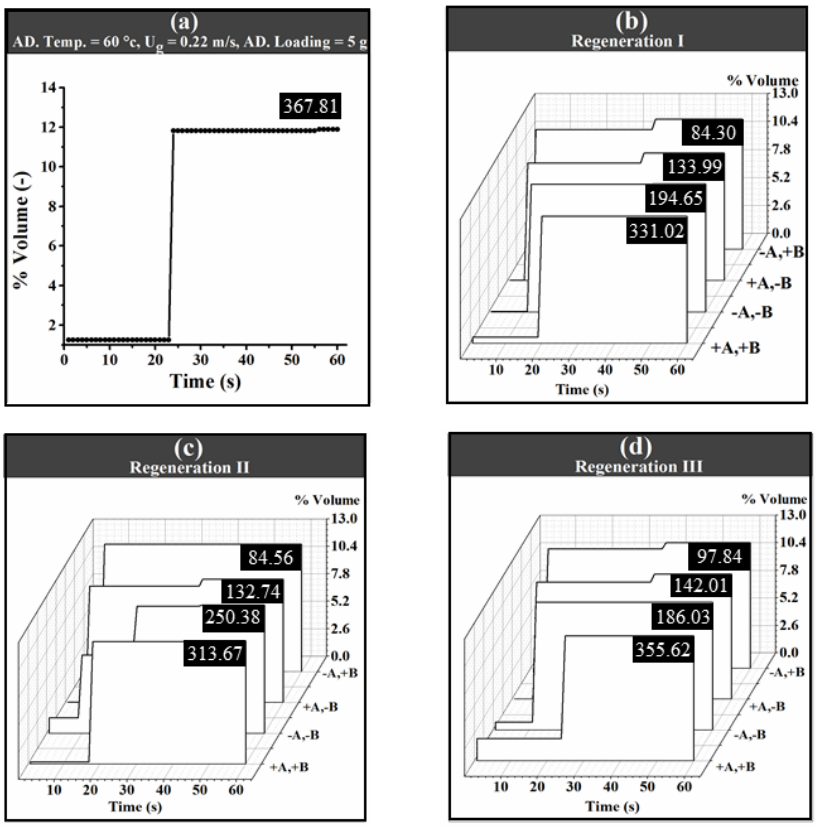

Figure 38 Sorption capacity of heat regenerated sorbent

(a) Fresh sorbent

(b) Regeneration I sorbent

(c) Regeneration II sorbent

(d) Regeneration III sorbent

Thermal mass decomposition of the fresh sorbent by the STA was chosen to explain the interaction between regeneration temperature and regeneration time. In Figure 39, normally, the application of hydro treatment on the sorbent before enrering CO_2 sorption process causes low regeneration temperature (120°C - 150°C) [18]. Thus, $KHCO_3$ could be converted to K_2CO_3 at the low value of regeneration temperature in this study. The poorest CO_2 adsorption capacity was found with the regeneration

condition of both low regeneration temperature and time. As the result obtained from Figure 38 (a), the long regeneration time removed entire surface water as shown in the schematic moisture diagram of Figure 39 (b), the DG curve shows the major change of mass 3.53% and 3.32% more which occurs at the temperature lower than 100 °C and in the range between 225 – 275 °C, respectively. The DTG curve is used to characterize the peak of the major changes. Due to the loss of surface waters, the first major change was characterized by the peak which located at 94.6 °C. In the porous materials, the loss of inter structural water which covered the surface in the deeper inner pore, dominated the major loss in the range of temperature 200 – 400 °C. For the γ-Al_2O_3 support, inter structural water was characterized by the peaks at 236.1 and 271.6 °C.

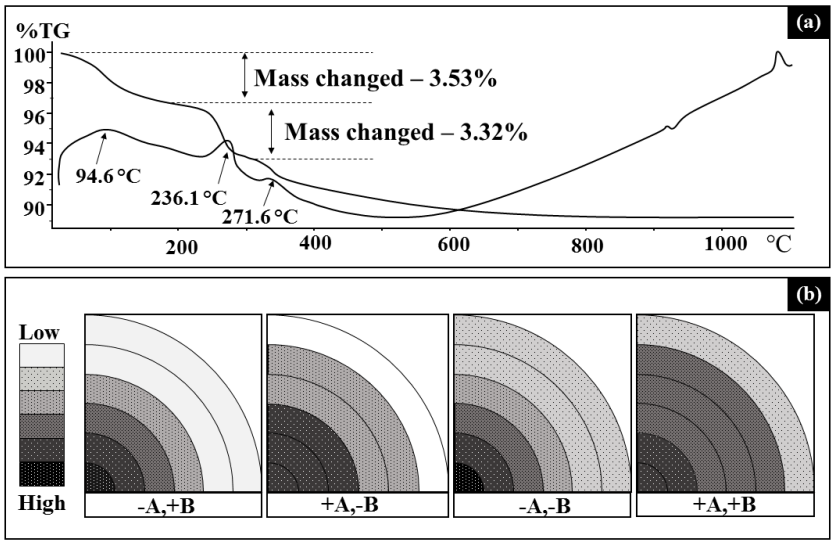

Figure 39 Thermal decomposition of the sorbent

(a) TG and DTG curves

(b) Schematic moisture diagram

The fair CO_2 sorption capacity occurred at the regeneration condition of high regeneration temperature together short regeneration time. At this high temperature, the

surface water was removed. Due to the short period of regeneration time, some inter structural water which remove from the deeper locations of the pore but did not have enough time to diffuse out of the pore. The remained water covered some part of the sorbent surface which helps promote the CO_2 adsorption reaction in the next cycle.

At both low regeneration temperature and regeneration time provided the good CO_2 adsorption capacity because this temperature is sufficient to reverse the thermal equilibrium of adsorption reaction and the heat is not high enough to evaporate the unreacted surface water which promotes the adsorption reaction in the next cycles.

The excellent CO_2 adsorption capacity was found at the condition of both high regeneration temperature and regeneration time. The applied heat at high temperature for a long regeneration time could remove a lot of inter structural water in the deep inner pore. Those unreacted water occupied on the surface of sorbent. The relegalization of the inter structural water respect to the regeneration temperature and regeneration time could be the explanation of the interaction.

4.3.3. Economical perspective of using heat regeneration

Table 13 displays the energy that is used in the varying regeneration condition. The regeneration time was provided into 2 periods. The first period was used to elevate the regeneration temperature with the ramp rate of 3 °C /min. The second period was the holdup time (regeneration time, B). The recovery percent was the ratio of the average CO_2 capture capacity of 3 cycles to the capture capacity of the fresh sorbent. The last column represents the energy that has been used in each trail which obtained from the multiplication between ramp power of the furnace and ramp time added with the multiplication between hold power and regeneration time.

Table 13 Energy intensity using by regeneration

Regeneration conditions	Ramp time (minute)	Holdup time (minute)	Recovery (%)	Energy (kilojoule)
(-A,-B)	56.7	2.0	57.2	8,093
(-A,+B)	56.7	20.0	24.2	10,037
(+A,-B)	90.0	2.0	37.0	12,726
(+A,+B)	90.0	20.0	90.7	14,670

The results from the Table 13 shows that the excellence CO_2 recovery of 90.7 % required the highest regeneration energy. As mentioned in the previously section, not only the regeneration condition of both low regeneration temperature and regeneration time provided such a good CO_2 capture capacity but also some the less energy compare to those regeneration conditions. The recovery percent is just about 30% behind but it consumed almost a half less than the energy that used in the best one. Thus, this would be the optimization which would become the ground work design of sorbent regeneration unit using heat.

The optimum operating condition which obtained from this work will be used as the boundary condition in computational fluid dynamic code to design an alternative for CO_2 sorption reactor. The continuous sorption will design as circulating fluidization reactor. The kinetic data of CO_2 sorption will be used to design the height of riser-sorber and determine the minimum amount of sorbent. After that optimum regeneration temperature and regeneration time will provide the sufficient information to design the dimension of the downer-heat regenerator. Solid recirculating rate between riser-sorber

and downer-heat regenerator will be the scaling factor for the application in various size of coal power plant.

4.4. Effect of operating parameters of potassium carbonate supported on gamma alumina (K_2CO_3/γ-Al_2O_3) on CO_2 capture capacity using depressurized regeneration

From the statistical analysis, potassium carbonate (K_2CO_3) supported on gamma alumina (γ-Al_2O_3), which prepared through impregnation method and employed to adsorb CO_2 under turbulent fluidized bed regime in a glass riser-sorber, could be regenerated by the depressurized regeneration. The sorption capacity of CO_2 was not depended on regeneration time and regeneration cycle. The P-value of regeneration pressure less than 0.05 showed its significant effect on the CO_2 sorption capacity for the next sorption There was no trace element of inactive species, $KAl(CO_3)(OH)_2H_2O$) on the regenerated sorbent. The obtained meso-pore type IV surface area did not affect by the regeneration cycle. The CO_2 capture capacity depended on the moisture which remained on the sorbent surface. The accumulation of water near the pore entrance reduced the average pore diameter and increased the average pore volume after passing the regeneration cycle with low depressurization degree. The regenerated sorbent could be used to adsorb about 95 percentage of the capture capacity obtained from the fresh sorbent at depressurized regeneration level of 0.2 atm and short regeneration time.

4.4.1. CO_2 capture capacity of depressurization regenerated sorbent

The effect of regeneration operating parameters and their interactions on CO_2 fluidization sorption system was mainly evaluated by capture capacity which directly displayed amount of CO_2 in unit of milligram per gram of active site (or sorbent). The

results from the varying parameters in the certain range using 2^3 factorial design analyses are shown in Table 14. The maximum CO_2 adsorption capacity of 365.09 mg-CO_2/g-sorbent was obtained from Run 7 which obtained from the first regeneration and operating parameters were kept at the maximum values.

Figure 40 (b) – (d) exhibit the concentration profiles of varying regeneration conditions of the first, the second and the third cycles, respectively. The CO_2 capture capacity of each operation was briefly estimated from the area between y-axis and the filled area. In each regeneration cycle, the CO_2 capture capacity was high when the regeneration operated at high depressurization degree (+A). The lower CO_2 capacity was observed when the depressurization was kept at low level (-A). The regeneration time between the experimental range had slightly affected on the sorption capacity at condition +A, but had large effect at condition -A.

Figure 41 compares the CO_2 capture capacity of each regeneration condition with the variation of the regeneration cycle to the value obtained from the sorption of the fresh sorbent. The high level of depressurization with high and low regeneration time is shown in Figure 41 (a) and (b), respectively. The capacity after regeneration with the operation of high depressurization degree was slightly lower than the capture capacity obtained from the fresh sorbent. Therefore, the regeneration cycle had no effect to the capture capacity or the capture capacity was independence from the regeneration cycle. In addition, the sorbent which has been prepared and utilized in the sorption process can be re-usable by the application of depressurized regeneration processes.

Table 14 Effect of depressurization operating regeneration parameters to CO_2 capture capacity

Run	*A*	*B*	*C*	Capture capacity (mg-CO_2/g-sorbent)
1	-1	-1	-1	265.64
2	-1	-1	1	65.96
3	-1	1	-1	195.55
4	-1	1	1	226.41
5	1	-1	-1	355.92
6	1	-1	1	340.36
7	1	1	-1	365.09
8	1	1	1	339.48
9	-1	1	0	360.13
10	1	-1	0	300.59
11	1	1	0	348.26
12	-1	-1	0	81.65

Where; A is regeneration temperature which ranged in the between 0.8 to 0.2 atm, xB is regeneration time which ranged in the between 2 to 20 minute, C is regeneration cycle which operated for 3 cycles.

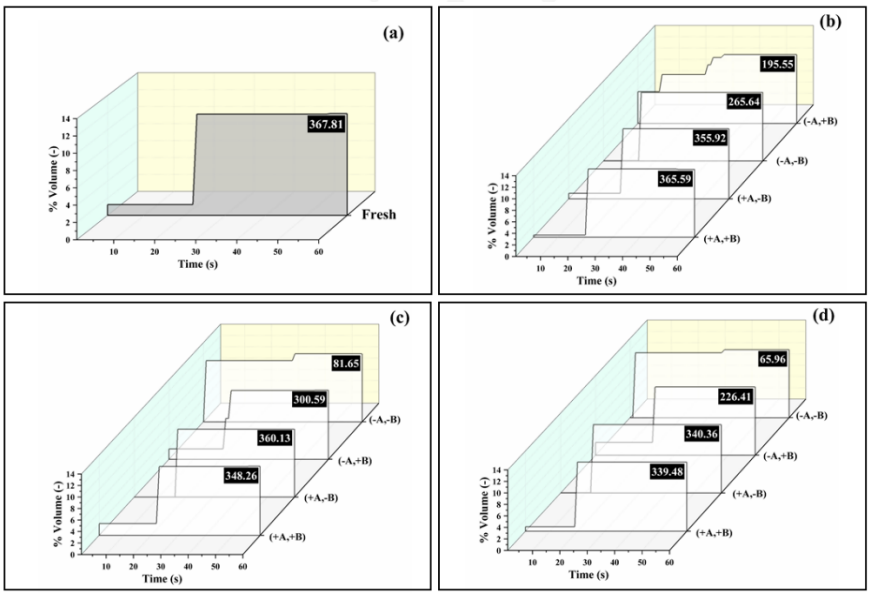

Figure 40 Breakthrough curves of depressurizatio of regenerated sorbent

(a) Fresh sorbent

(b) Regeneration I sorbent

(c) Regeneration II sorbent

(d) Regeneration III sorbent

About the effect of regeneration cycle in the low level of depressurization, the (-A, +B) condition provided the fair sorption capacity in the range of 195 to 300 mg-CO_2/g-sorbent. The trend of sorption capacity obtained from (-A,-B) condition was different from those regeneration conditions which exhibited the decreasing in capture capacity with the next regeneration cycle.

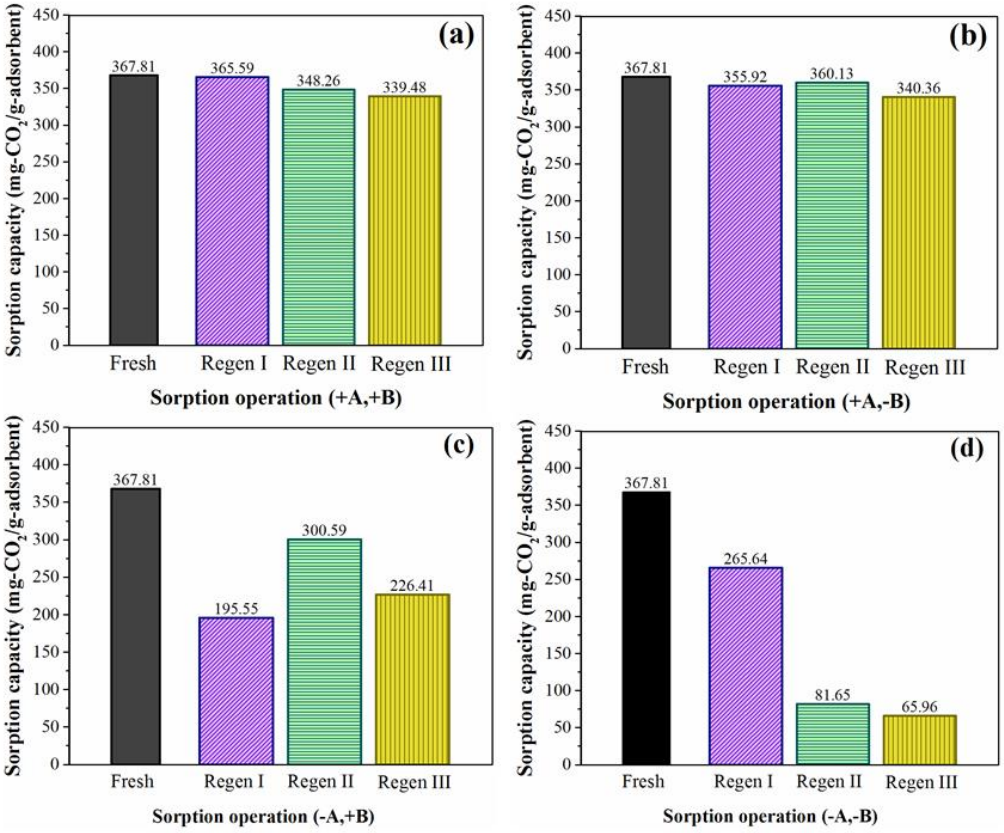

Figure 41 The effect of depressurized regeneration cycle

(a) Regeneration condition (+A,+B)

(b) Regeneration condition (+A,-B)

(c) Regeneration condition (-A,+B)

(d) Regeneration condition (-A,-B)

4. 4. 2. Statistical analysis (2^3 factorial design (plus four runs)) for the depressurized regeneration operating parameters

Due to the complexity in data interpretation, 2^3 factorial design (plus four runs) analyses had been used to determine the effect of each regeneration parameters to CO_2 sorption capacity. The data were transformed by square root. Then, the normal probability plot in Figure 42 was used to screen out the significant operating parameters of the depressurized regeneration. Due to the deviation from the normal line, only regeneration pressure was selected to consider its important degree. Therefore, the regeneration time and regeneration cycle had no effect on the CO_2 adsorption capacity.

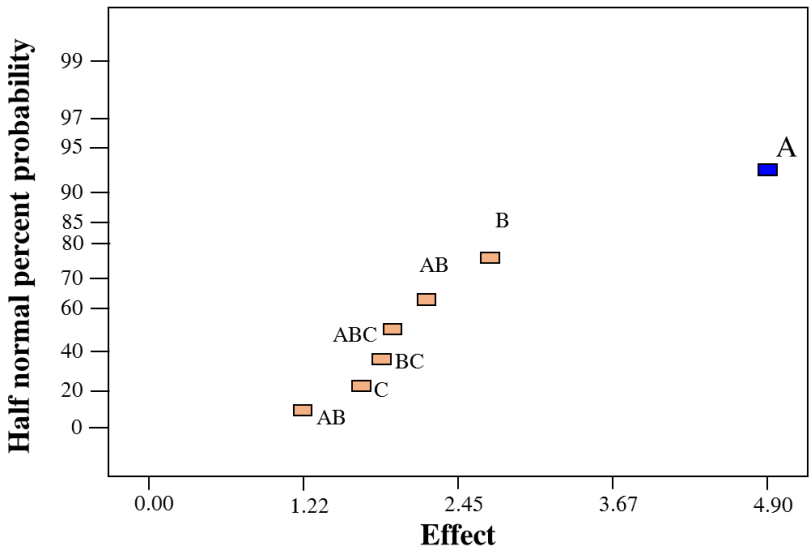

Figure 42 Normal probability plot of depressurized regeneration parameters.

Analysis of variance (ANOVA) of 2^3 factorial experimental design (plus four runs) was applied to determine the degree of significance for each affected parameter to a CO_2 concentration output of the experiment. The results are shown in Table 15. Regeneration pressure was the only parameters obtained from the normal probability plot which has P-value less than 0.05. Also, this could be confirmed that regeneration time and regeneration cycle did not have the statistical meaning to the CO_2 capture capacity.

Table 15 The analysis of variance (ANOVA) of depressurization regenerated sorbent

Sources	Sum of squares	Degree of freedom	Mean Square	F-Value	P-Value
Model	71.94	1	71.94	7.89	0.0185
A	71.94	1	71.94	7.89	0.0185
Residual	91.16	10	6.93		
Total	163.10	11			

Figure 43 shows an influence of main effects on the CO_2 adsorption capacity. Due to the data transformation, the main effect graphs were the plots between the square root of CO_2 capture capacity and each of the average individual operating parameter. Increasing regeneration depressurized level and regeneration time exhibited the positive trend to the magnitude of CO_2 adsorption capacity as shown in Figure 43 (a) and (b), respectively. Increasing the degree of depressurization increased the output ranging from 14.1 to 18.5; on the other hand, increasing regeneration time showed slightly less positive trend ranging from 15.3 to 17.8. The effect of regeneration cycle

is shown in Figure 43 (c). Increasing the regeneration cycle affected the output in the same range as regeneration time but in the opposite direction trend. Due to the results as shown in the Figure 43, the range that affected by the regeneration time and regeneration cycle did not have statistical significant to the square root of the sorption capture capacity. Therefore, the depressurization concept can be considered as an alternative method for the compact size regeneration unit at the same sorption temperature of 60 °C which was suitable for a continuous sorption-regeneration unit.

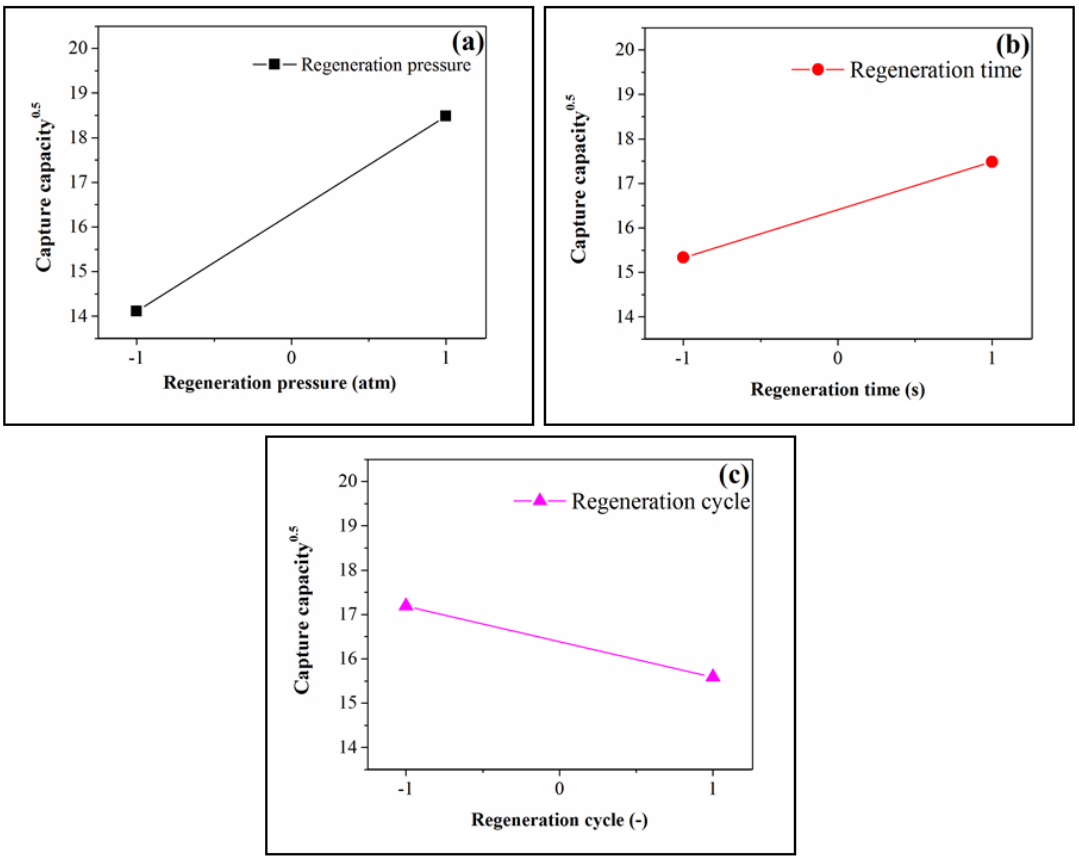

Figure 43 Effect of depressurization operating parameters and their interactions

(a) Effect of regeneration pressure

(b) Effect of regeneration time

(c) Effect of regeneration cycle

4.4.3. Sorbent characterization of depressurization regenerated sorbent

In this part, the reasons for the good sorption capacity obtained from (+A,+B) condition and the poor sorption capacity obtained from (-A,-B) were explained. Figure 44 shows texture properties of fresh sorbent and the spent sorbent after the third regeneration. The (a) showed the fresh sorbent had sharper spike than the regenerated sorbents since it was higher crystallinity. After sorption and regeneration for several times, the sorbents reduced their crystallinity. However, the shape of the peaks from (+A,+B) and (-A,-B) condition were similar. In summary, the particle crystallinity thus did not affect the sorption capture capacity.

Normally in heat regeneration, the low sorption capacity was caused by the formation of a high thermal stability species, ($KAl(CO_3)(OH)_2H_2O$) by an unwanted side reaction. This species required more energy to convert ($KAl(CO_3)(OH)_2H_2O$) back to the active species K_2CO_3. This inactive species reduced surface coverage of the active site which led to poorer sorption at the next regeneration cycle. However, the inactive species formation can be prevented by the hydro-treatment by adding the water to sorbent surface before starting the sorption as proposed in this study. Consequently, there was no observation of such a trace of the inactive species pattern in the regenerated sorbent.

The FTIR patterns help differentiate the trace of the other kind of inactive species by detecting the difference in absorbed energy by different kind of bonding. Figure 44 shows FTIR pattern which displayed the same results as those obtained from the XRD pattern. The shape absorbance pattern of fresh sorbent was different from the regenerated sorbents but the location of the peaks was about the same. There were no

observation of the difference in the shape and the location of each peak obtained from the different regeneration conditions. Thus, the capture capacity did not only affect by the less particle crystallinity and the formation of the inactive species as expected.

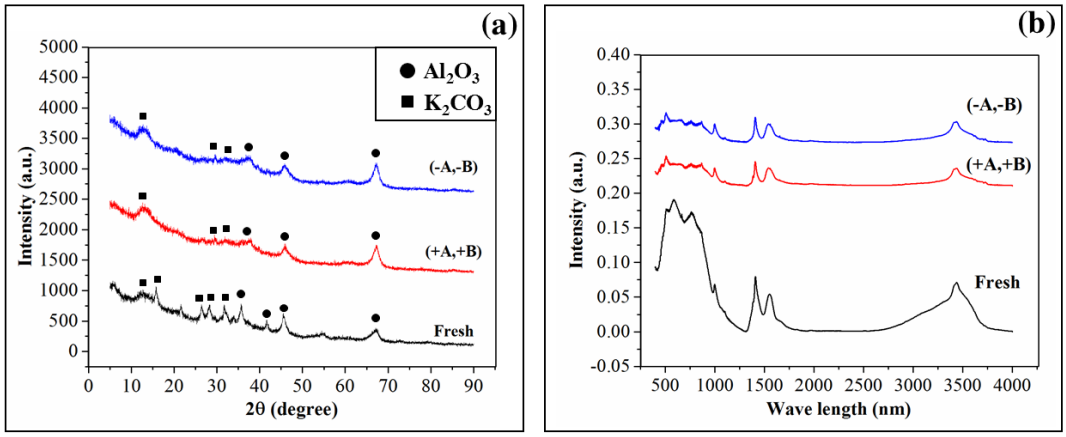

Figure 44 Textural properties depressurization regenerated sorbent

(a) XRD pattern

(b) FTIR pattern

Figure 45 shows the N_2 adsorption isotherm of sorbent particles. The numbers in each figure represented BET surface area in the unit of m^2 per gram of sorbent particle. The support γ-Al_2O_3 had the highest surface area as shown in Figure 45 (a). After the impregnation, the surface area reduced about 31 percentage to 84 m^2/ g as shown in Figure 45 (b) because some sorbent surface was occupied by active species. The isotherms in condition (+A,+B) and (-A,-B) were displayed in Figure 45 (c) and (d), respectively. After passing through three regeneration cycles, the regenerated sorbent still had the same surface area as the fresh sorbent.

The hysteresis of sorption isotherm shown in Figure 45 reflected the pore type of the sorbent to be the meso-pore type IV which characterized by the bent at the low

pressure and hysteresis loop at the high pressure. This pore type was composed by the various pore sizes mainly in the meso-pore range. The impregnation and depressurized regeneration did not change the pore type. Thus, the change in sorption capacity was proved not to cause by the change in both surface area and pore type.

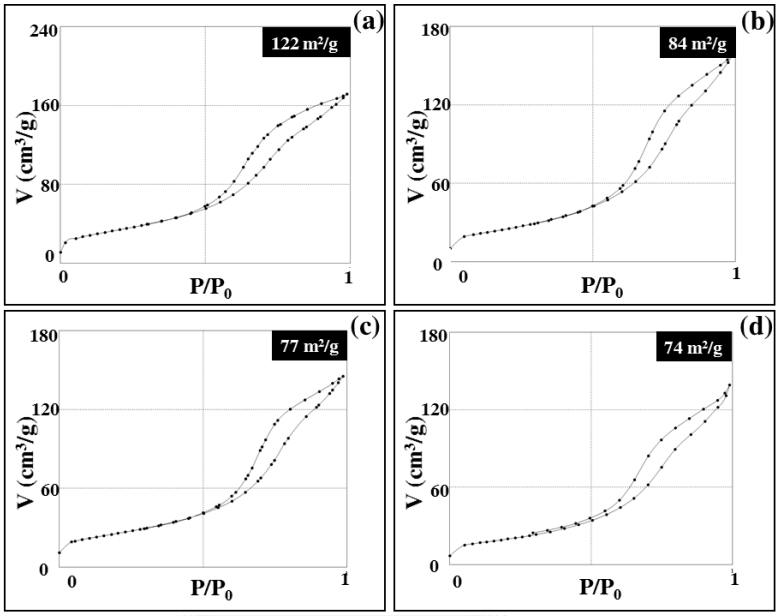

Figure 45 Nitrogen sorption isotherm of the drpressurization regenerated sorbent

(a) Support γ-Al_2O_3

(b) Fresh sorbent

(c) The third regenerated sorbent from condition (+A,+B)

(d) The third regenerated sorbent from condition (-A,-B)

The interpretation of N_2 sorption isotherm provided more details of the pore of the sorbent with different regeneration conditions. Figure 46 (a) shows the average pore diameter of sorbent with different regeneration conditions. The more regeneration cycle, the smaller pore diameter was observed. Also, the decreasing trend of the diameter of (+A,+B) regeneration condition was less than the (-A,-B) regeneration

condition. As the result of no inactive species, no change in the textural properties, the delocalization of surface water might be the cause of the poorer sorption capacity at the lower depressurization degree.

Figure 46 presents an average pore volume of sorbent with different regeneration conditions. The averages pore volume of the regenerated sorbent were independence of the regeneration cycles when the system was operated with (+A,+B) regeneration condition. The variation of pore volumes was in the range of 17 – 24 cm^3 per gram of sorbent with (-A,-B) condition. For the average pore volume, it was increased with the regeneration cycle which started from 17 to 27 cm^3 per gram of sorbent. This became the hypothesis is that the increasing in average pore volume led to the poor sorption capacity in the regenerated sorbent. The details and the proves of the assumption will be explained in the next section.

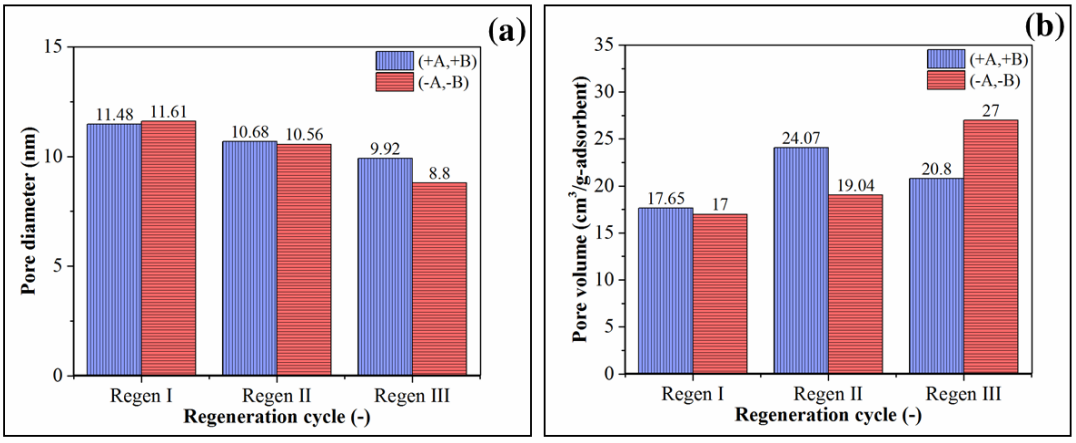

Figure 46 Pore analysis of the drpressurization regenerated sorbent

(a) Average pore diameter

(b) Average pore volume

4.4.4. Delocalization of the surface water hypothesis

From all the results, mass transfer was summarized as a rate limiting step for CO_2 sorption when using solid sorbent. The hydro treatment process was considered to increase the amount of water on sorbent surface. Based on the results as shown in sorbent characterization section and the delocalization of the surface water hypothesis, the possible schematic diagram, to explain the effect of depressurized regeneration on the sorbent pore with different operating conditions was drawn as shown in Figure 47.

Figure 47 (a) shows the meso-pore of sorbent which was covered by the surface water (water 1 and water 2). The thickness of the water layer was increased by the hydro treatment before performing the sorption in the riser-sorber. Depressurization can shift the equilibrium backward as shown in equation (1) and also reduces amount of water on the sorbent surface. Therefore, the thickness of water layer became thinner as shown in Figure 47 (b). In this study, the vacuum pump was used to reduce the pressure in the sorber-riser which was loaded with the used sorbent and, then immediately followed by the hydro treatment for two minutes. Some water would be added on the regenerated sorbent (water 3) as shown in Figure 47 (c) and (d).

Under the (+A,+B) regeneration condition, the pressure was reduced to 0.2 atm. Therefore, the regenerated sorbent could pull the water back into the deeper pore than when the operation took place at 0.8 atm. The weak force at the low depressurization degree allowed some water to cover on the surface outside the pore. This water was substituted for the loss water during the regeneration. The amount of water which was pulled back into the pore could consider being the same amount as the one before the regeneration due to small change of the average pore diameter and poring volume when the regeneration operated under the high depressurization degree.

At lower depressurization degree, only small amount of water was pulled back into the pores as shown in Figure 47 (d). Due to the weak pull back force, the water could not reach the deeper position in the pore to compensate the loss water during the regeneration. The water was accumulated only at the entrance of the pore leading to the increase of average pore volume but the decrease of the average pore diameter.

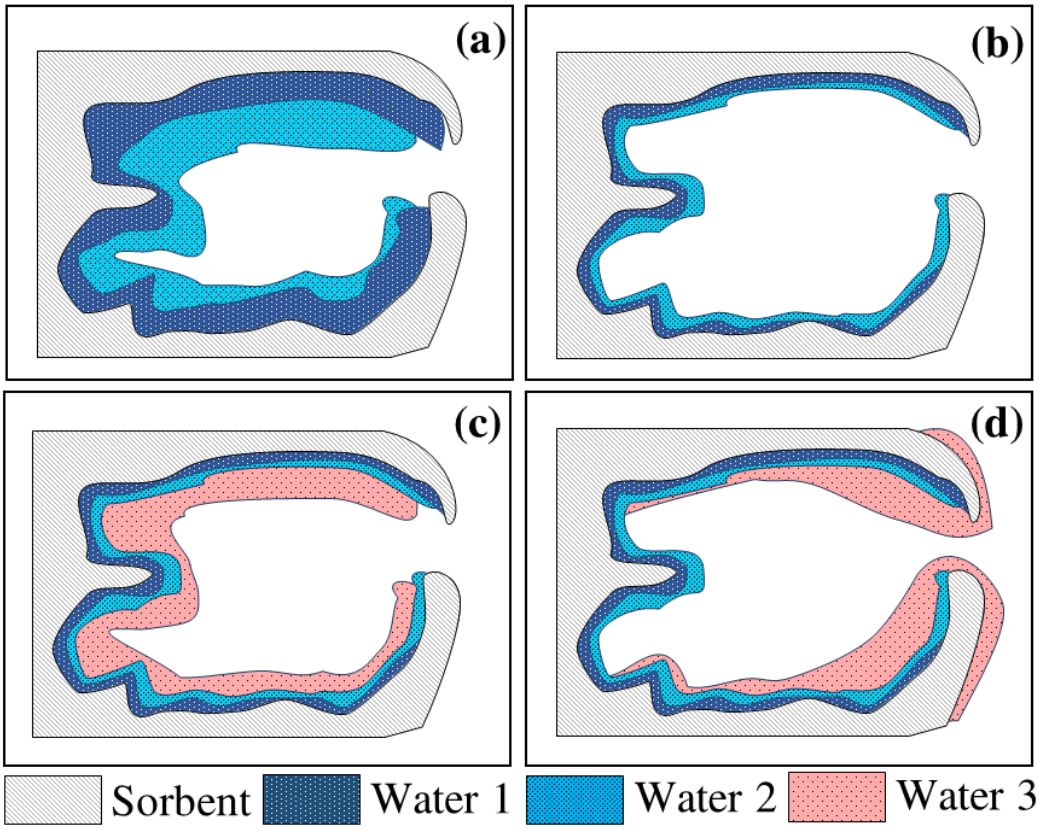

Figure 47 Schematic diagram of water on depressurization regenerated sorbents

(a) Fresh sorbent

(b) Regenerated sorbent

(c) Regenerated sorbent with (+A,+B) condition after hydro treatment

(d) Regenerated sorbent with (-A,-B) condition after hydro treatment

TG (Thermogravimetric analysis) and DTG (Differential thermogravimetric analysis) curves in Figure 48 were used to confirm the above proposed explanation. Mass decomposition with the progressive temperature is shown in the TG curve. The heating rate was 3 °C per minute, ranging from 30 to 1100 °C. The gradients of TG curve of each temperature were plotted as the DTG curve. The peak location on DTG curve was used to determine oxidation stage of the particles. The sorbent in this study had such a good thermal stability. Therefore, the oxidation stage at the temperature less than 300 °C was due to the loss of water from the particle surface.

Figure 48 (a) shows the curve of the sorbent which obtained from the high depressurization level. Mass decomposition of 6.15 percent was characterized by the DTG peak at temperature of 89.3 °C which was represented the major loss of the water. Figure 48 (b) shows the curves for the sorbent which generated under the low depressurization level. The mass decomposition was separated into two parts. The first decomposition of 1.68 percent was characterized by the peak at 53.9 °C on the DTG curve and the major mass loss of 5.56 percentage characterized by the peak at 106.0 °C.

The peaks on DTG curve can be used to show the location of the remained water after passing the regeneration and the hydro treatment. The higher temperature peak represented the water on the sorbent surface in the deeper location of the sorbent pore. Therefore, the interpretation for the single peak as seen in Figure 48 (a) was that the water was removed from the same location. But, the double peaks on Figure 48 (b) illustrated that water was removed from the two different locations.

The mass decomposition results confirmed the hypothesis of the remaining water on regenerated sorbent surface as shown in Figure 47. The single peak of the DTG curve was due to the decomposition of water in the meso-pore. On the other hand, the first peak at the lower temperature as shown in Figure 48 (b) was the loss of the water which attached on the surface outside the pore, while the major mass loss of the water was due to the decomposition of the water in the pore.

The low regeneration properties which led to the low capture capacity in this study was not caused by the inactive species as mentioned in the Introduction part but the location of water deposition. For the poor capture capacity sorbent, the active site located outside of the pore and the entrance of the pore where it was reacted with CO_2 to form the $KHCO_3$. Then, the solid product from the sorption blocked the pore. Consequently, the active site inside the pores could not react with the CO_2 which was the main cause of the low capture capacity when the low depressurization degree was applied as the regeneration method.

The main point for the sorbent generation for CO_2 sorption was not only the prevention of the formation of the unwanted inactive species but also the appropriate method to deal with the remained water on the sorbent. The sorbent should be moistening with the water in the pore to prevent the blocking of the solid sorption product. The accumulation position of the remained water could be adjusted by using high depressurization regeneration degree.

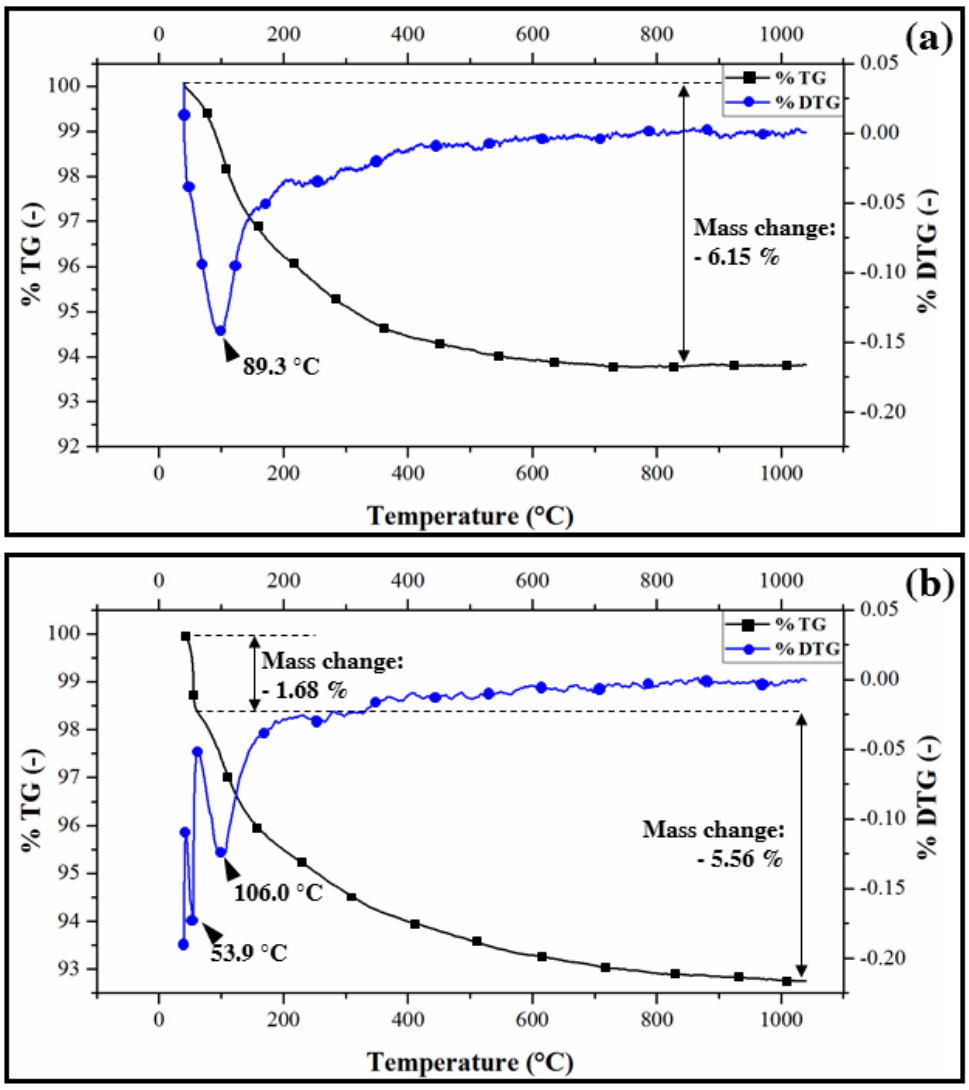

Figure 48 Thermal decomposition depressurization regenerated sorbents

(a) TG and DTG curves for high regeneration pressure

(b) TG and DTG curves for low regeneration pressure

4.5. CO_2 sorption in circulating fluidized bed reactor under circulating turbulent fluidized bed

The effect of operating parameters and their interactions on CO_2 in CTFB was mainly evaluated by capturing capacity which directly displays amount of CO_2 in unit of milligram per gram of active site (or sorbent). The results from the varying

parameters in the certain range using 2^4 factorial design analyses is shown in Table 16. The maximum CO_2 adsorption capacity of 170.34 mg-CO_2/g-sorbent obtained from Run 2 which gas velocity was kept at maximum value but all the rest operating parameters were kept at the minimum values. The poor range of CO_2 adsorption capacity (less than 90 mg-CO_2/g-sorbent) tendency provided by the maximum value of solid recirculating rate. Other combinations of the fair sorption capacity approximately around 100 mg-CO_2/g-sorbent which consider as pair sorption capacity.

The normal probability plot in Figure 49 was used to screen out the effect of operating parameters and interactions that had statistical meaning to the change of CO_2 sorption capacity. The result from the Figure 49 shows that the main effect of *A* and *C* have high effect to the capture capacity. The interaction *AC*, *AD* and *BCD* affect the capture capacity. Due to the selection of interaction *BCD*, the interaction *BC*, *CD* and *BD* together of the main effects B and *D* were also selected to the test their effect by using analysis of variance.

Analysis of variance (ANOVA) of 2^4 factorial experimental design was applied to determine the degree of significance of the parameters and their interaction to an output of the experiment. All of the effected parameters and interactions were analyzed by using P-value. The results of the analysis of variance is shown in Table 17. Parameters which provided the P-value less than 0.05 is considered as statistically effected parameter to the interested output. Thus, the results of normal probability plot were verified. Focusing on the P-value, the much lower value than 0.05, the higher influence it has on an output.

Table 16 Effect of depressurized operating regeneration parameters on CO_2 capture capacity

Run	A	B	C	D	CO_2 capture Capacity (mg-CO_2/g-sorbent)
1	1	102	600	1	47.21
2	1.5	50	300	1	170.34
3	1	102	300	12	144.13
4	1	50	300	12	129.74
5	1.5	50	600	12	104.34
6	1.5	102	300	12	134.36
7	1	50	300	1	125.04
8	1	102	300	1	89.17
9	1.5	102	300	1	117.60
10	1	50	600	12	67.39
11	1.5	50	600	1	102.91
12	1.5	102	600	12	84.72
13	1	102	600	12	54.67
14	1.5	50	300	12	141.95
15	1.5	102	600	1	135.66
16	1	50	600	1	40.54

Where; A is superficial gas velocity which ranged in the between 1 to 1.5 m/s, B is solid circulation rate which ranged in the between 50 to 100 $kg/m^2.s$, C is the initial sorbent loading which ranged in the between 300 to 600 g and D is depressurized regeneration time which ranged in the between 1 to 12 minute.

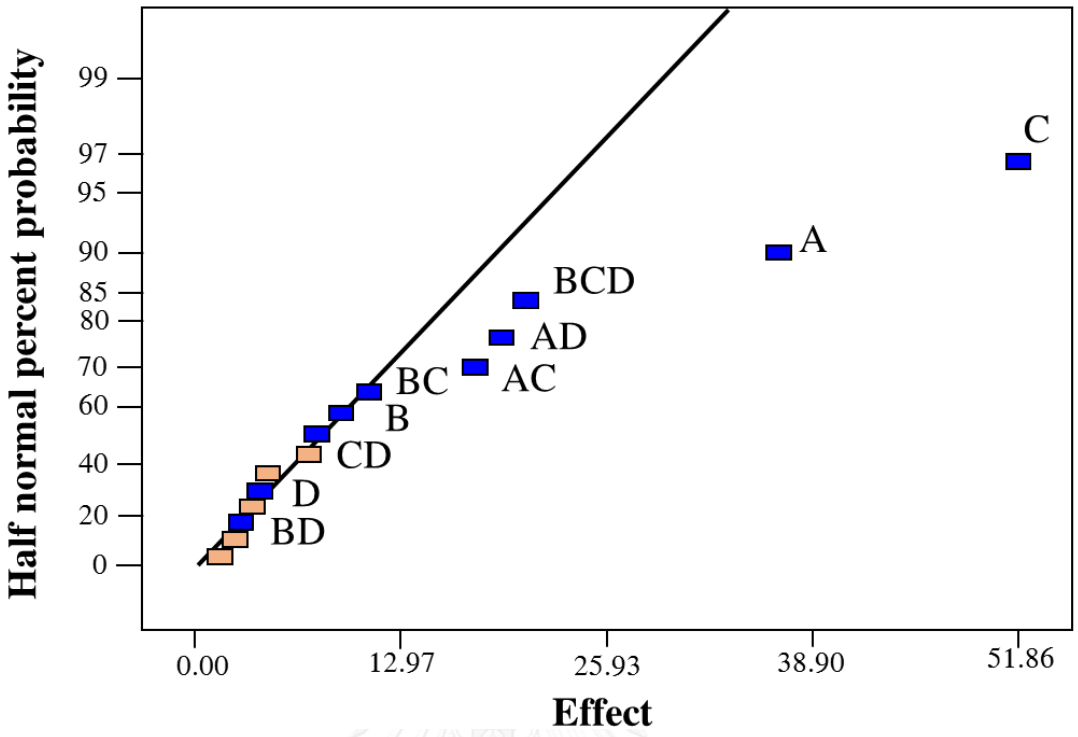

Figure 49 Normal probability plot of effected parameters for CO_2 sorption in CTFB

From Figure 49, it could be concluded that only the main effect of *A* and *C* and the interaction of *AC*, *AD* and *BCD* have significant effect on the capture capacity. In the range of operation as shown in Table 17, the initial sorbent loading has more effect than the inlet gas velocity while the effected interactions are in the same level on each other.

Figure 50 shows the main effect of each operating parameters with the CO_2 sorption capacity. The positive trend of superficial gas velocity to the output is shown in Figure 50 (a). Gas velocity in this study; ranging in circulating turbulent fluidization regime, affect to the mixing property. The more gas velocity increase, the more kinetic energy of the sorbent increase. This is a cause of the good mixing property at higher superficial gas velocity.

Table 17 The analysis of variance (ANOVA) of the capture capacity using CTFB

Sources	Sum of squares	Degree of freedom	Mean Square	F-value	P-value
Model	21859.05	10	2185.91	28.49	0.0009
A	5401.09	1	5401.09	70.40	0.0004
B	349.14	1	349.14	4.55	0.0861
C	10758.45	1	10758.45	140.23	<0.0001
D	67.37	1	67.37	0.88	0.3917
AC	1254.20	1	1254.20	16.35	0.0099
AD	1504.09	1	1504.09	19.60	0.0068
BC	493.74	1	493.74	6.44	0.0521
BD	34.98	1	34.98	0.46	0.5295
CD	249.84	1	249.84	3.26	0.1310
BCD	1746.14	1	1746.14	22.76	0.0050
Residual	383.61	5	76.72		
Total	22242.66	15			

Solid recirculating rate is one of the main effect that shows the negative trend to the output as shown in Figure 50 (b). This surprise trend are also explained by the mixing property. Normally, the more recirculating rate *B*, the more solid fraction in the riser increase. Thus, at the high solid recirculating rate, the kinetic energy which dissipated on each individual particle was decreased. This lead to the lack of moving

ability and then form a cluster. The cluster formation reduces the rate of CO_2 sorption because the rate limiting step for CO_2 sorption using solid metal carbonate sorbent is the step that CO_2 transfers through to the cluster to reach the active site on the sorbent.

Figure 50 (c) shows the main effect of the initial sorbent loading which also exhibited the negative trend to capture capacity as same as *B*. However, the reason of the poor capture capacity when it has high initial sorbent loading could not explain by the mixing properties. After each trail of the experiments, the packing sorbent were found at the downer bottom. The more initial loading, the more accumulation were found. Thus, there were some of active sorbents that did not circulate to capture CO_2 in the sorber-riser as expected. The design of the downer regenerator in this study was not applicable in larger scale because the initial sorbent loading is not independent on the capture capacity. There are two ways to reduce the effect of the initial sorbent loading. First, the active sorbent must be compressed as pellet. However, the shape and the size of the pellet is the crucial in the future study for the commercialized scale. If the same sized of the sorbent particle will be used, another way is the application of CFD to determine the appropriate dimension of the downer and its inclination for the downer bottom.

The regeneration time of depressurized regeneration is independence of the sorption capacity as shown in Figure 50 (d). The trend is considered as a promise trend to develop the circulating fluidized bed for CO_2 sorption. The short regeneration time is easily achieved by the compact size regeneration downer. The CFD is such a powerful tool to find the design is that reach the criteria.

The effected interactions which were screened out by the analysis of variance are shown in Figure 51. Increasing superficial gas velocity while keeping initial sorbent loading and the regeneration time at the minimum or the maximum value provide the higher capture capacity. Moreover, there is the limit of the gas velocity that could not exceed the transport velocity (U_{tr}) which is the highest velocity to perform CTFB. If A greater than U_{tr}, the fast fluidized bed which was characterized by a core annular will take place in the sorber-riser. This fluidization regime has such a low mixing property and also provides poor CO_2 sorption capacity.

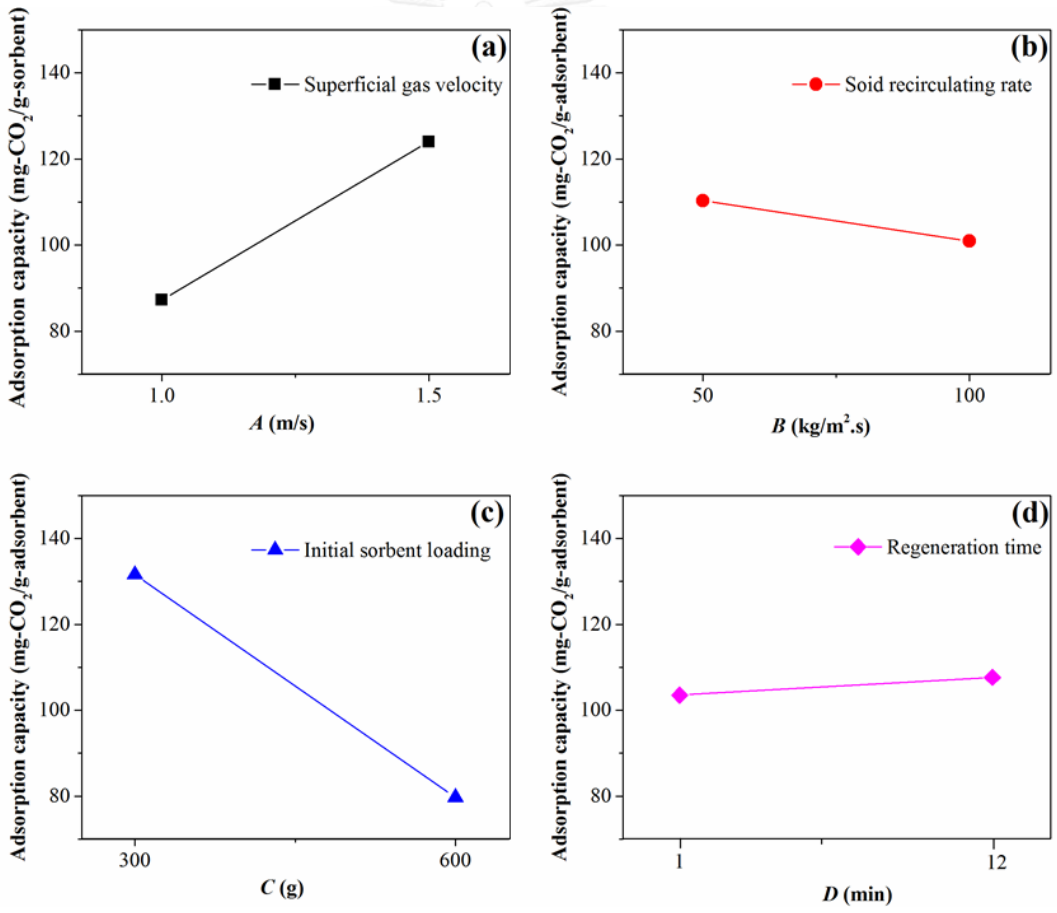

Figure 50 Main effect of CO_2 sorption in CTFB

(a) Effect of superficial gas velocity *(*A*)*

(b) Effect of solid recirculating rate (*B*)

(c) Effect of initial solid sorbent loading (*C*)

(d) Effect of regeneration time (*D*)

Focusing on the interaction of superficial gas velocity, *A*, and initial sorbent loading, *C*, the high value initial sorbent loading has the higher gradient than the trend obtained from the low initial sorbent loading. This implied that the negative trend when increasing initial sorbent loading as shown in Figure 50 (c) could be resolved by increasing superficial gas velocity. Thus, the extrapolation might be found the magnitude of gas velocity; ranging in CTFB that the main effect of initial sorbent loading was diminished by the gas velocity.

The promising trend is found with the interaction between the short regeneration time with the increase in gas velocity. The short in regeneration time refers to the compact size of the regenerator downer and the increase in superficial gas velocity shows the expansion capacity for the large scale.

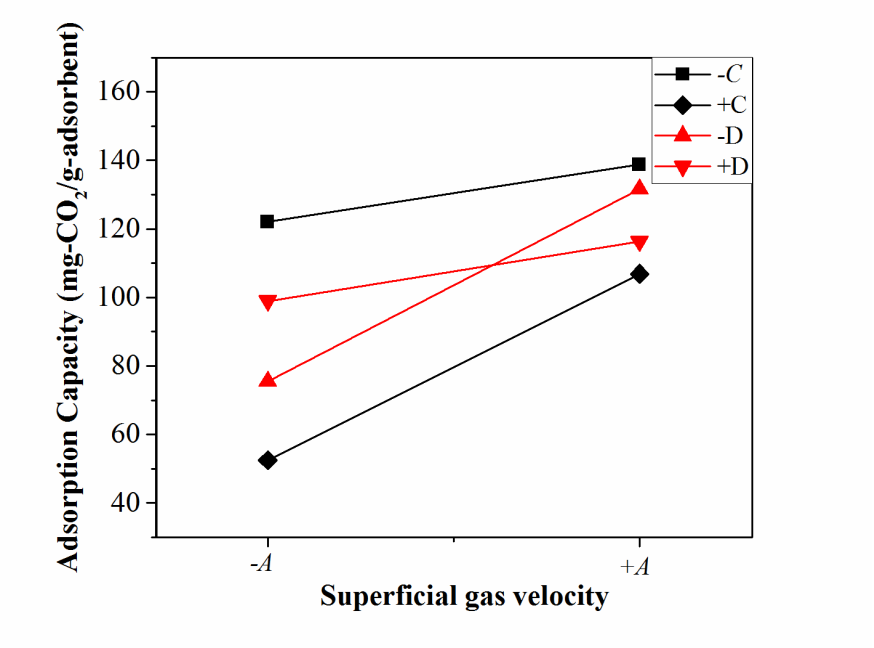

Figure 51 Interactions effect of the operating parameters using CTFB

Superficial gas velocity is the most important parameter and the increasing in its magnitude with the variation of the other operating parameters showed the positive trend to the output which is the expected trend for the scaling up. Equation (42) is the regression model obtained from the analysis of variance which can be used to predict the CO_2 capture capacity (Q) at the various sorption operation.

$$Q = 105.61 + 18.37A - 25.93C + 8.85AC - 9.70AD - 10.45BCD \qquad (42)$$

The response surfaces were constructed to investigate indept effect of gas velocity with a variation of solid recirculating rate while kept the initial loading at the average value (450 g). The influence of the greater magnitude of gas velocity provided the higher sorption capacity as shown in Figure 52 (a) to (d). Increasing magnitude of A dominated the effect interaction of B and D to obtain the good sorption capacity (higher than 130 mg-CO_2/g-sorbent) as shown in Figure 52 (a), (b) and (c) but not the

operation with (+B,-D) as shown Figure 52 (c). At the increasing of *A* provided such a fair sorption capacity. This is going to a concern for the fine tune in the future pilot study.

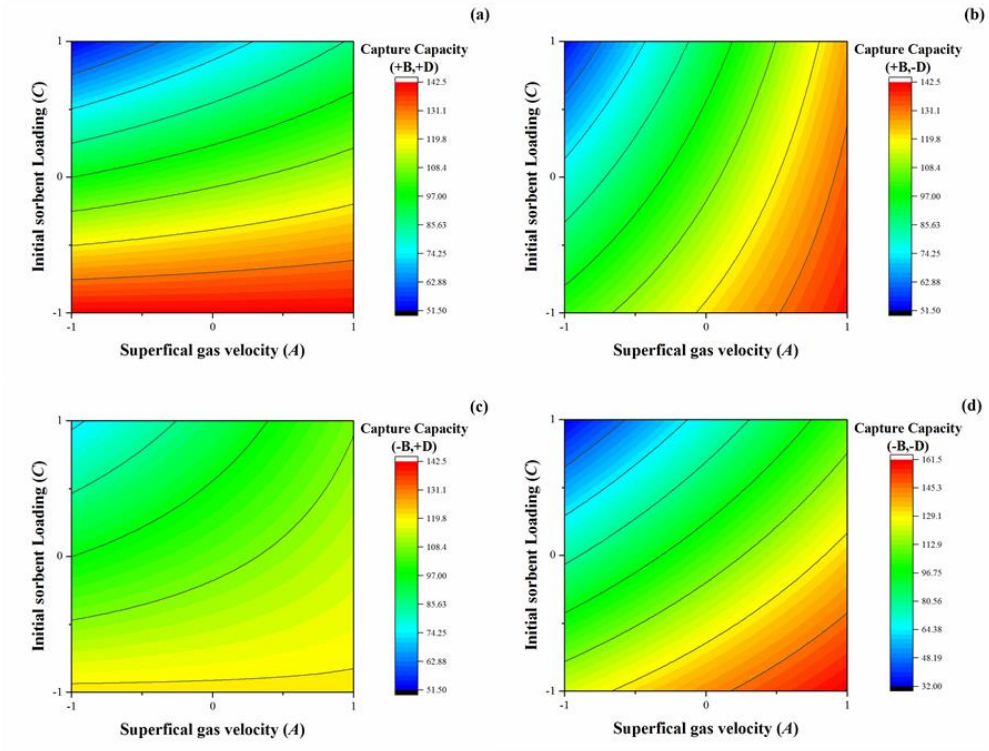

Figure 52 Response surfaces of the CO_2 capture capacity using CTFB

(a) Effect of superficial gas velocity (*A*) at high solid recirculating rate (+*B*) and long regeneration time (+*D*)

(b) Effect of superficial gas velocity (*A*) at high solid recirculating rate (+*B*) and short regeneration time (-*D*)

(c) Effect of superficial gas velocity (*A*) at low solid recirculating rate (-*B*) and long regeneration time (+*D*)

(d) Effect of superficial gas velocity (*A*) at low solid recirculating rate (-*B*) and short regeneration time (-*D*)

4.6. CO_2 Capture in multi single stage sorber-riser

The most common technology for post-combustion of CO_2 capture is the amine solvent scrubber. The energy consumption for capturing CO_2 from flue gases using amine solvent technology is 15 to 30% of the power plant electricity production. Hence, there is a need to develop more efficient methods of removing CO_2. A circulating fluidized bed using sodium or potassium carbonates is potentially such a process, since their high decomposition pressures allow regeneration at low temperatures using waste heat rather than steam from the power plant. But equilibrium data for the sorbents require the use of several cooled stages to achieve high CO_2 conversions. Here a method of computing such a number of stages for a given CO_2 conversion was developed using multiphase computational fluid dynamics. The high rates of sorption and cluster formation in the risers lead to mass transfer control of the reactions. Earlier studies had shown the possibility that CO_2 can be captured from existing power plants using dry sodium or potassium carbonates in bubbling or circulating fluidized beds. But due to equilibrium limitations, previous designs could not capture 80 % or more of the CO_2. The mass transfer limitation is benefit, since the rate of CO_2 removal is then not controlled by variable rates of reactions. It was found that it required 6 equilibrium stages to remove 96 percent of CO_2 with the initial mole fraction of 0.15 in a sorption riser. The maximum average sorption temperature was 52.5 °C. To remove more CO_2, the temperature of the next stage was reduced by 5 °C.

4.6.1. CFD model selection for the single stage sorber-riser

Figure 53 depicts the startup of the simulation and the area-averaged Na_2CO_3 solid sorbent volume fraction profiles. Figure 53 (a) shows the particle volume fraction

every 5 seconds. Initially, the bed was free of particles. By 25 seconds the 7 m tall bed was full of particles. Figure 53 (b) shows the area average particle volume fractions at various times. At the bottom of the bed the particle concentration is considerably higher than those at the top. For our assumption, the dense bed is needed for maximizing the rate of CO_2 capture.

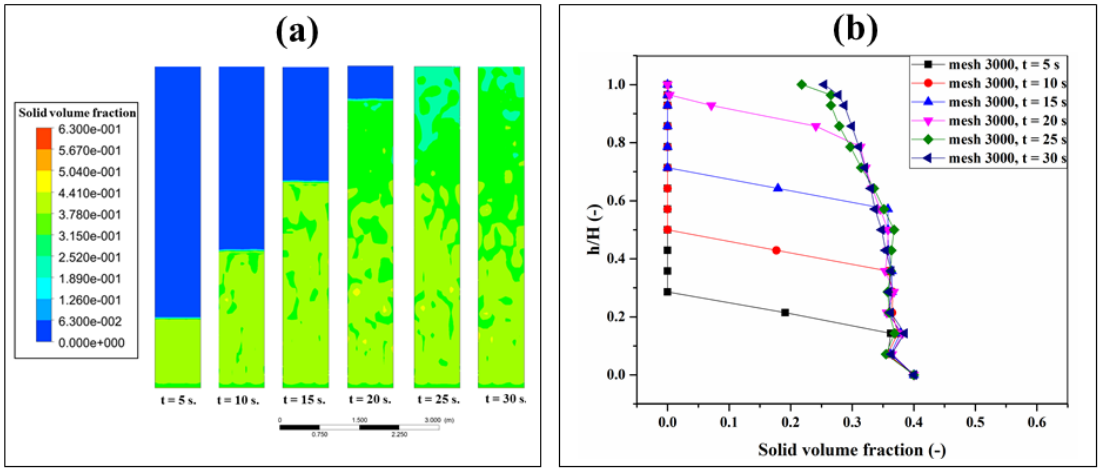

Figure 53 Compute solid volume fraction for the single stage sorber-riser

(a) Solid volume fractions at various times

(b) Average solid volume fractions at various times

Figure 54 (a) shows the grid selection study. It shows that grid independence is obtained as 3000 meshes. With higher grid, the obtained results were not altered. Figure 54 (b) shows a comparison of the computed solid volume fractions to experiments conducted a two-dimensional riser in Thailand using similar sorbent particles [63]. The results were successfully matched with the experimental information.

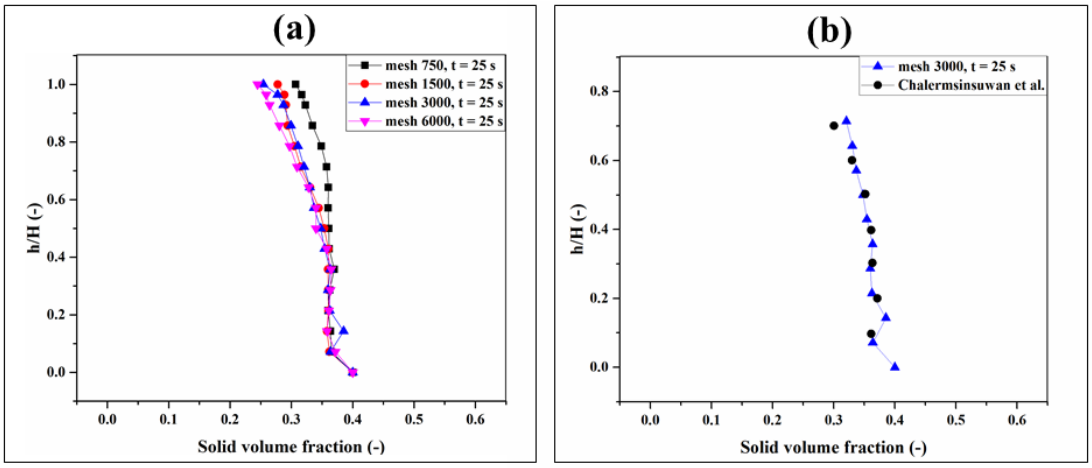

Figure 54 Grid selection and simulation validation for the single stage sorber-riser

(a) Grid selection study

(b) Comparison to the experiments [63]

4.6.2. Hydrodynamics of particles in the single sorber-riser

Figure 55 (a) shows the root mean square particle velocities for various dimensionless heights along the various dimensionless radial positions. The results show that there is no down flow at the walls and that the mean velocities are flat parabolic. At lower section in the riser, the axial velocity profiles are not strongly asymmetric, due to the entrance effect. However, the axial velocity profile becomes more symmetric, when the height of the riser moves higher.

The time-averaged velocity profiles of the vertical velocity along the various dimensionless radial position shows in Figure 55 (b). It exhibits non-asymmetric at all heights. This is because of the cluster formation in CTFB sorber-riser. Focusing on the positions near the riser walls (r/R = - 0.8 to -1.0 and 0.8 to 1.0), the average vertical velocities are positive which refers to no downward flow near to the walls. Due to the

disappearance of core-annular, the flow regime in this sorber-riser is characterized by a circulating turbulent fluidized bed [63].

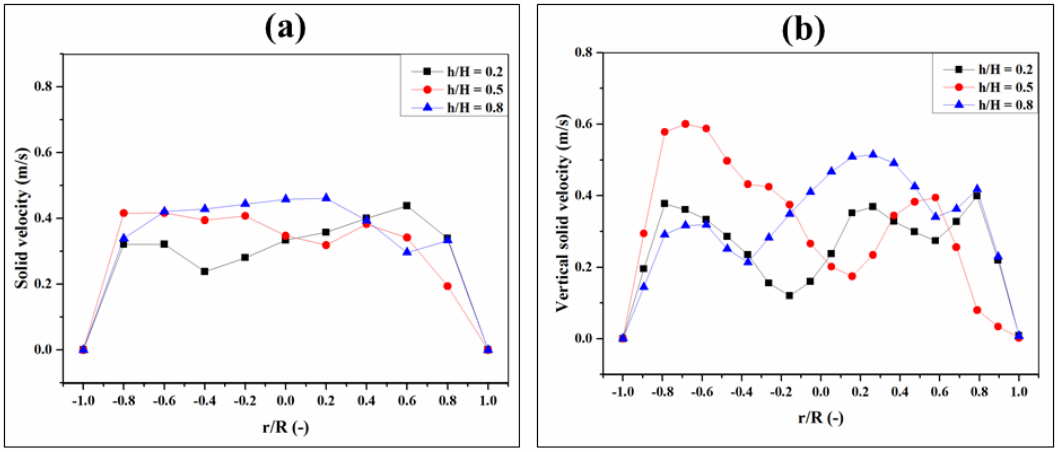

Figure 55 Radial particle velocity distributions in the single stage sorber-riser

(a) Mean particle velocity

(b) Vertical particle velocity

Figure 56 shows the contour of solid-sorbent volume fraction profile. It is clearly demonstrated that the clusters were formed throughout the riser. Cluster size could be determined by the area of each specific cluster position which shows by the enlarge section of Figure 8. The smaller cluster is formed near the top of the riser while the larger cluster is found in the lower section of the riser due to the higher particle concentration.

Figure 56 Cluster formation in the single stage sorber-riser

Figure 57 shows the computed turbulent granular temperatures and a theoretical expression for the granular temperature with the constant,

$$\mu / kv^2 = 0.006 \qquad (42)$$

obtained from the curve fit to the data.

The FLUENT code itself computes the laminar granular temperature. The turbulent granular temperature is defined as the average of the normal Reynolds stresses, which is the average of the three squares of the velocity fluctuation components in the three directions. For two- dimensional simulation, the velocity fluctuations in the nonflow or radial directions, x- and z- directions, are assumed to be equal. The turbulent granular temperature (θ_t) was calculated as follows:

$$\theta_t(t,x) \approx \frac{2}{3}\overline{v}_x\overline{v}_x + \frac{1}{3}\overline{v}_y\overline{v}_y \qquad (43)$$

where $\overline{v}_x\overline{v}_x$ and $\overline{v}_y\overline{v}_y$ are the square of the velocity fluctuations in x-direction and y-direction respectively.

The granular temperture in Figure 57 can be compared to that in Roy Jackson's book (2010), Figure 6.24, based on Sinclair-Jackson (1989) [43] and Hrenya-Sinclair (1997) [44] models, for a volume fraction of particles of the order of one percent. Their highest computed granular temperature is 2 m^2/s^2. Due to the much higher particle concentration in this study, shown in Figure 57, the granular temperature here is considerably lower. Note that at maximum packing the granular temperature will be zero.

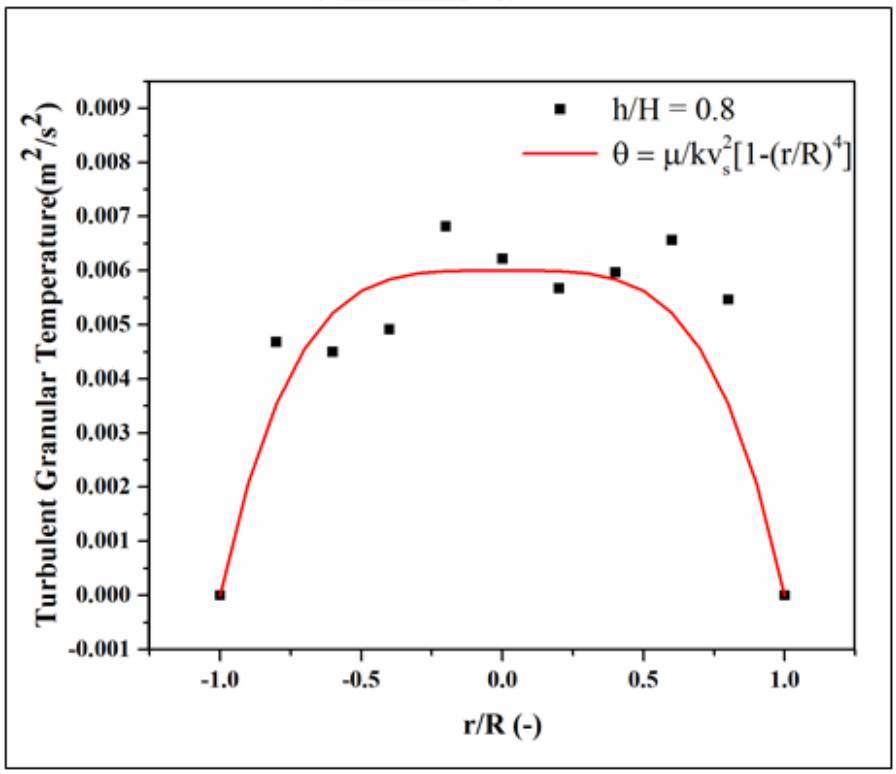

Figure 57 Solid turbulent granular temperature

4.6.3. CO_2 capture in the single stage sorber-riser

Since the CO_2 sorption is the exothermic reaction, the increasing temperature profiles indicate the position where the reaction taking place inside the reactor. Focusing on the temperatures inside the riser, the higher the temperature, the more sorption reaction took place. Figure 58 shows the particle temperature distributions. Figure 58 (a) shows the contour development of the particle temperatures as a function of the start-up time. After 25 seconds, the temperature has reached quasi steady-state. Figure 58 (b) show the cross-sectional average solid temperatures. At the quasi steady-state, the particle temperature rises only 6 °C. Such a small temperature rise is a large advantage of using circulating fluidized bed for CO_2 capture over that of using bubbling beds. This advantage is due to the fact that the adiabatic temperature in the riser, with particle inflow and outflow, is two orders of magnitude smaller than that for bubbling beds due to two orders of magnitude higher inflow and outflow of mixture density [38]. Figure 58 (c) shows the enlargement of solid temperature distribution near the bottom of the reactor ($h/H = 0.0$ to 0.25) at 30 s. The hot spot near the walls is about two degrees higher than the center temperature because the fact that the particle velocity near the walls is much lower than that at the center, as shown in Figure 58 (b). This suggests that large diameter risers with multiple inlet jets will be preferred which not have a large radial temperature distribution. Figure 58 (d) shows the small rise in the cross-sectional average solid temperature near the bottom (h/H = 0.0 to 0.25). The rise in temperature occurred near the very bottom of the reactor only, since this is where the rate of reaction is the highest.

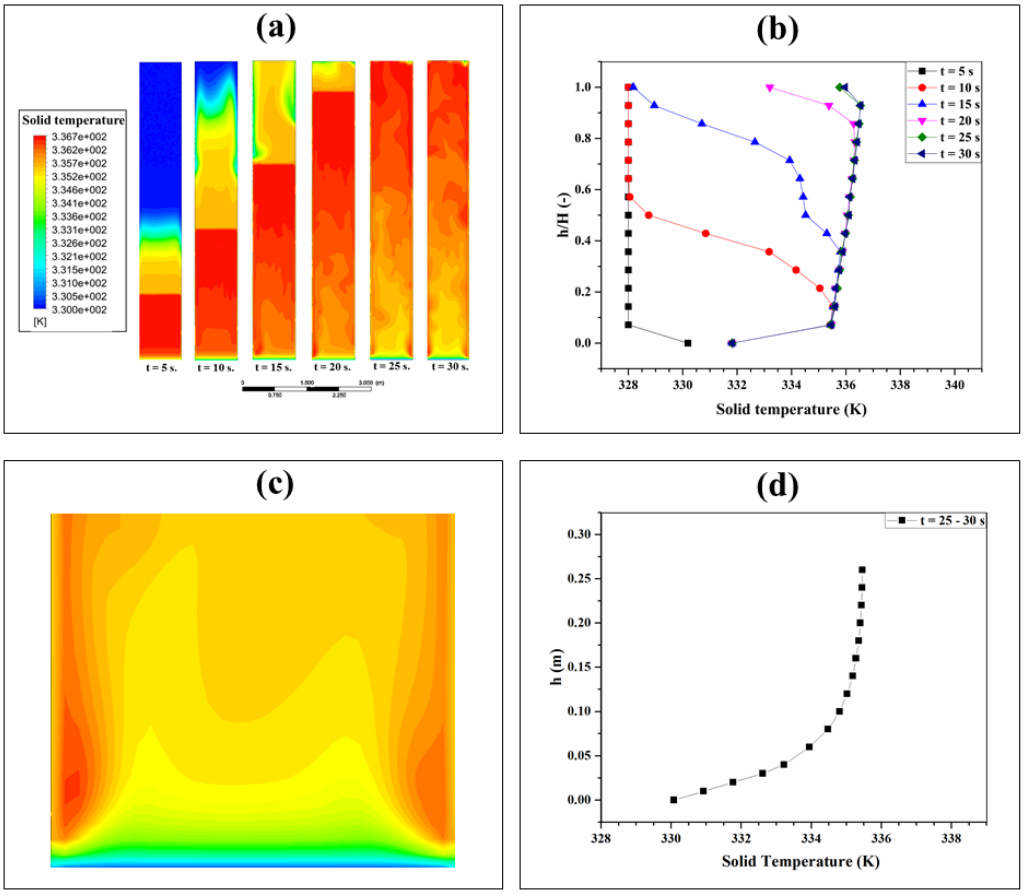

Figure 58 Solid Temperature in the single stage sorber-riser

(a) Solid temperature as a function of start-up time

(b) Cross-sectional average solid temperature

(c) Solid temperature distribution near the bottom at 30 s

(d) Cross-sectional average solid temperature near the bottom

Figure 59 shows the gas phase temperature distributions which exhibit the same overall trend as solid temperatures. The temperature reached the quasi steady state at 25 s as shown in Figure 59 (a). The gas temperature is only about one degree lower than that for the particles. Figure 59 (b) shows that the temperature drastically increases

at the short length above the bottom. The hot spot in the gas phase is smaller than those in the solid phase as shown in Figure 59 (c). The gas temperature is slightly changed above the position h/H higher than 0.10. The details of gas temperature rising is shown Figure 59 (d). From h equal to 0 to 25 m, gas temperature increases by 6 °C which is similar to solid temperature.

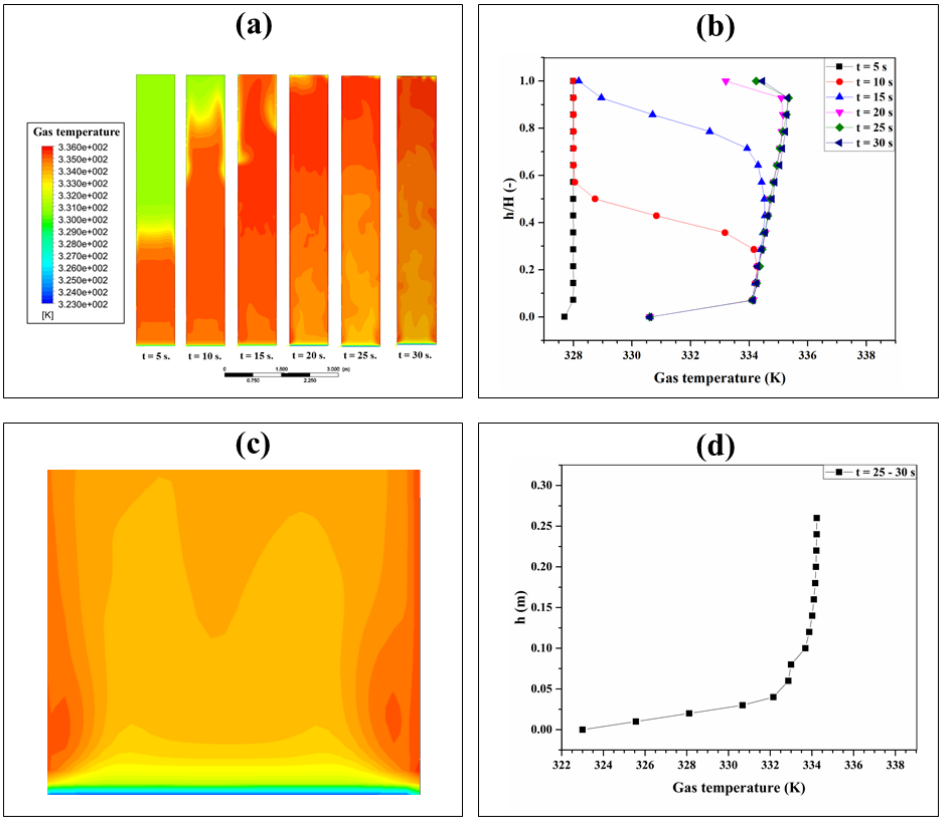

Figure 59 Gas Temperature in the single stage sorber-riser

(a) Gas temperature as a function of start-up time

(b) Cross-sectional average gas temperature

(c) Gas temperature distribution near the bottom at 30 s

(d) Cross-sectional average gas temperature near the bottom

The temperature change in the riser reflected the CO_2 removal from the flue gas and it would relate to the concentration of CO_2 remaining inside the riser. The percent CO_2 removal was calculated by equation (33)

$$\%\ CO_2\ removal = \frac{X_{CO_2(in)} - X_{CO_2}}{X_{CO_2(in)}} \times 100 \qquad (44)$$

Where:

$X_{CO_2(in)}$ is an initial concentration of CO_2 in the stimulated flue gas.

X_{CO_2} is an CO_2 content in the treated gas after adsorption.

Figure 60 (a) shows CO_2 weight fraction profile along the riser. The concentration is drastically dropped within small height near the bottom section. Figure 60 (a) is the zoom figure in the section of highly change in the CO_2 concentration as shown by Figure 60 (b). The figure shows that CO_2 weight fraction is dropped from the initial concentration of 0.22 to 0.07. The concentration of CO_2 above h equal to 0.25 m slightly increases due to the backward reaction pronounced more as the temperature increases. Under the sorption temperature of 52.5 °C (the average tempertature between solid and gas), the calculation using equation (44) showed that 67.32 percent of CO_2 was removed near the height of 0.25 m. from the bottom and the rest was slowly removed until reached the exit at the height of 7 m. Figure 60 (c) shows the weight fraction of $NaHCO_3$ which is a solid product obtained from sorption. The profile is similar to those temperature profiles of gas and solid phases as shown in Figure 58 and Figure 59. Focusing on the lower riser part, the plot in Figure 60 (d) clearly demonstrates the opposite trend to the CO_2 profile as shown in Figure 60 (b). The

weight fraction increases from zero to 0.8 percent. This means that the sorption reaction requires only small amount of Na_2CO_3 to capture 67.32 % of CO_2 concentration. Since 67.32 % of CO_2 concentration was removed within 0.25 m. of the riser, this height is considered to be an effective sorption zone. Thus, this information is important for designing a riser and will be used in the second part of this study to show that the total riser height can be reduced by almost an order magnitude.

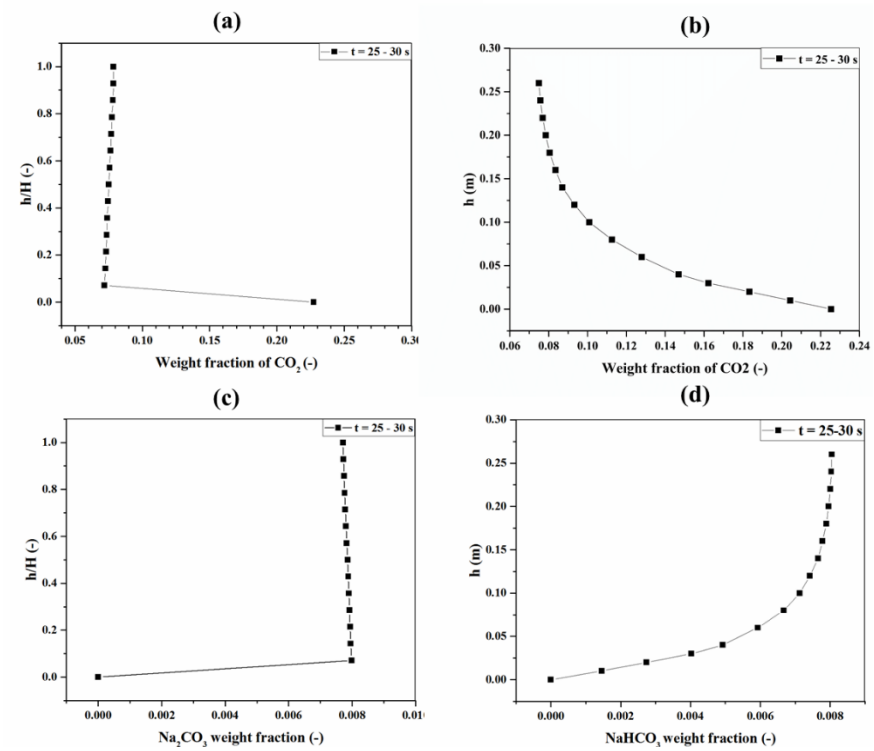

Figure 60 Weight fraction profile of CO_2 in the single stage sorber-riser

(a) CO_2 along the riser height

(b) CO_2 near the bottom section

(c) $NaHCO_3$ along the riser height

(d) $NaHCO_3$ near the bottom section

Figure 61 (a) shows the breakthrough CO_2 sorption curve measured at the exit of the riser. The residence time for the CO_2 to travel from the entrance to the exit was about 8 s. Then, this system took about 7 s to reduce the CO_2 mass fraction to the breakthrough concentration about 67 percent in the first stage of sorber-riser. At the breakthrough concentration, Figure 61 (a) shows that to remove more CO_2, more sorber-riser stages are necessary. Figure 61 (b) shows the corresponding gas temperature behavior. The temperature rise is due to exothermic reaction but it is not very large as already explained earlier. The gas temperature increases along the reaction time while the CO_2 decreases. Both trends of the CO_2 mass fraction and gas temperature were constant after 15 s due to the equilibrium limitation of using Na_2CO_3 sorbent. From the thermal sensitivity plot, Figure 61 (a) shows that the next stages for more CO_2 sorption must be operated with the lower temperature than the previous stage.

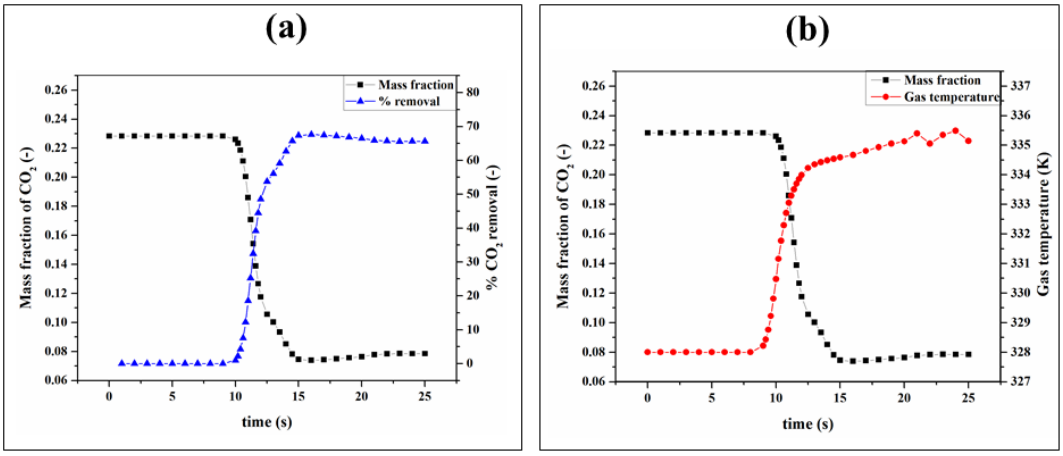

Figure 61 Transient CO_2 capture in the single stage sorber-riser

(a) Removal percent of CO_2

(b) Thermal sensitivity to CO_2 sorption

Figure 62 shows the equilibrium curve and the number of stages needed for CO_2 capture. The inlet CO_2 concentration is 15 mole percent (mass fraction about 0.22) and the inlet solid temperature is 55 °C, located by point C. In stage 1, the fraction decreases to the equilibrium curve, Line AB to point D. The temperature rises only a few degrees as already explained. To continue the sorption the gas has to be cooled. It is cooled by 5 °C. Then the exit gases enter the second stage riser of the identical dimensions to stage 1, point E. The CO_2 concentration decreases to point F on the equilibrium curve with a rise in temperature. Then the gas is cooled again by 5 °C and is introduced into stage 3, point G. The mass fraction of CO_2 is again decreases with a rise in temperature. The process is repeated until stage 6 to capture 96.26 per cent CO_2.

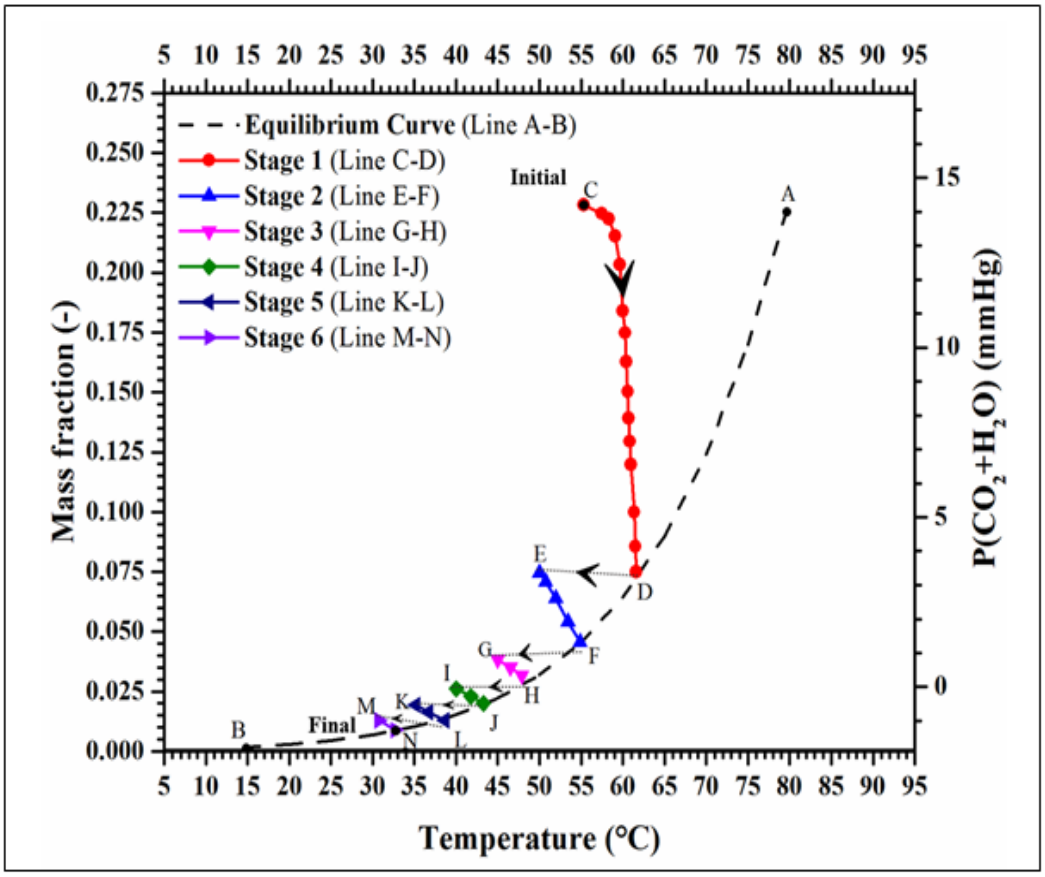

Figure 62 Number of stages for CO_2 capture

Table 18 summarizes this CO_2 removal information. This method is similar to the classical technique for the calculation of the number of plates in a distillation column in that there is an equilibrium curve and operating lines. The capture of CO_2 using liquid amines also uses the equilibrium curves and operating lines, but without consideration of flow and concentration distributions in the sorbers. This table clearly demonstrates that not only the residence time but also the equilibrium must be considered to increase the capture percentage. Understanding the effects of equilibrium for CO_2 sorption leads to the more efficacy compact design of a commercialized sorption unit.

Table 18 Summary of CO_2 sorption in multi single-stage sorber-riser

Stage	Gaseous condition				% CO_2 removal
	CO2 mass fraction	CO2 mole fraction	Temperature [°C]	DT [°C]	
1	0.2284	0.15	52.5	6	67.32
2	0.0746	0.048	47.5	4.86	83.16
3	0.0385	0.0246	42.5	3.79	88.54
4	0.0262	0.0167	37.5	3.5	91.32
5	0.0198	0.0126	32.5	3.25	94.32
6	0.013	0.0083	27.5	2.96	96.27
Exhausted	0.0085	0.0054	30.46	-	-

4.6.4. Sherwood Number

The study of Chalermsinsuwan *et al.* shows how to compute the dimensionless mass transfer coefficients in fluidized beds, called the Sherwood numbers (Sh).

Table 19 Kinetic Constants in multi single-stage sorber-riser

Stage	$k_{eff}[s^{-1}]$	$k_{eq}[s^{-1}]$	$k_{mass}[s^{-1}]$	Sh
1	1.951	19.190	2.172	0.372
2	1.230	356.559	1.235	0.211
3	0.731	861.093	0.732	0.125
4	0.532	1899.465	0.532	0.091
5	0.801	4214.787	0.801	0.137
6	0.801	9042.221	0.801	0.137

Table 19 summarizes the computed effective first order rate constants and the Sh base on cluster diameters. The first order rate effective rate constant (k_{eff}) is calculated by using equation (45) shown below.

$$k_{eff} = \frac{\Delta C}{C} \cdot \frac{v}{L} \qquad (45)$$

where,

$L = 0.52$ m, (The lowest height that the concentration of CO_2 is constant)

$v = 1$ m/s,

$\Delta C =$ the difference between the inlet and outlet CO_2 concentration in each stage.

$C =$ the average concentration between inlet and outlet in each stage.

k_{eq} is the first order rate constant for reversible reaction that is determined from the logical loop as shown in the Figure 20, and is obtained using equation (46).

$$k_{eq} = \frac{r_{eq}}{[CO_2]} \qquad (46)$$

and where,

$$r_{eq} = r_{fw} - r_{bw} \qquad (47)$$

k_{mass} represents the mass transfer of the active species which determined by equation (48).

$$\frac{1}{k_{eff}} = \frac{1}{k_{eq}} + \frac{1}{k_{mass}} \qquad (48)$$

Table 19 shows that the computed mass transfer coefficients are orders of magnitude smaller than the rates of reactions. Hence, for fast reaction mass transfer controls the rate of reactions and therefore the suitable height of reactor is much shorter than that initial design. Breault (2006) was aware of this phenomenon for a long time and has given a similar explanation [11].

Table 19 also shows the computed Sherwood numbers. They are less than 2 for every stage due to the cluster formation. They are calculated using equation (49) with the method of Chalermsinsuwan *et al.* 2010 [38], where

$$Sh = \frac{k_{mass} d_p}{D} \qquad (49)$$

$$D = d_{cl} * \mathrm{Re}\, stress \qquad (50)$$

and where,

d_p = solid particle diameter

D = diffusivity of gas in the cluster

d_{cl} = computed cluster diameter

Re*stress* = Reynold stress

4.7. CO_2 Capture in a multi-stage sorber-riser

A 1 m in diameter and 3.55 m tall fluidized bed riser internally with water tubes, which required 6 equilibrium stages of riser-sorber for capturing about 95 percent of CO_2 emitted from a coal power plant, were designed to replace the multi single risers (1 m in diameter and 7 m tall). At the optimum operating condition, the temperature of the cooling tubes in the bottom, the middle and the top of the riser were kept constant values at 50 40 and 30 °C, respectively. The hot water (57 °C) from lowest exchanger section can be used to pre-heat the spent sorbent for the regeneration in a downer. The rest of the heat for the regenertion is obtained from the stack gas (100 – 130 °C). This new concept promises to reduce the energy consumption for CO_2 removal from flue gas. The only energy requirement is for pumping fluid and fluidizing particles in the bed. Earlier studies had shown that CO_2 can be captured from existing power plants using dry sodium or potassium carbonates in bubbling or circulating fluidized beds. But due to equilibrium limitations, previous designs could not capture 80% or more of the CO_2.

4.7.1. CFD model selection for the multi-stage sorber-riser

As stated above, the simulations were carried out using the CFD method described in section 4.6 of this dissertation. Figure 63 (a) shows the grid independence study. The model with 7,200 meshes was selected to study the effect of three operation modes because the average percent error decreases from 1 percent to 0.1 percent when the calculation meshes increase from 6000 to 7200 and 7200 to 10000. The average of gas temperature with the interval of 5 s was selected to determine quasi-steady. Figure 63 (b) shows the average gas temperature profiles along the riser height in different periods of operating time. Focusing at the top 30 percent of the riser, the average gas temperature tends to decrease with the increase in the interval time. The average temperature in the time interval of 30 - 35 s is less than that of 35 – 40 s about a half of degree celsius. Therefore, it was found that after 30 s, the average gas temperature is independent of the operating time as shown in Figure 63 (b) and the system was reached the quasi-steady state.

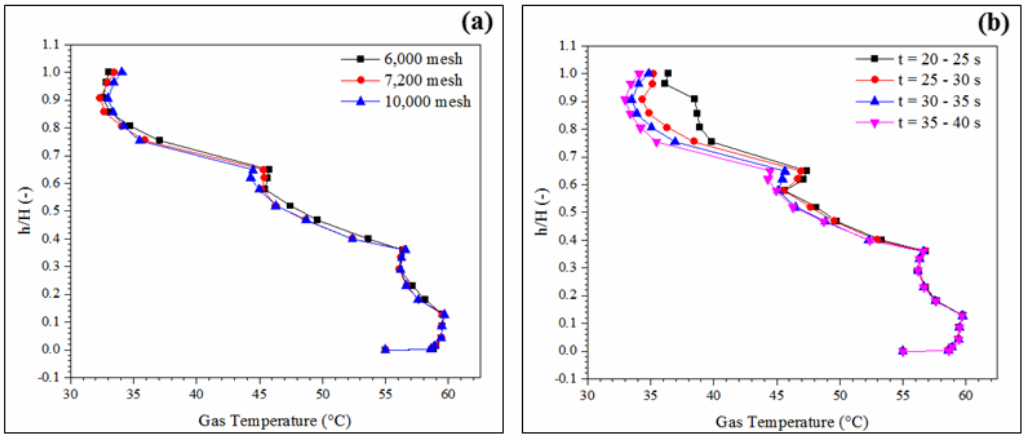

Figure 63 Modeling selection and simulation validation for the multi-stage sorber-riser

(a) Grid independence

(b) Quasi-steady-state determination

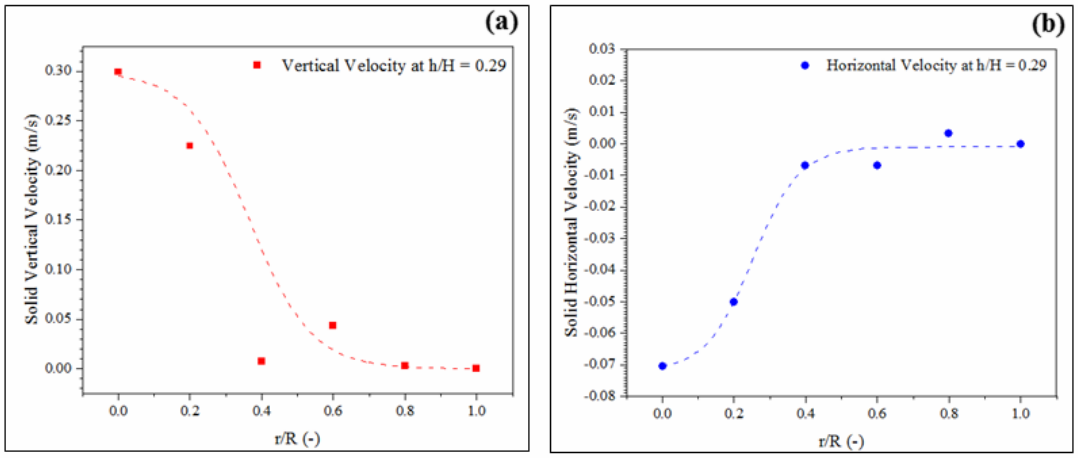

Figure 64 Particle velocity in the multi-stage sorber-riser

(a) Solid vertical velocities for operation I at the inlet section

(b) Solid horizontal velocities for operation I at the inlet section

Figure 64 shows the trends of the velocities along the radial positions. This figure shows a typical velocity for operation I with the dimensionless height of 0.29. The flow in the riser is complex due to the fluctuation of turbulence regime and is dominated by a cluster formation. Figure 64 (a) shows the vertical velocities versus the dimensionless riser radius. The dashed curve shows the trend of vertical particle velocity. The flow near the wall is much lower than that at the center due to the friction between the fluid and the riser wall. The average velocities are positive along the radial position and refer to only upward motion of the particles even at the position close to the wall. Thus, there is no back mixing which leads to low efficiency of the system. This flow distribution is governed by inlet condition. Here, the constant inlet velocity was used. In practice, multiple jets will be used. Figure 64 (b) shows the horizontal velocities versus the dimensionless riser radius. The dashed lines in negative or positive

signs represent the move away or toward the riser wall, respectively. Such a small magnitude of the horizontal velocity demonstrates that the same number of particles moves toward the riser.

4.7.2. Hydrodynamics of particles in the multi-stage sorber-riser

Figure 65 (a) shows the solid volume fraction distribution along the dimensionless height. It was found that the bed is very dense with solid fraction of 0.45. This condition is favored for high CO_2 capture, since the rate of sorption is proportional to the particle concentration. The solid fraction seems to be constant in some short range of height where the cooling tubes are presented, since the cooling tubes behave like a baffle which helps distributing of the particles. There are the variations of solid fraction at the position where fluid exit from the cooling section to the sorption section where no cooling tube is installed. Figure 65 (b) shows the contour of solid volume fraction. Some clusters were formed at the intersection between the sorption section and the cooling section.

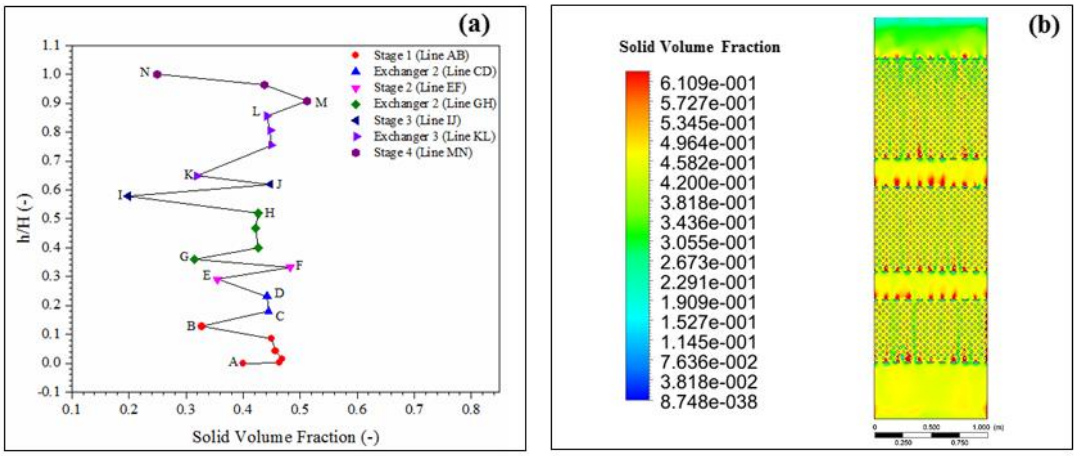

Figure 65 Solid volume fraction in the multi-stage sorber-riser

(a) Solid volume fraction profile for operation I

(b) Contour of solid volume fraction for operation I at t = 37.5 s

4.7.3. CO_2 capture in the multi-stage sorber-riser

Figure 66 shows the temperature profiles for the 4 stages of sorption and 3 cooling sections. The corresponding particles and gas temperatures of three operation conditions are shown in Figure 66 (a) to (d). The gas and solid temperatures on each stage are nearly equal due to the good heat transfer.

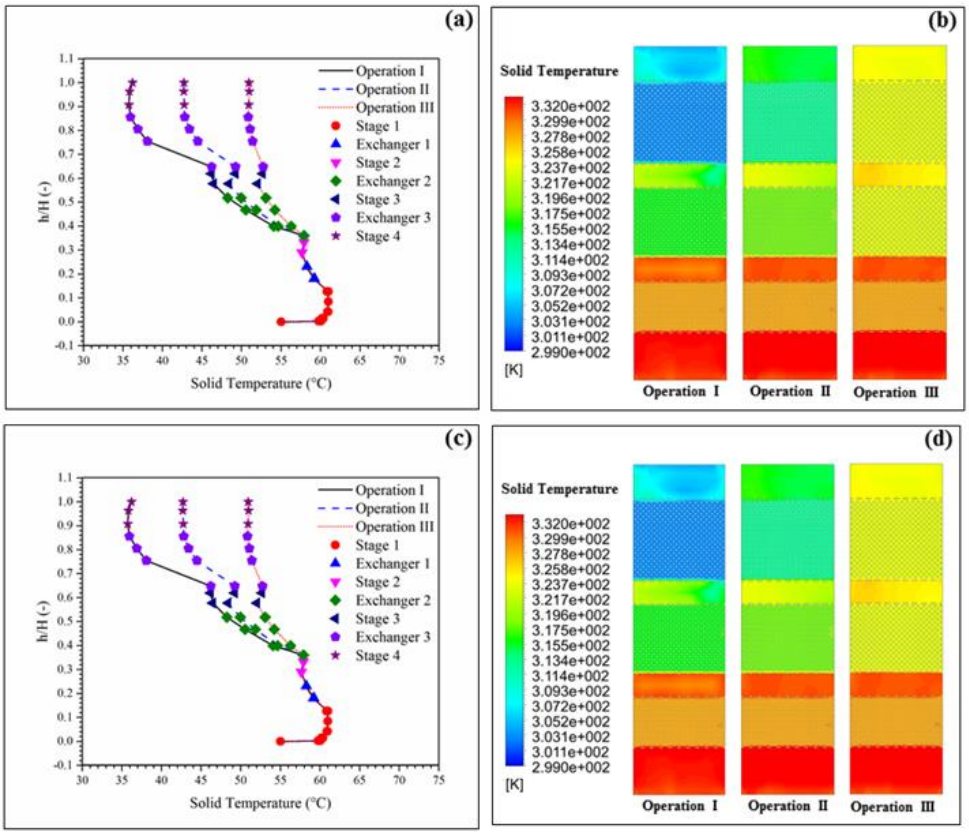

Figure 66 Temperatures for operation conditions I, II and III

(a) Gas temperature profiles

(b) Effect of operating conditions on gas temperature at t = 37.5 s

(c) Solid temperature profiles

(d) Effect of operating conditions on solid temperature at t = 37.5

The gas temperature and solid temperature of the 3 operation conditions are the same up to the dimensionless height of 0.3 above the riser entrance as the result of the same cooling temperature of 50 °C in the first cooling section. Above the bottom section, including cooling sections 2 and 3 and sorption sections 3 and 4, the temperatures of operation I and II deviate from the operation III. Due to the appropriate number of the cooling tubes in each cooling section, the gas temperature could be manipulated by the temperature of the cooling tubes. This leads to multi-stage sorption in a single riser. The output temperatures of the solid phase are slightly higher than the gas phase due to the higher thermal conductivity of solid phase than the gas phase. This difference in temperatures can be reduced by expanding the length and the number of the cooling tubes in each cooling section.

Figure 67 shows the CO_2 mass fraction in each section of the riser. Most of the CO_2 is removed in the first sorption stage. The inlet concentration of CO_2 is much higher than the equilibrium concentration at the initial sorption temperature of 55 °C. This provides the high driving force in this sorption stage. Therefore, most of the heat is generated in stage 1 and will be utilized to preheat the used sorbent in the regeneration - downer. The effect of operation temperatures becomes apparent when the riser height is above the second sorption stage. CO_2 concentration decreases in the cooling sections and slightly increases at the sorption sections due to the higher driving force at lower temperature. The profiles obtained from the different operations show the improvement of CO_2 sorption compared to the part I of this study.

Actually, the CO_2 sorption occurred only in the short length of 25 cm above the riser entrance, if there is no cooling section to remove the heat being generated by the sorption. The constant temperature of the cooling tubes of the operation III allows the riser to adsorb as an iso-thermal process. The multi-stage effect becomes more prominent with the operation I and II than the operation III as shown by Figure 67 (b). This is due to the reduction of the temperatures in each section of the operation I and II, but not in the operation III. The contour of CO_2 mass fraction demonstrates that the multi-stage CO_2 sorption can be performed in a single riser with the cooling sections. Thus, the temperature of cooling section becomes a crucial factor to control percent removal of CO_2.

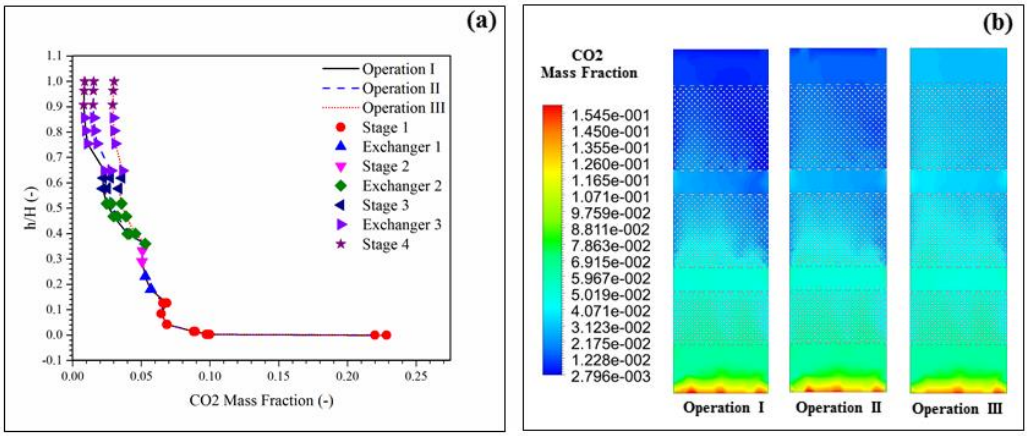

Figure 67 Mass fraction of CO_2 for operation conditions I, II and III

(a) Mass fraction of CO_2 profiles

(b) Effect of operation conditions on mass fraction of CO_2 at t = 37.5 s

Figure 68 shows the mass fractions of Na_2CO_3 in each section. The oscillations of the mass fractions are due to varying temperatures and fluctuation of solid volume

fractions as shown in Figure 65. Therefore, it is difficult to notice the difference of average mass fraction in the period of 5 s as shown in Figure 68 (a). Only about 8 percent of the sorbent was consumed to capture CO_2. Figure 68 (b) shows instantaneous contour at time equal 37.5 s. The mass fraction contour of the operation III shows a slightly higher of Na_2CO_3 mass fraction than those of the operation I and II.

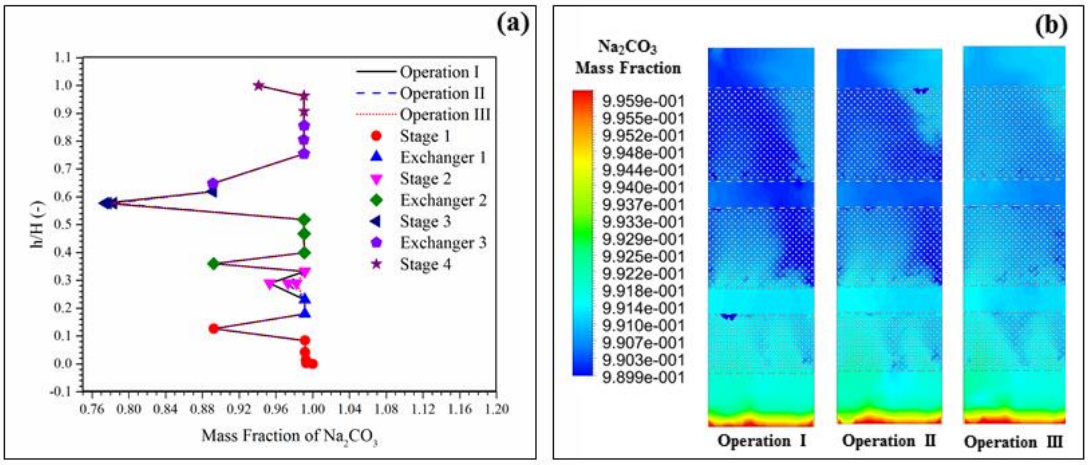

Figure 68 Mass fraction of Na_2CO_3 for operation conditions I, II and III

(a) Mass fraction of Na_2CO_3 profiles

(b) Effect of operation conditions on mass fraction of Na_2CO_3 at t = 37.5 s

Figure 69 (a) and (b) show the operating lines and the equilibrium curve for the sorbent. Figure 69 (a) is for the multiple single-stage risers described in part I of this paper. Figure 69 (b) is the operating line for a single multi-stage riser, as described in detail here. As stated earlier, the inlet flue gas is at 55 °C. Its inlet concentration has the mole fraction of 15 percent CO_2 and 15 percent H_2O and the rest is nitrogen. The main difference between multiple riser system and single multi-stage riser system is the number of the risers in the system. The operation from stage 1 to 6 was obtained from a series of 6 risers (1 m in diamter and 7 m tall) where the outputs of the previously

riser were used as the inputs of the next riser. The sorption temperature of the next riser was reduced by 5 °C. It required 6 equilibrium stages to remove about 95 percent of the initial concentration. The present multi-stage riser is that the multi-stage riser described here is only one short riser-sorber. Figure 69 (b) shows that the operation I can remove CO_2 up to 96 percent as the same as the operation of the 6 single stage risers in series. The equiribrium limitation in CO_2 sorption using Na_2CO_3 is overcome by introducing cooling sections inside the sorption riser. Thus, the alternative design which was addressed in this work can be considered as a compact efficient sorption unit compared to the tall conventional absorber column using liquid amine.

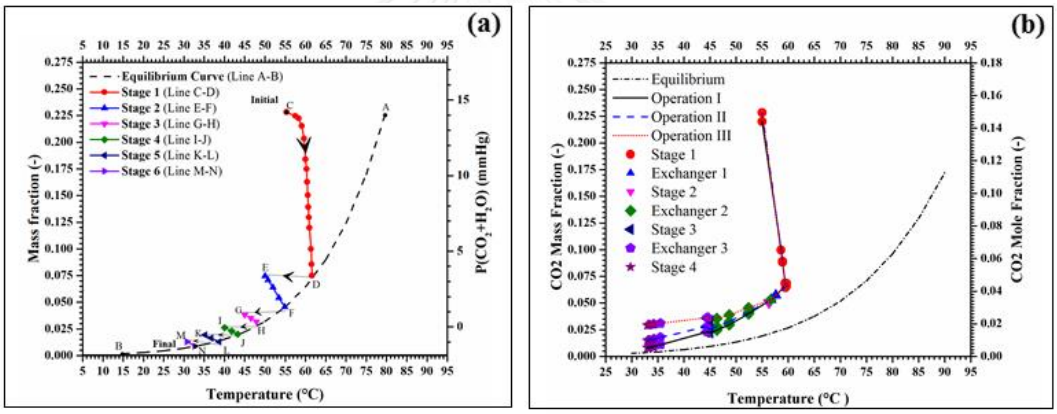

Figure 69 Operating lines and equilibrium curve for CO_2 and sorbent Na_2CO_3

(a) Multiple riser system

(b) Single multi-stage riser

Figure 70 is a summary outcome of operation I which is included some important boundary conditions and the results which were obtained from ผิดพลาด! ไม่พบแหล่งการอ้างอิง and Figure 67. Similarly to the study of Oyenekan and Rochelle [105], the flue gases enter the sorber at 55 °C. In section A, the temperature rises to 59.70 °C due to the evolution of the heat of sorption. The mixture is then cooled to 56.21 °C in

cooling section B. In the next section C, the sorption stage 1 without the cooling tubes, the temperature rises less than 1°C. To significantlly decrease the temperature of gas-solid mixture, cooling section D was designed larger than the first cooling section. The gas-solid mixing exits the cooling section at 44.30 °C. In the section E, the sorption stage 3, the rise in temperature is small due to the low CO_2 concentration. In the 90 cm tall cooling section F, the temperature of the mixture decreased to 33.38 °C. Finally, in section G, only 0.1 percent CO_2 was removed. Therefore, this section may be removed to reduce the total height of the riser from 355 cm down to 305 cm. The 3 meters height of the sorber is about one tenth of the 30-meter tall aqueous amine absorber of Oyenekan and Rochelle [105].

This reduction in height of the sorption column is due to the high sorption rate of porous carbonate pellets used in this study. The hot cooling water leaving section B can be used for regeneration of the used sorbent. The coolant temperatures leaving the upper 2 sections is too low to be used for regeneration. The pressure drop shown in Figure 70 is the gauge pressure. The entering pressure is equal to 3236 kPa, as shown in Figure 70. The pressure drop was calculated from the CFD code. It can be used to determine the electrical energy needed to operate a compressor. This energy input will be the principal energy needed for this CO_2 capture system, since the energy for regeneration is supplied by the hot cooling water from stage one and the energy recovered from cooling the flue gas from about 150 to 55 °C [105].

The average values of gas temperature, solid temperature, CO_2 concentration and mass fraction of Na_2CO_3 as shown in Figure 9 will become a crucial set of boundary conditions to determine a suitable design of the cyclone where the treated gas and the

used sorbent are separated and the downer where used sorbent is regenerated. The complete CO_2 sorption system will provide a precise approximation for actual performance and the real cost for CO_2 sorption.

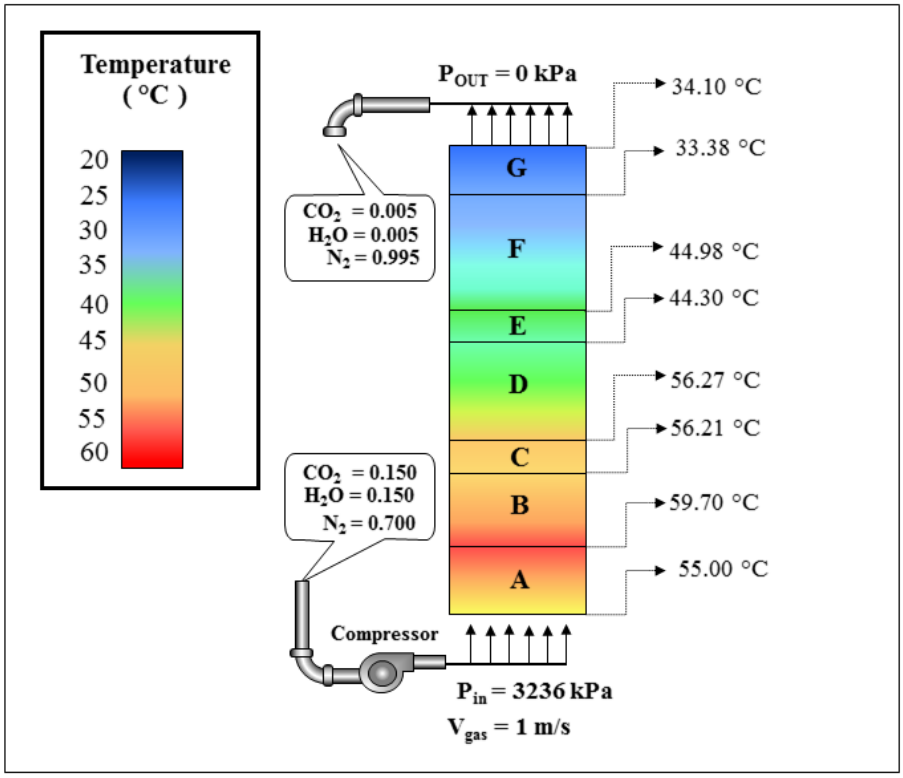

Figure 70 The summary result of the operation I

Table 20 Summary of the multi-stage riser for three different mode of operation

Operation	Section Named	Gaseous condition			DT [°C]	% removal (by Mass)
		[CO_2] mass fraction	[CO_2] mole fraction	Temp. [°C]		
I	Stage 1	0.2284	0.1500	55.00	+4.70	70.00
	Cooling 1	0.0567	0.0361	59.70	-3.49	76.91
	Stage 2	0.0507	0.0337	56.21	+0.06	77.76
	Cooling 2	0.0528	0.0337	56.27	-11.97	89.16
	Stage 3	0.0220	0.0145	44.30	0.68	90.14
	Cooling 3	0.0231	0.0152	44.98	-11.60	96.22
	stage 4	0.0082	0.0056	33.38	0.72	96.13
	Exhaust	0.0088	0.0060	34.10	-	-
II	Stage 1	0.2284	0.1500	55.00	+4.75	74.91
	Cooling 1	0.0573	0.0364	57.72	-1.03	77.89
	Stage 2	0.0505	0.0322	56.15	+0.12	76.90
	Cooling 2	0.0528	0.0337	56.55	-8.46	88.88
	Stage 3	0.0254	0.0166	46.97	+0.52	87.73
	Cooling 3	0.0280	0.0184	47.67	-7.09	93.47
	stage 4	0.0149	0.0103	40.32	+0.52	93.25
	Exhaust	0.0154	0.0108	40.84	-	-
III	Stage 1	0.2284	0.1500	55.00	+5.82	74.96
	Cooling 1	0.0572	0.0364	59.24	-0.93	77.90
	Stage 2	0.0505	0.0322	57.63	+0.24	76.89
	Cooling 2	0.0528	0.0337	57.89	-4.83	85.25
	Stage 3	0.0337	0.0218	52.01	+0.64	84.07
	Cooling 3	0.0364	0.0239	52.73	-1.89	87.23
	stage 4	0.0292	0.0289	50.91	+0.02	86.76
	Exhaust	0.0302	0.0197	50.93	-	-

Table 20 summarizes the outcomes obtained from three modes of operation applied to the system. The CO_2 concentration which was introduced in each section were presented in the unit of mass and mole fraction. The third column (**Temp**.) under the gaseous condition section of the table is the inlet temperature of each section. After the adsorption, the change in the temperature between the inlet and the outlet of each

section is also displayed in the next column (**DT**). The percent CO_2 removal which shows in the last column of the table was calculated by equation (44).

4.7.4. Sherwood numbers and scale-up

Table 21 Kinetic constants and Sherwood numbers

Operation	Section Named	Kinetic Constant			Approximation cluster diameter	Re Stress	Diffusivity	Sh
		k_{eff} [s^{-1}]	k_{eq} [s^{-1}]	k_{mass} [s^{-1}]				
A	Stage 1	1.2731	16.2740	1.38	1.167678	0.00057	0.0006711	1.029
	Stage 2	0.7906	68.9983	0.80	0.342717	0.00701	0.0024021	0.166
	Stage 3	0.6875	434.8201	0.69	0.031348	0.03450	0.0010815	0.318
	stage 4	2.2324	1508.9339	2.24	0.134432	-	-	-
B	Stage 1	1.2758	16.2740	1.38	0.468819	0.04343	0.0203626	0.034
	Stage 2	0.0823	77.1501	0.08	0.426976	0.02502	0.0106821	0.004
	Stage 3	0.5748	235.3937	0.58	0.024163	0.05915	0.0014293	0.202
	stage 4	1.4532	469.3292	1.46	0.327413	-	-	-
C	Stage 1	1.2759	16.2740	1.38	1.031511	0.00468	0.0048226	0.144
	Stage 2	0.0802	54.6194	0.08	0.10504	0.00576	0.0006047	0.066
	Stage 3	0.3472	97.7552	0.35	0.022148	0.02481	0.0005495	0.317
	stage 4	0.4602	114.3271	0.46	0.153936	-	-	-

Table 21 summarizes the rate constants and the computed Sherwood numbers for the three modes of operation. This information will be useful for scaling up the present riser to risers of about 8 meters in diameter to handle large flowrate of flue gas generated by 300 MW conventional fossil fuel power plants. In place of using kinetic rates of reactions the mass transfer coefficients computed here may be used as an input which complied in the user define function. The present one diameter reactor will be

useful for constructing a pilot plant to test the new concept that promises the capture of CO_2 with very small amount of energy consumption.

4.8. Heat regenerator downer

Figure 71 (a) depicts the startup of the simulation and the area-averaged the solid volume fraction profiles which was averaged every 5 seconds. Initially the lower part of the downer was free by the particles. By 5 seconds the 1 m tall downer was full of particles. The profile of the time interval 5 to 10 s and 10 to 15 s are similar. Therefore, the qausi-steady stage is determined after 5 seconds. Figure 71 (b) shows the grid selection study. It shows that grid independence is obtained for 6000 meshes. Thus, the calculation grid of 6000 and the area weight average during the time interval 5 to 10 s were used to display the regeneration results.

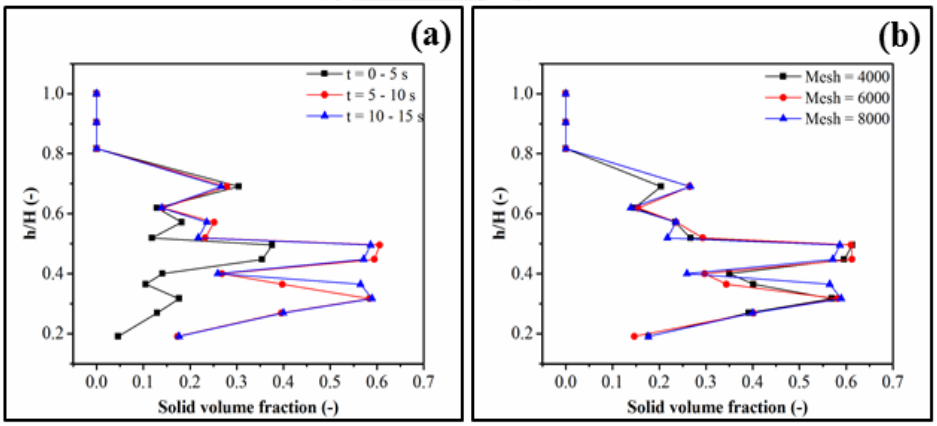

Figure 71 Modeling selection and simulation validation

for heat regeneration-downer

(a) Grid independence

(b) Quasi-steady-state determination

Solid volume fraction is one of the most important factor to determine regenerator- downer performance. The big baffle which located at the bottom of the cyclone separated the falling sorbent into two part as Shown in Figure 72 (a). The two smaller baffle provided the wider angle for the downward solid flow to the left and right side of the downer. The tubes temperature in the first half of the upper section were set at 60 °C for the pre-heating process. The upper section of the downer shows such a dense solid volume fraction at the center. The baffles at the middle part of the downer help for more uniform solid volume fraction at the lower part of the downer which also occupied by the tubes but their surface temperature was set at 130 °C. After the collision with those baffles, sorbent loss their kinetic energy lead to the accumulation of sorbent in the middle downer section. Then the solid uniformly flow through the bottom of the riser.

Figure 72 (b) shows area weight average of solid volume fraction along the vertical direction. The averages are in the range of 0.2 to 0.6 which can consider as a high solid concentration system. The variation is due to the installation of baffles.

Before the results as shown in Figure 72, there were a number of the simulations which used the different dimensions, number and the location of the baffle and the tube. Only the design as presented in this work could provide a uniform solid volume fraction distribution which is a key for the higher performance regeneration downer.

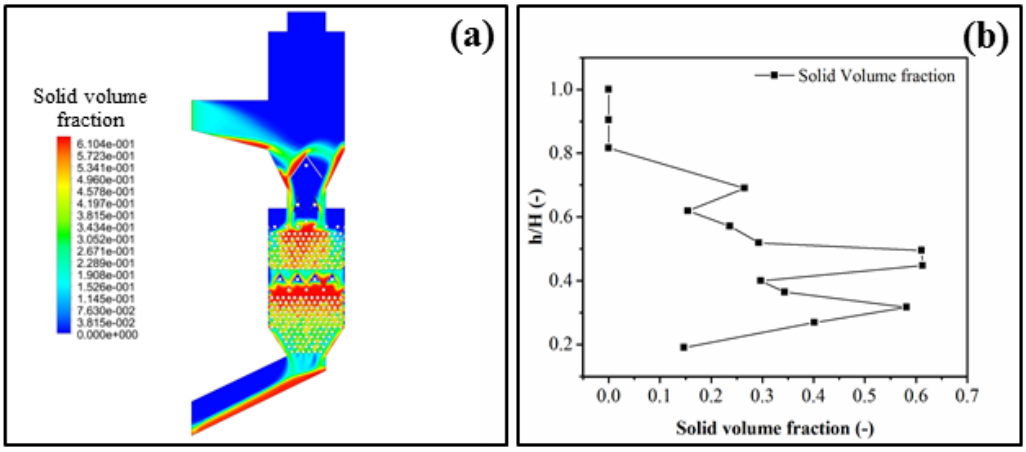

Figure 72 Solid volume fraction in the heat regeneration-downer

(a) Contour of solid volume fraction

(b) Solid volume fraction profile

Complete regeneration is monitored by the mass fraction of the sodium bicarbonate ($NaHCO_3$). After the regeneration at the regenerator-downer, the mass fraction of $NaHCO_3$ decreases and becomes zero at the downer bottom as shown in Figure 73 (a). Mass fraction of sodium carbonate (Na_2CO_3) is shown in Figure 73 (b). The reverse tread of Na_2CO_3 had been address to demonstrate that all of $NaHCO_3$ convert to Na_2CO_3. Thus, the compete regeneration can be done in the designed regeneration-downer.

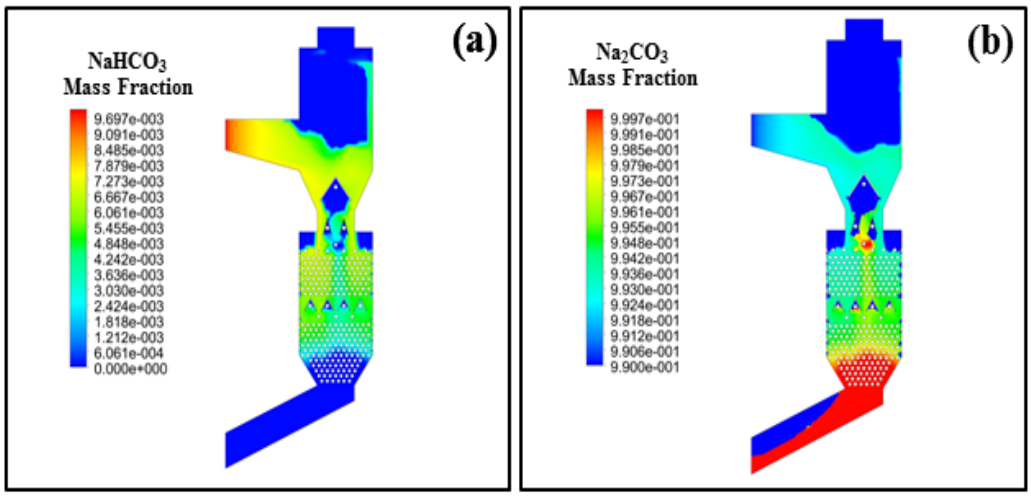

Figure 73 Contour of species in the solid phase

(a) Mass fraction of sodium bicarbonate $NaHCO_3$

(b) Mass fraction of sodium carbonate Na_2CO_3

For the application in a circulating fluidized bed reactor, not only Na_2CO_3 phase but also a proper outlet regenerated should be reached the temperature of 55 °C. The solid temperature is presented in Figure 74. The inlet temperature is increased from the temperature of 30 °C. For the upper downer section, the temperature slightly increases when compared to the bottom section as shown in Figure 74 (a). Because the sorbent was slowed down together with high surface temperature. The temperature of the upper downer section is equal to the temperature of the cooling tube at the bottom of the multi-stage riser (60 °C) and temperature of the lower downer section is the same the stack gas which exhausted from power plant (130 °C). Therefore, the temperature is drastically increased when sorbent passed through the middle part toward the bottom of the downer.

In the downer with the various size, location and dimension of the baffle, the number and the dimension of the tubes were studied for the several designs to obtain

temperature profile as shown in Figure 74 (b). The trend is that the temperature drop toward the direction of the downer bottom and the output average temperature of solid is about 55 °C which is the same as the inlet temperature of the solid phase of the multi-stage riser. Therefore, the regeneration-downer as shown in Figure 24 is the suitable design for CO_2 sorption in circulating fluidized bed.

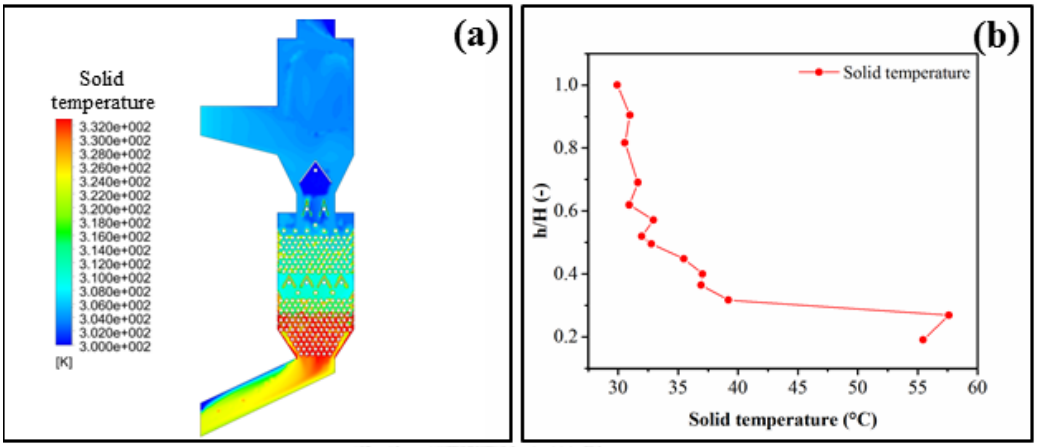

Figure 74 Solid temperature in the heat regeneration-downer

(a) Contour of Solid temperature

(b) Solid temperature profile

CHAPTER V
CONCLUSION AND RECOMMENDATION

5.1 Conclusion

In this dissertation, it was shown that CTFB could be operated in a conventional circulating fluidized bed reactor with the single gas feed stage. The hydrodynamics of the CTFB are similar to the conventional turbulent fluidized bed which has a highly uniform solid fraction along the vertical direction while solid particles can circulate throughout the system as fast fluidization. This regime can occur when U_g is higher than U_c but lower than U_{tr}. For CTFB performing, riser height is the crucial design parameter. The riser height must be lower than the maximum bed expansion.

The suitable height of the riser depended on the properties of used solid particles. In this dissertation, the expansion of the solid bed was considered by using Geldart classification and dimensionless *Ar*. Geldart group B particles had a higher ability to expand more than the group A. In Geldart group B, lower *Ar* particles had more ability to expand. Therefore, the CTFB occurred in 126 micron average diameter sand particles at a lower U_g than those with 260 micron average diameter.

The main effects of adsorption temperature, superficial gas velocity and sorbent loading had statistically significant meanings to CO_2 adsorption capacity. The analysis of variance demonstrated that the interaction between adsorption temperature and superficial gas velocity and the interaction between adsorption temperature and initial sorbent loading had an influence on CO_2 sorption capacity. The highest CO_2 capacity was obtained at sorption temperature of 60 °C, superficial gas velocity of 0.22 m/s and initial sorbent loading of 5 g. CO_2 sorption in a turbulent fluidized bed regime obeys

the exothermic equilibrium reaction to convert K_2CO_3 to $KHCO_3$, but it also produces the byproduct ($KAl(CO_3)(OH)_2$) which has drawbacks for regeneration.

Due to the statistical analysis, the sorbent which passed the hydro treatment and adsorbed CO_2 under turbulent fluidized bed regime can be regenerated by the heat regeneration. Focusing on the main effect operating parameters, both regeneration temperature and regeneration time promoted the positive trend to CO_2 sorption capacity. The response surface which obtained from the regression model revealed interaction between the effected operating parameters. The surface and inter molecular water which characterized by the DTG curve peaks lower 100 °C and between 200 – 400 °C played an important role to the interaction. The CO_2 capture capacity depended on the moisture which remained in the sorbent. Thus, the short regeneration time provided CO_2 capture capacity higher than the long regeneration at the low regeneration temperature. In contrast, longer regeneration time is better than the short period of regeneration at high temperature. This resulted by the inter structural water relocated to the sorbent surface and helped to promote the adsorption of the next cycle. The economical aspect showed two purposes of heat regeneration. The fresh sorbent could be replaced by the regenerated sorbent obtained from both high regeneration temperature and time which had CO_2 capture capacity about 90.7 % of fresh sorbent. In the design of CO_2 adsorption unit, the heat regeneration at low regeneration temperature in the short period time was sufficient to maintain the process.

The CO_2 sorbent with hydro treatment employed in a sorption process under turbulent fluidized bed regime and regenerated with depressurization was investigated for its adsorption activity. According to the statistical analysis, only the regeneration

pressure provided the positive trend on CO_2 adsorption capacity. The inactive species, $KAl(CO_3)(OH)_2H_2O$) was not found on the regenerated sorbent. Pore type of the sorbent was classified as meso-pore type IV and its type was not changed after passing the depressurized regeneration. The CO_2 capture capacity depended on the moisture which remained in the sorbent. The low depressurization degree (pressure at 0.8 atm) could not pull back the water during the hydro-treatment comparing to the high depressurization degree (pressure at 0.2 atm). The weak pull back force after the low depressurization degree could not take water into the deep pore. Thus, the water accumulation that took place on the sorbent surface and near the pore entrance was become an obstacle and blocked the active site in the pore to capture CO_2. For economical aspect, the fresh sorbent could be replaced by the regenerated sorbent obtained from high depressurized regeneration level of – 0.8 atm at short regeneration time. The CO_2 capture capacity of regenerated sorbent was about 95 percentage of the capture capacity obtained by the fresh sorbent.

The circulating fluidized bed reactor with perform three different steps; sorption in riser, gas-solid separation at cyclone and regeneration at downer can be used to capture CO_2 continuously. The positive trend of the increasing in superficial gas velocity showed the promise trend for the commercial use. The concern is the regenerator downer design which showed the negative trend of the initial sorbent loading to the sorption capacity which could be resolved by the increase in the inclination angle of the bottom or the compressed sorbent particle into a pellet with the larger diameter. The regression model had been addressed for the CO_2 capturing load with the variation of the operating parameters. The results and data interpretation in this

work is foundation concepts for the design of continuous CO_2 capture unit using solid sorbent.

The 90 percent or more CO_2 in fluidized bed using potassium or sodium carbonate sorbents multi-staged sorption is necessary due to equilibrium limitations. In this study, a method of determining the number of stages as function of per cent CO_2 removal was developed. This method is similar to the classical technique for the calculation of the number of plates in a distillation column in that there is an equilibrium curve and operating lines.

The 1 m in diameter and 3.55 m tall fluidized bed riser with cooling sections can solve the equilibrium limitation of CO_2 sorption on Na_2CO_3 sorbent. The operation I, which the temperatures of the cooling sections B D and F were kept at 50, 40, and 30°C, respectively, could provide more than 95% CO_2 capture. It is the same performance as the use of 6 multi-risers operated in series.

This riser does not need large amount of energy from the power plant, like steam used in case of conventional amine absorbers-strippers. The only substantial energy needed is a relatively small amount of electricity to fluidize the solid sorbent particles in short risers. To regenerate the sorbent, the downer uses waste heat transferring from the cooling section and the heat removing from the flue gas.

The sorbent could be regenerated by the application of heat. There are two sources of the heat which utilized for the regeneration. The heat which obtained from the sorption utilized by the cooling tubes for the sorbent pre-treatment at the upper part of the downer and the completion of the regeneration can be achieved by the heat that utilized by the flue gas. The proper size, number and the installation location as shown

in this work can complete the regeneration. All of the used sorbent ($NaHCO_3$) converts to be the active sorbent (Na_2CO_3). The regenerated sorbent has the temperature of 55 °C which is the same as the inlet temperature for CO_2 sorption in the multi-stage riser. Therefore, the alternative design for CO_2 sorption in the circulating fluidized bed reactor using solid sorbent Na_2CO_3 can be used as a continuous process to handle the larger CO_2 load from the large scale coal power plant.

5.2 recommendation

- The operating and design parameters should be used to define a new simple variable rather than V^* for CTFB determination. The methodology for CTFB prediction should be addressed to revise the new flow regime diagram.

-The effect of moisture in the synthesis flue gas on CO_2 sorption capacity should be studied.

- Equilibrium curves of CO_2 with different metal group I carbonate compound should be next step to be studied before the pilot scale study. The concentration of CO_2 supposed to be regulated ranging between 5 to 20 percent by volume.

- Transport phenomena of the multiphase flow which represented in term of dimensionless number should be included in the kinetic reactions which were coded in user define function of Fluent program.

- Indept pressure loop study of the circulating fluidized bed for CO_2 sorption should be done by simulating the response to water condensation arguments.

REFERENCES

[1] Gall ET, Nazaroff WW. New directions: Potential climate and productivity benefits from CO2 capture in commercial buildings. Atmospheric Environment. 2015;103:378-80.

[2] Rosenqvist Å, Milne A, Lucas R, Imhoff M, Dobson C. A review of remote sensing technology in support of the Kyoto Protocol. Environmental Science & Policy. 2003;6:441-55.

[3] Shan L, Li H, Meng B, Meng J, Yu Y, Min Y. Improvement of CO2 Capture Performance of Calcium- based Absorbent: Modified with Palygorskite. Chinese Journal of Chemical Engineering.

[4] Veneman R, Hilbers T, Brilman DWF, Kersten SRA. CO2 capture in a continuous gasósolid trickle flow reactor. Chemical Engineering Journal. 2016;289:191-202.

[5] Hiremath V, Jadhav AH, Lee H, Kwon S, Seo JG. Highly reversible CO2 capture using amino acid functionalized ionic liquids immobilized on mesoporous silica. Chemical Engineering Journal. 2016;287:602-17.

[6] Choi S, Drese JH, Eisenberger PM, Jones CW. Application of amine-tethered solid sorbents for direct CO2 capture from the ambient air. Environmental science & technology. 2011;45:2420-7.

[7] Trends in Atmospheric Carbon Dioxide. 2016.

[8] Richner G, Puxty G, Carnal A, Conway W, Maeder M, Pearson P. Thermokinetic properties and performance evaluation of benzylamine-based solvents for CO2 capture. Chemical Engineering Journal. 2015;264:230-40.

[9] Duyar MS, Ramachandran A, Wang C, Farrauto RJ. Kinetics of CO2 methanation over Ru/γ-Al2O3 and implications for renewable energy storage applications. Journal of CO2 Utilization. 2015;12:27-33.

[10] Kishor R, Ghoshal AK. High molecular weight polyethyleneimine functionalized three dimensional mesoporous silica for regenerable CO2 separation. Chemical Engineering Journal. 2016;300:236-44.

[11] Socolow R, Desmond M, Aines R, Blackstock J, Bolland O, Kaarsberg T, et al. Direct air capture of CO2 with chemicals: a technology assessment for the APS Panel on Public Affairs. American Physical Society; 2011.

[12] Smil V. Energy myths and realities: bringing science to the energy policy debate: Government Institutes; 2010.

[13] Ayobi M, Shahhosseini S, Behjat Y. Computational and experimental investigation of CO2 capture in gasósolid bubbling fluidized bed. Journal of the Taiwan Institute of Chemical Engineers. 2014;45:421-30.

[14] Kongkitisupchai S, Gidaspow D. Carbon dioxide capture using solid sorbents in a fluidized bed with reduced pressure regeneration in a downer. AICHE J. 2013;59:4519-37.

[15] Lin Y-J, Rochelle GT. Approaching a reversible stripping process for CO2 capture. Chemical Engineering Journal. 2016;283:1033-43.

[16] Goel C, Bhunia H, Bajpai PK. Novel nitrogen enriched porous carbon adsorbents for CO2 capture: Breakthrough adsorption study. Journal of Environmental Chemical Engineering. 2016;4:346-56.

[17] Rosenqvist Å, Milne A, Lucas R, Imhoff M, Dobson C. Corrigendum to "A review of remote sensing technology in support of the Kyoto Protocol" [Environ. Sci. Policy 6 (2003) 441ó455]. Environmental Science & Policy. 2003;6:551.

[18] Lee SC, Choi BY, Ryu CK, Ahn YS, Lee TJ, Kim JC. The effect of water on the activation and the CO2 capture capacities of alkali metal-based sorbents. Korean Journal of Chemical Engineering. 2006;23:374-9.

[19] Park YK, Choi WC, Kang NY. CARBON DIOXIDE CAPTURE APPARATUS. U.S. Patent Application In: TECHNOLOGY KRIOC, editor. Daejeon

KoreaJan 21, 2016.

[20] Gidaspow MOaD. kinetics of the reaction of CO2 with solid K2CO3. institute of gas technology 1975.

[21] Michael Onischak DG. In: Li NN, editor. Recent Developments in Separation Science: CRC press; 1972. p. 73-93.

[22] Rochelle GT. Amine scrubbing for CO2 capture. Science. 2009;325:1652-4.

[23] Nelson TO, Coleman LJ, Green DA, Gupta RP. The dry carbonate process: carbon dioxide recovery from power plant flue gas. Energy Procedia. 2009;1:1305-11.

[24] Holt N. Evaluation of Innovative Fossil Fuel Power plants with CO2 removal. EPRI Interim Report to DOE NETL December 2000.

[25] Gidaspow D, Onischak M. Process for regenerative sorption of CO2. US patent 3,865,924. In: Technology IoG, editor. Chicago, Illinois, US.1975.

[26] Onischak M, Gidaspow D. Separation of gaseous mixtures by regenerattive sorption on porous solid: part I A fluid porous solid reaction model with structural changes and Part II Regenerative separation of CO2 Chemical Rubber Co., Cleveland Ohio; 1972.

[27] Nelson TO, Coleman LJ, Green DA, Gupta RP. Carbon Dioxide Recoveryfrom Power Plant Flue Gas Using Supported Carbonate Sorbents in a Thermal-swing

Process. Proc of Sixth Annual Conference on Carbon Capture and Sequestration. Pittsburgh, PAMay 7ó20; 2007.

[28] Pan Y-x, Liu C-j, Wiltowski TS, Ge Q. CO2 adsorption and activation over γ-Al2O3-supported transition metal dimers: A density functional study. Catalysis Today. 2009;147:68-76.

[29] Lee SC, Kwon YM, Chae HJ, Jung SY, Lee JB, Ryu CK, et al. Improving regeneration properties of potassium-based alumina sorbents for carbon dioxide capture from flue gas. FUEL. 2013;104:882-5.

[30] Zhao C, Chen X, Zhao C. Carbonation behavior of K2CO3 with different microstructure used as an active component of dry sorbents for CO2 capture. Industrial & Engineering Chemistry Research. 2010;49:12212-6.

[31] Peng T-H, Lin C-L, Wey M-Y. Development of a low-temperature two-stage fluidized bed incinerator for controlling heavy-metal emission in flue gases. Appl Therm Eng. 2014;62:706-13.

[32] Zhao C, Chen X, Zhao C, Wu Y, Dong W. K2CO3/Al2O3 for capturing CO2 in flue gas from power plants. Part 3: CO2 capture behaviors of K2CO3/Al2O3 in a bubbling fluidized-bed reactor. Energy & Fuels. 2012;26:3062-8.

[33] Zhao C, Chen X, Zhao C. K2CO3/Al2O3 for capturing CO2 in flue gas from power plants. Part 2: Regeneration behaviors of K2CO3/Al2O3. Energy & Fuels. 2012;26:1406-11.

[34] Zhao C, Chen X, Zhao C. K2CO3/Al2O3 for capturing CO2 in flue gas from power plants. Part 1: Carbonation behaviors of K2CO3/Al2O3. Energy & Fuels. 2012;26:1401-5.

[35] Liang Y, Harrison D, Gupta R, Green D, McMichael W. Carbon dioxide capture using dry sodium-based sorbents. Energy & Fuels. 2004;18:569-75.

[36] Jaiboon O-a, Chalermsinsuwan B, Mekasut L, Piumsomboon P. Effect of flow patterns/ regimes on CO2 capture using K2CO3 solid sorbent in fluidized bed/circulating fluidized bed. Chemical Engineering Journal. 2013;219:262-72.

[37] Jaiboon O-a, Chalermsinsuwan B, Mekasut L, Piumsomboon P. Effect of flow pattern on power spectral density of pressure fluctuation in various fluidization regimes. Powder Technology. 2013;233:215-26.

[38] Chalermsinsuwan B, Kuchonthara P, Piumsomboon P. CFD modeling of tapered circulating fluidized bed reactor risers: Hydrodynamic descriptions and chemical reaction responses. Chemical Engineering and Processing: Process Intensification. 2010;49:1144-60.

[39] Kim H, Miller DC, Modekurti S, Omell B, Bhattacharyya D, Zitney SE. Mathematical modeling of a moving bed reactor for post-combustion CO2 capture. AICHE J. 2016.

[40] Jackson R. The mechanics of fluidised beds: part I: the stability of the state of unifrom fluidisation. Transactions of the Institution of Chemical Engineers. 1963;41:1-10.

[41] Jackson R. The Mechanics of fluidised bed : Part II The motion of fully developed bubbles

Transactions of the Institution of Chemical Engineers. 1963;41:22-8.

[42] Anderson T, Jackson R. Fluid mechanical description of fluidized beds. Stability of state of uniform fluidization. Industrial & Engineering Chemistry Fundamentals. 1968;7:12-21.

[43] Sinclair J, Jackson R. Gas-particle flow in a vertical pipe with particle-particle interactions. AICHE J. 1989;35:1473-86.

[44] Hrenya CM, Sinclair JL. Effects of particle-phase turbulence in gas-solid flows. AICHE J. 1997;43:853-69.

[45] Jackson R. The dynamics of fluidized particles: Cambridge University Press; 2000.

[46] Mostofi Reza M. CFD Simulations of Particulate Two-Phase and Three Phase Flows, Ph.D thesis: Illinois Institute of Technology; May 2002.

[47] Gidaspow D. Multiphase Flow and Fluidization. San Diego: Academic Press; 1994. p. 61-72.

[48] Collier J. Convective and Condensation 2nd ed: McGraw-HIll book Company; 1972.

[49] Breault RW. A review of gasó solid dispersion and mass transfer coefficient correlations in circulating fluidized beds. Powder technology. 2006;163:9-17.

[50] Breault RW, Guenther C. Mass transfer coefficient prediction method for CFD modeling of riser reactors. Powder Technology. 2010;203:33-9.

[51] Chalermsinsuwan B, Kuchonthara P, Piumsomboon P. Effect of circulating fluidized bed reactor riser geometries on chemical reaction rates by using CFD simulations. Chem Eng Process. 2009;48:165-77.

[52] Kashyap M, Gidaspow D. Computation and measurements of mass transfer and dispersion coefficients in fluidized beds. Powder Technology. 2010;203:40-56.

[53] Kashyap M, Gidaspow D. Measurements and computation of low mass transfer coefficients for FCC particles with ozone decomposition reaction. AICHE J. 2012;58:707-29.

[54] Pannala S. Computational Gas-Solids Flows and Reacting Systems: Theory, Methods and Practice: Theory, Methods and Practice: IGI Global; 2010.

[55] J. F. Davision DH. Fluidization. London and Newyork: Academic press; 1971.

[56] Geldart D. Types of gas fluidization. Powder Technology. 1973;7:285-92.

[57] Ren J, Mao Q, Li J, Lin W. Wavelet analysis of dynamic behavior in fluidized beds. Chemical Engineering Science. 2001;56:981-8.

[58] Yang T-Y, Leu L-p. Study of transition velocities from bubbling to turbulent fluidization by statistic and wavelet multi-resolution analysis on absolute pressure fluctuations. Chemical Engineering Science. 2008;63:1950-70.

[59] Xiong Q, Aramideh S, Kong S-C. Modeling effects of operating conditions on biomass fast pyrolysis in bubbling fluidized bed reactors. Energy & Fuels. 2013;27:5948-56.

[60] Abdelghany EAM, Abdelkareem MA, Mahmoud IH. Behavior of Ultrafine versus Superfine Powders in a Binary-Mixture Semi-Batch Circulating Fluidized Bed. Chemical Engineering & Technology. 2014;37:723-9.

[61] Bi HT, Grace JR. Flow regime diagrams for gas-solid fluidization and upward transport. International Journal of Multiphase Flow. 1995;21:1229-36.

[62] Chaiwang P, Gidaspow D, Chalermsinsuwan B, Piumsomboon P. CFD design of a sorber for CO2 capture with 75 and 375 mircron particles. Chemical Engineering Science. 2014;105:32-45.

[63] Chalermsinsuwan B, Boonprasop S, Nimmanterdwong P, Piumsomboon P. Revised fluidization regime characterization in high solid particle concentration circulating fluidized bed reactor. International Journal of Multiphase Flow. 2014;66:26-37.

[64] Chalermsinsuwan B, Gidaspow D, Piumsomboon P. In-depth system parameters of transition flow pattern between turbulent and fast fluidization regimes in high solid particle density circulating fluidized bed reactor. Powder Technology. 2014;253:522-36.

[65] Chalermsinsuwan B, Piumsomboon P, Gidaspow D. Kinetic theory based computation of PSRI riser: Part II—Computation of mass transfer coefficient with chemical reaction. Chemical Engineering Science. 2009;64:1212-22.

[66] Tamadondar MR, Azizpour H, Zarghami R, Mostoufi N, Chaouki J. Using particle trajectory for determining the fluidization regime in gasósolid fluidized beds. Advanced Powder Technology. 2012;23:349-51.

[67] Yerushalmi J, Cankurt NT. Further studies of the regimes of fluidization. Powder Technology. 1979;24:187-205.

[68] Grace JR. Contacting modes and behaviour classification of gas—solid and other two-phase suspensions. The Canadian Journal of Chemical Engineering. 1986;64:353ó 63.

[69] Du B, Fan LS, Wei F, Warsito W. Gas and solids mixing in a turbulent fluidized bed. AICHE J. 2002;48:1896-909.

[70] Monazam ER, Shadle LJ, Mei JS, Spenik J. Identification and characteristics of different flow regimes in a circulating fluidized bed. Powder Technology. 2005;155:17-25.

[71] Bai D, Shibuya E, Masuda Y, Nakagawa N, Kato K. Flow structure in a fast fluidized bed. Chemical Engineering Science. 1996;51:957-66.

[72] Chu KW, Yu AB. Numerical and experimental investigation of an "S-shaped" circulating fluidized bed. Powder Technology. 2014;254:460-9.

[73] Lee SC, Cho MS, Jung SY, Ryu CK, Kim JC. Effects of alumina phases on CO2 sorption and regeneration properties of potassium-based alumina sorbents. Adsorption. 2014;20:331-9.

[74] Lee SC, Kwon YM, Ryu CY, Chae HJ, Ragupathy D, Jung SY, et al. Development of new alumina-modified sorbents for CO 2 sorption and regeneration at temperatures below 200 C. FUEL. 2011;90:1465-70.

[75] Guo Y, Zhao C, Li C, Lu S. Application of PEIóK 2 CO 3/AC for capturing CO 2 from flue gas after combustion. Applied Energy. 2014;129:17-24.

[76] Lee SC, Chae HJ, Choi BY, Jung SY, Ryu CY, Park JJ, et al. The effect of relative humidity on CO 2 capture capacity of potassium-based sorbents. Korean Journal of Chemical Engineering. 2011;28:480-6.

[77] Zhao W, Sprachmann G, Li Z, Cai N, Zhang X. Effect of K 2 CO 3· 1.5 H 2 O on the regeneration energy consumption of potassium-based sorbents for CO 2 capture. Applied Energy. 2013;112:381-7.

[78] Bi H, Grace J. Flow regime diagrams for gas-solid fluidization and upward transport. International Journal of Multiphase Flow. 1995;21:1229-36.

[79] Vepsäläinen A, Shah S, Ritvanen J, Hyppänen T. Interphase mass transfer coefficient in fluidized bed combustion by Eulerian CFD modeling. Chemical Engineering Science. 2014;106:30-8.

[80] Joshi JBS, M. M. A circulation cell model for bubble columns Transactions of the Institution Chemical Engineering. (1979);57:244-51.

[81] Joshi JB RV, Gharat SD. Sparged loop reactor Canadian Journal of Chemical Engineering.68:705-41.

[82] Tamadondar M, Azizpour H, Zarghami R, Mostoufi N, Chaouki J. Using particle trajectory for determining the fluidization regime in gasósolid fluidized beds. Advanced Powder Technology. 2012;23:349-51.

[83] Grace JR. Contacting modes and behaviour classification of gas—solid and other two-phase suspensions. The Canadian Journal of Chemical Engineering. 1986;64:353-63.

[84] Rhodes M, Sollaart M, Wang X. Flow structure in a fast fluid bed. Powder Technology. 1998;99:194-200.

[85] Chu K, Yu A. Numerical and experimental investigation of an "S-shaped" circulating fluidized bed. Powder Technology. 2014;254:460-9.

[86] Grace JR. High-velocity fluidized bed reactors. Chemical Engineering Science. 1990;45:1953-66.

[87] Bi H, Zhu J. Static instability analysis of circulating fluidized beds and concept of high-density risers. AICHE J. 1993;39:1272-80.

[88] Kim SW, Kirbas G, Bi H, Lim CJ, Grace JR. Flow behavior and regime transition in a high-density circulating fluidized bed riser. Chemical Engineering Science. 2004;59:3955-63.

[89] Grace JR. Reflections on turbulent fluidization and dense suspension upflow. Powder Technology. 2000;113:242-8.

[90] Qi X, Zhu H, Zhu J. Demarcation of a new circulating turbulent fluidization regime. AICHE J. 2009;55:594-611.

[91] Zhu J. Circulating turbulent fluidization—a new fluidization regime or just a transitional phenomenon. Particuology. 2010;8:640-4.

[92] Qi M, Barghi S, Zhu J. Detailed hydrodynamics of high flux gasó solid flow in a circulating turbulent fluidized bed. Chemical Engineering Journal. 2012;209:633-44.

[93] Qi M, Zhu J, Barghi S. Particle velocity and flux distribution in a high solids concentration circulating turbulent fluidized bed. Chemical engineering science. 2012;84:437-48.

[94] Zhu H, Zhu J. Comparative study of flow structures in a circulating-turbulent fluidized bed. Chemical Engineering Science. 2008;63:2920-7.

[95] Zhu H, Zhu J. Gas-solids flow structures in a novel circulating-turbulent fluidized bed. AICHE J. 2008;54:1213-23.

[96] Park C, Basu P. A model for prediction of transient response to the change of fuel feed rate to a circulating fluidized bed boiler furnace. Chemical Engineering Science. 1997;52:3499-509.

[97] Al-Sherehy F, Grace JR, Adris A-EM. The influence of distributed reactant injection along the height of a fluidized bed reactor. Chemical engineering science. 2005;60:7121-30.

[98] Chalermsinsuwan B, Piumsomboon P, Gidaspow D. A computational fluid dynamics design of a carbon dioxide sorption circulating fluidized bed. AICHE J. 2010;56:2805-24.

[99] Chalermsisuwan B TT, Piumsomboon P. Characterization regime in circulating fluidized bed rector with high solid particle concentration using computational fluid dynamics. Korean J Chem Eng. 2014;31:350-63.

[100] Jaiboon O-a, Chalermsinsuwan B, Mekasut L, Piumsomboon P. Effect of flow patterns/ regimes on CO 2 capture using K 2 CO 3 solid sorbent in fluidized bed/circulating fluidized bed. Chemical engineering journal. 2013;219:262-72.

[101] Krupay B, Amenomiya Y. Alkali-promoted alumina catalysts: I. Chemisorption and oxygen exchange of carbon monoxide and carbon dioxide on potassium-promoted alumina catalysts. Journal of Catalysis. 1981;67:362-70.

[102] Sengupta S, Reddy SA, Dongara R, Das AK, Bhunia H, Bajpai PK. Improvement in Regeneration Properties and Multicycle Stability for K2CO3/Al2O3 Adsorbents for CO2 Removal from Flue Gas. Energy & Fuels. 2014;28:5354-62.

[103] Jongartklang N, Chanchairoek S, Piumsomboon P, Chalermsinsuwan B. Correlations of kinetic parameters with various system operating conditions for CO2 sorption using K2CO3/Al2O3 solid sorbent in a fixed/fluidized bed reactor. Journal of Environmental Chemical Engineering. 2016;4:1938-47.

[104] Boonprasop S, Chalermsinsuwan B, Piumsomboon P. Design Parameters for Performing Circulating Turbulent Fluidization with a Single Feed Stage Fluidized Bed Reactor. Chemical Engineering and Technology. 2017;40:177-85.

[105] Oyenekan B, Rochelle G. Energy performance of stripper configurations for CO2 capture by aqueous amines. Industrial & Engineering Chemistry Research. 2006;45:2457ó464.

APPENDIX

CALCULATION

1. Solid Volume Fraction (ε_s)

$$\varepsilon_s = \frac{\Delta P}{\rho_p g \Delta h} \tag{5}$$

Where:

$\Delta P = 2642.80$ Pa, $\rho_p = 2642.80$ kg/m^3, $\Delta h = 0.15$ m, and $g = 9.81$ [m/s^2].

Thus,

$$\varepsilon_s = \frac{2642.803}{2642.80 \times 9.81 \times 0.15}$$

$$\varepsilon_s = 0.50$$

2. Archimedes number (Ar)

$$Ar = \frac{\rho_g (\rho_p - \rho_g) g d_p{}^3}{\mu^2} \tag{6}$$

Where:

$\rho_p = 1.16$ kg/m^3, $\rho_p = 2642.80$ kg/m^3, $g = 9.81$ m/s^2, $d_p = 0.00026$ m, and μ = 0.00002 Pa.s.

Thus,

$$Ar = \frac{1.16 \times (2650 - 1.16) \times 9.81 \times 0.00026^3}{000002^2}$$

$$Ar = 1352$$

3. V^*

$$V^* = \left[\frac{\rho_g{}^2}{g\mu_g(\rho_p - \rho_g)}\right]^{\frac{1}{3}}\left[U_g - \frac{G_s\varepsilon_s}{\rho_p(1-\varepsilon_s)}\right]$$

Where:

ρ_p = 1.16 kg/m^3, ρ_p = 2642.80 kg/m^3, g = 9.81 m/s^2, d_p = 0.00026 m, μ_g = 0.00002 Pa.s, U_g = 1.3 m/s, ε_s = 0.28, and G_s = 290 kg/m^2.s

Thus,

$$V^* = \left[\frac{1.16^2}{9.81 \times 0.00002 \times (2642.80 - 1.16)}\right]^{\frac{1}{3}}\left[1.3 - \frac{290 \pm 0.28}{2642.80(1-0.28)}\right]$$

$$V^* = 1.74$$

4. CO_2 capture capacity (q)

$$q = \frac{1}{m}\int_o^t Q(C_{in} - C_{out})dt$$

Where:

m = 0.85 g, C_{in} = the inlet concentration of CO_2 (% volume) [-], C_{out} = the outlet concentration of CO_2 (% volume) [-]. Q = the gas flow rate [g/S], and t = the sorption time [S].

Where, $\int_{o}^{t} Q(C_{in} - C_{out})dt$ is 0.276 which is the shaded area on the CO_2 concentration profile as in Figure A.

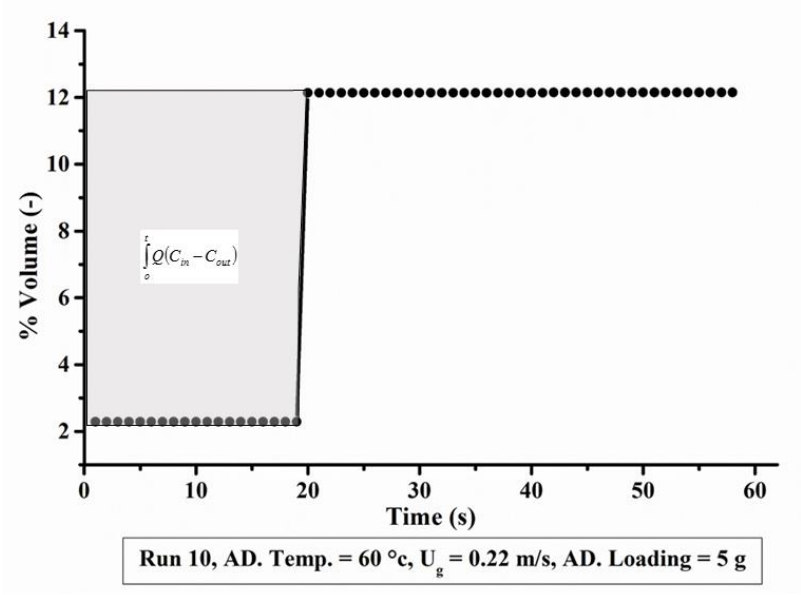

Figure A the integration value on breakthrough curve

Thus,

$$q = \frac{1}{0.85} \times 0.275$$

$q = 323.94$ mg of CO_2/g of sorbent

VITA

Mr. Sutthichai Boonprasop was born on 22nd January 1989 at Bangkok, Thailand. He received his Bachelor degree and Master degree in Chemical Technology from Faculty of Science, Chulalongkorn University, Thailand in 2011 and 2013 respectively. Then, he stated his doctorate program in 2013 academic year in the same place. He has received the Century Anniversary Chulalongkorn University Fund for Doctoral Scholarship (2013 - 2017). Sutthichai also served as a teaching assistant for undergraduate course Applied Mathematical I (2014), Fuel Laboratory (2015) and Physicochemical Measurement I (2017).

Sutthichai received Sakura Project fund to conduct the particle (sorbent) characterization study at Nagoya University (October – November 2015). He also supported by Overseas Research Experience Scholarship for Graduate Student to develop the simulation for an alternative design of Carbon dioxide sorption unit. He published his work in Chemical and Engineering & Technology journal with the title of "Design parameters for performing circulating turbulent fluidization with single feed stage fluidized bed reactor". His simulation works in the topics of "CO2 Capture in a Multistage CFB: Part I: Number of Stages" and "CO2 Capture in a Multistage CFB: Part II: Riser with Multiple Cooling Stages" got an acceptance from AIChE Journal. The publications will be published in the special volume to tribute to the journal founders: Roy Jackson, Particle Technology and Fluidization.